Hashemite Kingdom of Jordan

Hashemite University

Jordan Journal of Earth and Environmental Sciences

JJEES

An International Peer-Reviewed Scientific Journal

Financed by the Scientific Research Support Fund

http://jjees.hu.edu.jo/

Volume (6) Number (2) ISSN 1995-6681 December 2014/Rabi' Al-Awwal 1436

The Jordan Journal of Earth and Environmental Sciences (JJEES)

JJEES is an international peer-reviewed research journal, issued by the Deanship of Academic Research and Graduate Studies, the Hashemite University, in corporation with, the Jordanian Scientific Research Support Fund, the Ministry of Higher Education and Scientific Research.

SUBMISSION ADDRESS:

Professor **Eid A. Al-Tarazi**
Deanship of Academic Research and Higher Studies
Hashemite University, P.O. Box 150458, Postal Code 13115, Zarqa, Jordan.
Phone: +962-5-3903333 ext.4229
E-Mail: jjees@hu.edu.jo

Hashemite Kingdom of Jordan

Hashemite University

Jordan Journal of Earth and Environmental Sciences

JJEES

An International Peer-Reviewed Scientific Journal

Financed by the Scientific Research Support Fund

http:// jjees.hu.edu.jo/

ISSN 1995-6681

المجلة الأردنية لعلوم الأرض والبيئة
Jordan Journal of Earth and Environmental Sciences (JJEES)
http://jjees.hu.edu.jo

Hashemite University

Deanship of Scientific Research and Graduate Studies

TRANSFER OF COPYRIGHT AGREEMENT

Journal publishers and authors share a common interest in the protection of copyright: authors principally because they want their creative works to be protected from plagiarism and other unlawful uses, publishers because they need to protect their work and investment in the production, marketing and distribution of the published version of the article. In order to do so effectively, publishers request a formal written transfer of copyright from the author(s) for each article published. Publishers and authors are also concerned that the integrity of the official record of publication of an article (once refereed and published) be maintained, and in order to protect that reference value and validation process, we ask that authors recognize that distribution (including through the Internet/WWW or other on-line means) of the authoritative version of the article as published is best administered by the Publisher.

To avoid any delay in the publication of your article, please read the terms of this agreement, sign in the space provided and return the complete form to us at the address below as quickly as possible.

Article entitled:----------

Corresponding author: ----------

To be published in the journal: Jordan Journal of Earth & Environmental Sciences (JJEES)

I hereby assign to the Hashemite University the copyright in the manuscript identified above and any supplemental tables, illustrations or other information submitted therewith (the "article") in all forms and media (whether now known or hereafter developed), throughout the world, in all languages, for the full term of copyright and all extensions and renewals thereof, effective when and if the article is accepted for publication. This transfer includes the right to adapt the presentation of the article for use in conjunction with computer systems and programs, including reproduction or publication in machine-readable form and incorporation in electronic retrieval systems.
Authors retain or are hereby granted (without the need to obtain further permission) rights to use the article for traditional scholarship communications, for teaching, and for distribution within their institution.

☐ **I am the sole author of the manuscript**

☐ **I am signing on behalf of all co-authors of the manuscript**

☐ **The article is a 'work made for hire' and I am signing as an authorized representative of the employing company/institution**

Please mark one or more of the above boxes (as appropriate) and then sign and date the document in black ink.

Signed:_____ **Name printed:** _____

Title and Company (if employer representative) : _____

Date: _____

Data Protection: By submitting this form you are consenting that the personal information provided herein may be used by the Hashemite University and its affiliated institutions worldwide to contact you concerning the publishing of your article.

Please return the completed and signed original of this form by mail or fax, or a scanned copy of the signed original by e-mail, retaining a copy for your files, to:

Hashemite University
Deanship of Scientific Research and Graduate Studies
Zarqa 13115 Jordan
Fax: +962 5 3903338
Email: jjees@hu.edu.jo

Subscription

Jordan Journal of Earth & Environmental Sciences (ISSN 1995-6681)
An International Peer- Reviewed Research Journal
Published by the deanship of Research and Graduate Studies- The Hashemite University

Name:	الاســـــــــــم:
Specialty:.....	التخصـــــــــص:
Address:.....	العنـــــــــوان:
P.O. Box:.....	صنـــدوق البريـــــد:
City & Postal Code:	المدينة: الرمز البريدي:
Country:.....	الـــــــــــدولة:
Phone:.....	رقـــم الهاتـــــف:
Fax No:.....	رقـــم الفاكـــــس:
E-mail:.....	البريـــد الإلكترونـــي:
Method of payment:	طريقـــــة الدفـــع:
Amount Enclosed:.....	المبلـــــغ المرفـــق:
Signature:.....	التوقيـــــــــع:

Cheques should be paid to Deanship of Research and Graduate Studies- The Hashemite University

I would like to subscribe to the Journal:

For

- ☐ One year
- ☐ Two years
- ☐ Three years

One year Subscription Rates		
	Inside Jordan	Outside Jordan
Individuals	10JD	70$
Students	5JD	35$
Institutions	20JD	90$

Correspondence

Subscriptions and sales:

Prof. Dr. Eid Al-Tarazi
The Hashemite University
P.O. Box 330127- Zarqa 13115 - Jordan
Tel. +962-(0) 795651567 (mobile)
+962-5-3903333 - 4229 (office)
Fax: +962 5 3903338
Email: jjees@hu.edu.jo

JJEES
Jordan Journal of Earth and Environmental Sciences

JJEES
Jordan Journal of Earth and Environmental Sciences

Volume 6, Number 2, December, 2014
ISSN 1995-6681
Pages 45- 51

Removal of Aqueous Chromium (III) Ions Using Jordanian Natural Zeolite Tuff in Batch and Fixed Bed Modes

Ahmad M. Al-Haj-Ali* and Lana M. Marashdeh

Dept. of Chemical Engineering, University of Jordan

Received 3 September, 2014; Accepted 25 December, 2014

Abstract

The present study was undertaken to evaluate the capability of natural zeolite tuffto remove Cr(III) ions from aqueous solutions by physical chemical method under specified conditions. Investigationsinvolved shake-flasks experiments conductedusing 1.0-8.0 g/L doseof 355-500 µm zeolite particles in solution of 50 mg Cr(III)/L at initial pH of 4.0 and 22°Cas well as fixed-bedexperiments conducted using 4.8-14.4 cm bed height, 5.66-12.45 solution velocity, 50-100 mg/L initial metal concentration, size cuts in the range +355-850µmand initial pH of 4.0-5.5. The equilibrium adsorption capacity reached 19.6 mg/g and the data fitted well both Langmuir and Redlich-Peterson isotherms. Break points up to 2.5 hours were obtained at 5% breakpoint using fixed-beds of zeolite at the lower metal concentration and solution velocity but higher pH and bed depth. Mechanism of removal appears to be ion exchange of $Cr(OH)^{2+}$at pH≤ 6.0 and adsorption on zeolite surface of fine $Cr(OH)_3$ precipitate at pH> 6.0.

Keywords: Trivalent chromium, natural zeolite, adsorption isotherms, breakthrough curves, Jordan.

1. Introduction

Being used in many very important industrial applications, Chromiumplays a key role in many industries such as leather tanning, metal electroplating and other surface finishing, pigments, paints, textile, wood preservation, fire-retardant formulas, reaction catalysis, batteries, magnetic tapes and corrosion inhibition (Kirk-Othmer Encyclopedia, 2007). From these industries, there is a substantial disposal of chromium-containing process effluents and sludges that contaminate the soil, surface water and underground water before eventually entering the human food chain (Adriano, 2001).Chromium may exist in several oxidation states of which 0, 3 and 6 are stable enough to occur in the environment. Cr(VI) is much more soluble and due to the mobility of its species in water it constitutes a high health and environmental hazard. Cr(III) is the most chemically stable and best known oxidation state of chromium. In the presence of manganese oxides, Cr(III) can be easily oxidized to Cr(VI). According to Stumm and Morgan (1996), the interaction of trivalent chromium with the environment involves various chemical and physical processes including hydrolysis, complexation, redox reactions and adsorption.

The discharge limits from industrial effluents vary according to the fate or application of wastewater. For example, the maximum allowable concentration of total chromium in the Jordanian wastewater (both industrial and treated domestic sewage) standards is 0.01 mg/L for reuse in irrigation and discharge to streams and lakes; 0.02 mg/L for underground water recharge and 0.07 mg/L for discharge to the sea. Drinking water guideline value for Cr(III) recommended by World Health Organization (WHO) is 0.005 mg/L (WHO, 2011), which is adopted by the Jordanian standard for drinking water. Two engineering techniques for heavy metal removal are usually applied, namely chemical precipitation and ion exchange. These methods suffer from disadvantages such as non-selectivity, high cost and waste disposal problems. Natural zeolites are crystalline microporousaluminosilicates with well-defined structures that consist of a framework formed by tetrahedra of SiO_4 and AlO_4 connected through oxygen atoms. The frame-work contains channels and cavities with molecular dimensions from 0.3 to 1 nm occupied by alkaline and alkaline earth metal cations as well as water molecules. These cations possess the ability to move freely and can be exchanged by more selective cations from aqueous solutions (Wang and Peng, 2010).

Fixed beds of zeolite may be used as packing materials in subsurface barriers to control ground water pollution (Obiri-Nyarkoa *et al*., 2014). These applications are stimulated by the non-toxic nature of zeolites as well as their availability in many countries at low cost. Application of natural zeolites for the removal of heavy metals such as Pb(II), Cd(II), Ni(II), Zn(II), etc. has been reported in several studies considering both batch equilibrium and dynamic fixed-bed column experiments (Alvarez-Ayuso *et al*., 2003; Al-Haj-Ali and Al-Hunaidi, 2004; Baker *et al*., 2009; Karatas, 2012; Malamisa and Katsou, 2013).

In northeastern and central parts of Jordan, large deposits of natural zeolites, produced by alteration of basaltic glass, are present and estimated as geological reserves at 170 million tons. Currently, these minerals (mostly phillipsite and chabazite) are being mined and made commercially available for agricultural applications where they are used as a soil conditioner (Natural Resources Authority, 2006). Environmental applications of Jordanian zeolites, as

* Corresponding author. e-mail: ahmad.ay55@gmail.com

adsorbents and ion exchangers for pollutant removal, have been the subject of investigation over the last two decades. Published studies over the past two decades have shown that Jordanian zeolite tuffs, from different locations in Jordan, are efficient adsorbents for heavy metal removal from aqueous solutions and industrial wastewater (Al-HajAli and El-Bishtawi, 1997; Ibrahim *et al*., 2002; Taamneh and Al Dwairi, 2013).

The main objective of this study is to evaluate the ability of a major type of natural Jordanian zeolite, namely, Phillipsite tuff for the removal of Cr(III) ions under various adsorption conditions of zeolite and solution, both in batch and fixed-bed column modes. In particular, the adsorption capacity, mechanism and breakthrough times are sought for further consideration of the mineral application.

2. Methodology

2.1. Materials

The zeolite tuff used in this work was mined from Jabal Aritayn area in the northeastern part of Jordan and supplied by the Natural Resources Authority of Jordan. X-Ray Diffraction (XRD) analysis has shown that the raw zeolite tuff is rich in phillipsite and calcite ($CaCO_3$) is the major non-zeolitic impurity (Fig. 1).

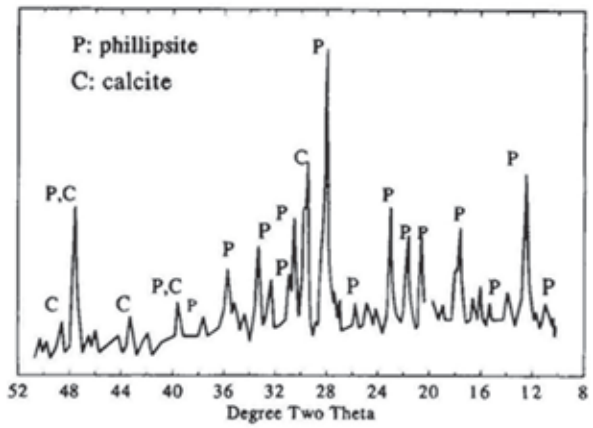

Figure 1: X-ray diffraction chart of zeolite tuff (P: phillipsite, C: calcite)

A scanning electron microscope of the mineral is shown in Fig. 2, indicating the heterogeneous surface and irregular shape of the mineral particles.

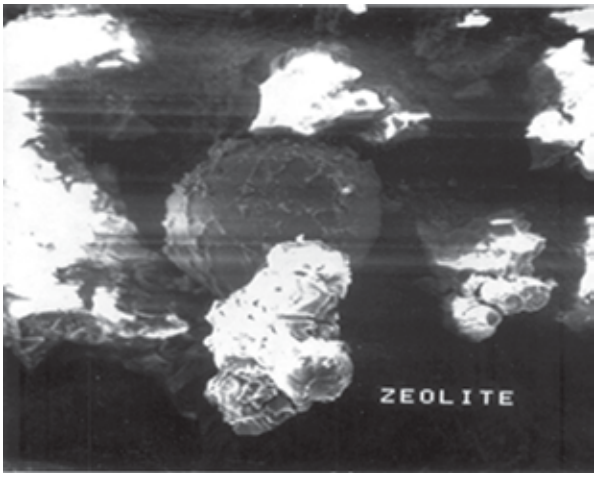

Figure 2: Scanning electron micrograph (SEM) of powdered zeolite

The mineral was crushed using a Jaw crusher and sieved into different size cuts; those of 355-500, 500-710 and 710-850 μm were selected for metal uptake experiments. These size cuts were washed with distilled water to remove all fines, immersed in 25g/L analytical grade sodium chloride solution for 48 hours to convert the zeolite into Na-form. The NaCl solution was then decanted and zeolite sample washed gently with distilled water to remove trace salt. Finally, the zeolite sample was oven-dried overnight at 100°C.

Table 1: Physical Properties of Unsieved and Size Cuts of Zeolite

Unsieved Zeolite: True Density: 2.380 g/cm^3 Bulk Density: 1.035 g/cm^3 Color: Yellowish Brown				
Size Range	Langmuir Surface Area (m^2/g)	BET Surface Area (m^2/g)	Total Pore Volume (cm^3/g)	Avg. Pore Diameter (Å)
355-500 μm	124	92.0	4. 02 x 10^{-2}	1.75
710-850 μm	120	90.0	3.90 x 10^{-2}	1.75

Various physical properties of unsieved zeolite and some size cuts are given in Table 1. Langmuir and Brunauer Emmett Teller (BET) surface areas and total pore volume and average pore diameter were determined for zeolite sieve cuts using a Quanta chrome Autosorb automated gas sorption system. Data are calculated and reported using Autosorb 1 program for nitrogen at 77K. Also, the chemical composition of raw zeolite (as received) was obtained by x-ray fluorescence (XRF) analysis and is given in Table 2.

Table 2: Chemical Composition of Raw Unsieved Zeolite (Weight Percent)

SiO_2	Al_2O_3	FeO	CaO	MgO	K_2O	Na_2O	TiO_2	Other
34.2	10.57	7.02	11.35	7.28	2.00	1.65	1.23	0.33

Analytical grade chromium chloride was used as source for Cr(III) ions. Stock solutions of 1000 mg Cr(III)/L were prepared by dissolving the exact weight of $CrCl_3.6H_2O$ in distilled-deionized water and used to provide the desired Cr(III) ion concentration by proper dilution. Glassware was cleaned by detergent and double rinsed thoroughly by tap water and distilled-deionized water.

2.2. Procedure and Analysis

2.2.1 Equilibrium Experiments

Adsorption capacity was determined by shake-flask batch experiments. A volume 150 mL of solution containing 50 mg/L was placed in a 250 mL Erlenmeyer flask. The initial pH was adjusted to a specified initial value of 4.0 while the final pH was left uncontrolled to determine how it changes during the process. An accurately-weighed zeolite mass in the range 0.12-1.2 g was added to the solution, thus making slurry concentration in the range 1.0- 8.0 g/L.A series of such flasks was then agitated at a constant speed in a laboratory shaker at room temperature of 22°C until equilibrium is attained, followed by separation of zeolite particles by filtration. A sample of the solid-free solution was analyzed for Cr(III) remaining concentration using UNICAM atomic absorption spectroscopy. Meanwhile, the final pH of the solution was measured using a calibrated pH meter.

2.2.2 Column Experiments

The apparatus used consists of a bench-mounted glass column, 1.5cm inside diameter and 90cm height. The column is gently packed with different masses of zeolite which provide different bed depths. The feed solution is pumped from a glass storage tank to an overhead constant-level tank made of plexi-glass and fed to the column through a glass flow meter. Flow control is achieved by valves fitted at the top and at the bottom of column. Samples from effluent solution

are withdrawn at predetermined time intervals and analyzed for metal ion concentrations using by atomic absorption spectroscopy. Experimental column variables and their tested ranges are given in Table 3.

Table 3: Breakpoint time in zeolite beds at various experimental conditions

Expt. #	Solution velocity, u (cm/min)	Bed Depth, H (cm)	Initial Cr(III) Concentration, Co (mg/L)	Particle Size Cut (μm)	5 % Breakpoint time, tB(min)
1	12.45	14.4	50	355-500	15
2	8.49	14.4	50	355-500	150
3	5.66	14.4	50	355-500	150
4	5.66	9.6	50	355-500	75
5	5.66	4.8	50	355-500	30
6	8.49	14.4	75	355-500	60
7	8.49	14.4	100	355-500	30
6	8.49	14.4	50	500-710	50
7	8.49	14.4	50	710-850	30

3. Results and Discussion

3.1. Adsorption Isotherms

The adsorptive capacity of a solid is concluded from equilibrium sets of data that need to be fitted to mathematical models to facilitate design of adsorption systems and broaden their application. Data on equilibrium uptake were fitted to the popular models of adsorption isotherms, namely; Langmuir, Freundlich and Redlich-Peterson equations which are favored by most researchers because of interpretable parameters and simple expression. These models have the following non-linear forms, respectively (Redlich and Peterson, 1959):

$$q_e = Q_L.b.C_e / (1 + b.C_e) \quad (1)$$

$$q_e = K_F.\ C_e^{1/n} \quad (2)$$

$$q_e = A_R.C_e / (1 + B_R.C_e)^g \quad (3)$$

The parameters of each isotherm model are obtained from the slope and intercept of the linearized form of the respective model. The Redlich-Peterson isotherm combines both Langmuir and Freundlich isotherms thus suggesting a hybrid mechanism of adsorption rather than the ideal monolayer adsorption. It has three constants, namely, A_R, B_R and g, which characterize the isotherm. In the above equation, constant "g" is the exponent, which lies between 0 and 1. Experimental data taken at an equilibrium time of 120 hours and the model predictions of q_e are compared in Figure 3, where Redlich-Peterson model showed the best fit. Fig. 4 confirms this by linear plot of C_e/q_e versus C_e^g with a correlation coefficient of 0.99.

The parameters of the three adsorption isotherms were obtained from linear regression analysis of equations 1, 2 and 3 and their values are given in Table 4 along with the correlation coefficients and standard deviations of error. These values were then inserted in the original isotherm models to predict the equilibrium uptake which yielded the following equations:

$$q_e = 19.6\ C_e / (1 + 0.13C_e) \quad (4)$$

$$q_e = 5.41\ C_e^{3.65} \quad (5)$$

$$q_e = 6.31\ C_e / (1 + 0.93\ C_e)^{0.75} \quad (6)$$

Table 4: Results of regression analysis for data fitting to adsorption isotherms

Langmuir	Fruendlich	Redlich-Peterson
Q_L = 19.6 b = 0.13 R^2 = 0.96	K_F = 5.41 n = 0.274 R^2 = 0.90	A_R = 6.31 B_R = 0.93 g = 0.75 R^2 = 0.99

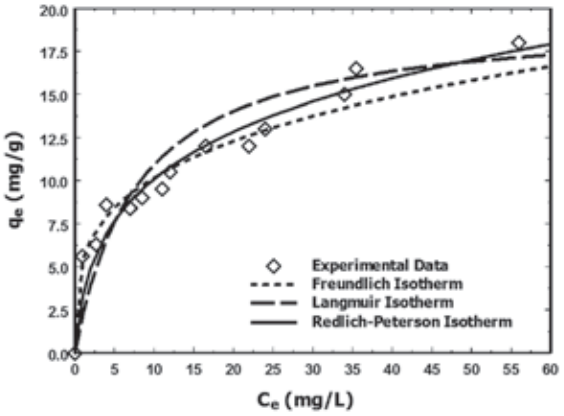

Figure 3: Equilibrium uptake modeled by different adsorption isotherms

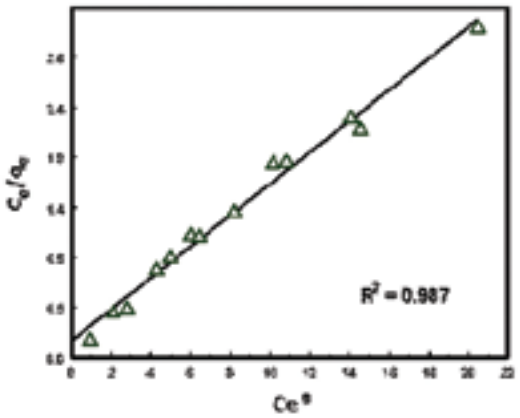

Figure 4: Linearized Redlich-Peterson model for Cr(III) adsorption by natural zeolite tuff

Figs. 3 and 4 clearly show that Redlich-Peterson model represents the experimental data quite well compared to the two other models. This is an indication that Cr(III) uptake mechanism is not purely monolayer coverage typically represented by Langmuir isotherm which is associated with chemisorption but rather a combination of both ion exchange and physical adsorption. Although the Redlich-Peterson model represented the experimental data better than Langmuir isotherm, the latter remains a tool to estimate the maximum adsorption capacity.

3.2. Final pH

In Fig. 5, the final pH attained in solution at equilibrium is plotted as a function of zeolite dose. The initial pH was adjusted at a fixed value of 4.0 and left to change with process

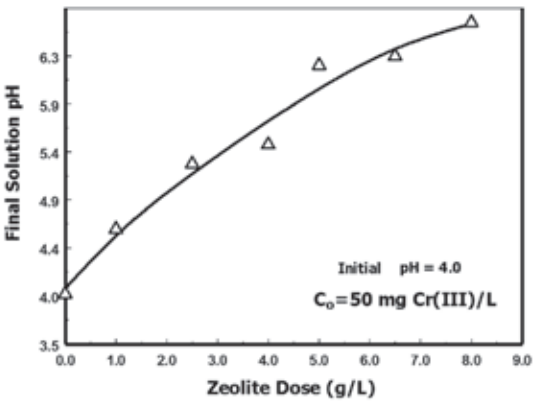

Figure 5: Equilibrium pH as a function of zeolite dose

variables. The increase of pH is mainly attributed to the release of alkaline metal ions from zeolite surface. In addition to naturally existing alkaline metals in zeolite, the major alkaline ion released during adsorption is sodium (Na^+) added in the zeolite pretreatment step. Uptake of cations, e.g. Cr^{3+} and H_3O^+ (hydronium) ions by zeolite would reduce solution acidity. Moreover, dissolution of alkaline impurities in zeolite tuff, mainly $CaCO_3$ (appeared as a significant constituent in the XRD analysis) is also responsible for part of the pH rising.

3.3. Breakthrough Curves

The effects of solution flow-rate, bed depth, initial concentration of Cr(III) ions in the feed, zeolite particle size and initial pH on the sorption behavior of Cr(III) ions are presented and discussed. The 5% break point time is taken as an indicator of zeolite bed efficiency and defined as the time required to reach the break point where C/C° = 0.05. It is well known, from the mass transfer theory of breakthrough curves (Reynolds and Richards, 1996), that the higher the breakpoint time, the higher is the adsorbate removal and the more efficient is the bed. Breakpoint time (t_B) values obtained from various breakthrough curves describing Cr(III) uptake by zeolite bed are given in Table 3 along with the respective column parameters.

3.3.1 Effect of Bed Depth

In Fig. 6, the bed depth was varied, keeping all other parameters constant as in given in Table 3. Obviously, the highest value of t_B (150 min) was obtained using the highest bed depth (14.4 cm). Decreasing the bed depth while keeping the solution velocity constant at 5.66 cm/min resulted in significantly shorter breakpoint times (75 minutes at 9.6 cm and only 30 minutes at 4.8cm). For the latter case, the C/C° versus time plot does not give the typical S-curve. It is concluded that at the conditions tested, a bed depth less than 9.6 cm (zeolite mass less than 20 g) will not give a satisfactory sorption performance.

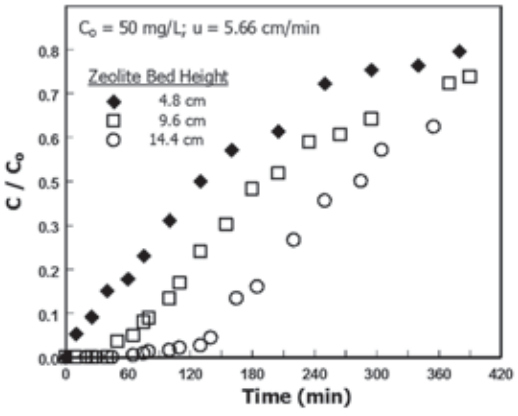

Figure 6: Breakthrough curves at variable bed depth

3.3.2 Effect of Solution velocity

Breakthrough curves, obtained using three solution velocities keeping other parameters constant (zeolite mass = 30 g equivalent to 14.4 cm of bed depth), are shown in Fig. 7. At 5% break point, t_B value of 150 minutes was obtained at flow rates of 5.66 and 8.49 cm/min, indicating a relatively efficient bed. However, the bed performance is unsatisfactory at higher solution velocities where the breakpoint time is very short (15 minutes) at 12.45cm/min. The effect of solution velocity on bed adsorption capacity is due to the difference in residence time of solution in contact with zeolite particles.

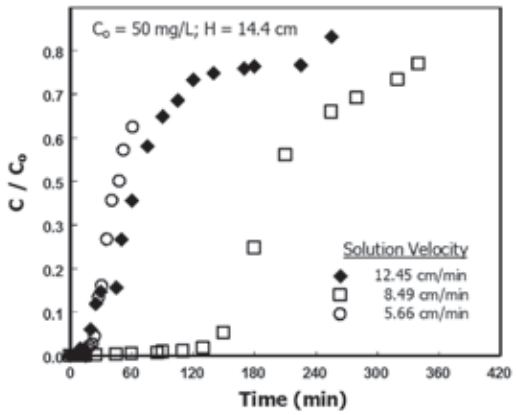

Figure 7: Breakthrough curves at variable solution velocity

3.3.3 Effect of Initial Cr(III) ion Concentration

Fig. 8 shows the effect of Cr(III) ion concentration in feed solution, C°, on breakpoint time is shown in maintaining a constant flow rate at 8.49 cm/min and bed depth at 14.4 cm. The slopes of breakthrough curves decreased as C° decreased, indicating better sorption behavior at the lowest C° of 50 mg/L, where the 5% breakpoint time reached 150 minutes compared to 60 and 30 minutes at the higher C° values of 75 and 100 mg/L, respectively.

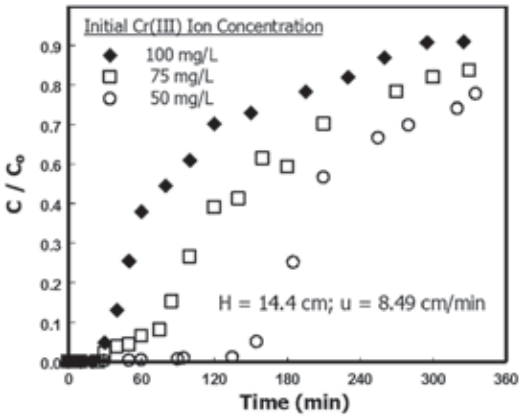

Figure 8: Breakthrough curves at variable initial Cr(III) concentration

3.3.4 Effect of Zeolite Particle Size

Fig. 9 shows that as the particle size of the zeolite bed increased, the 5% breakpoint time decreased. Values of t_B of 150, 50 and 30 minutes were obtained by when 355-500, 500-710 and 710-850 µm sieve cuts were used. Therefore, lower zeolite size fractions are preferred since they produce

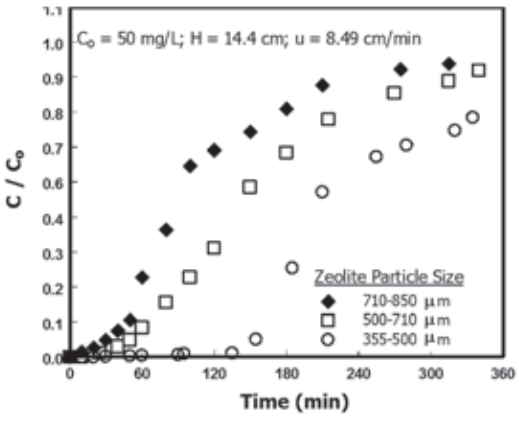

Figure 9: Breakthrough curves at variable zeolite particle size

higher surface area available for adsorption. In addition, the ion exchange capacity may change with particle size due to the variation of zeolite grade in the tuff mineral (Al-Haj Ali and El-Bishtawi, 1997; Ibrahim and Jbara, 2009). In practical applications, very small particles should not be used as they may cause pressure drop across the bed to rise, slow the process and increase energy consumption. If t_B is assumed to be a valid criteria for comparison, it can be concluded that particle size must be carefully selected to optimize Cr(III) removal capacity of zeolite beds with their operability.

3.3.5 Changes in pH

The changes of pH during chromium ion uptake in a typical breakthrough experiment are shown in Fig. 10. Starting with feed solutions initially adjusted to pH 4.0, the pH during sorption has risen sharply in the first 10 minutes to 6.9 then declined slowly and leveled off at 5.6. It is clear that the final pH is always higher than that of the particle-free solution.

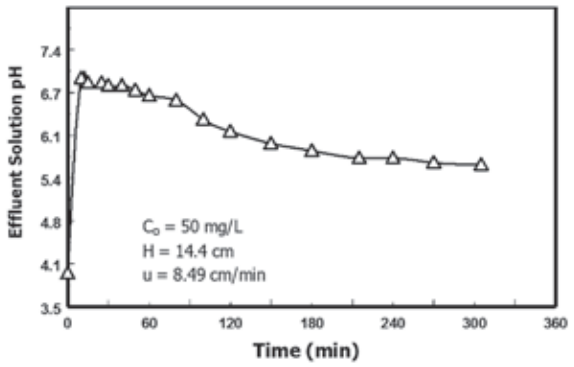

Figure 10: Change in effluent pH with time in fixed-bed

To explain this observation, several processes that occur during metal-zeolite contact and affecting the pH of the solutionwill be considered below:

a- Hydrolysis of zeolite: this occurs at low pH since the zeolite structure may be adversely affected by acids (Ibrahim, 2001).

b- Hydrolysis of metal ions: this results in lowering the pH (increased acidity).

c- Release of exchangeable alkaline metal ions from active site at the zeolite surface: the addition of Na^+ and possibly some K^+, Ca^{2+} or Mg^{2+} to the solution will drive the pH up (more alkalinity). Sodium ions are dominant because they have been added to the mineral in the preparation step to activate its sites for ion exchange.

d- Uptake of metal ions by zeolite: removal of cationic Cr(III) species will raise the pH (reduce acidity).

e- Uptake of protons or hydronium ions: removal of H^+ (or H_3O^+) will decrease solution acidity.

f- Dissolution of solid carbonate and hydroxide impurities in the zeolite tuff: these impurities will also contribute to the rise of pH.

The net pH value, measured at a given time, is the resultant of the effects of two or more processes working in opposite direction. Since the final pH is always higher than the initial pH (of solid-free solution), it seems that processes (c), (d) and (f) are more influential thus pushing the pH scale up to the alkaline side.The sharp rise in pH during the initial sorption stage is understood noting that the release of Na^+ ions into solution is an easy process due to their accessibility on the external surface of zeolite. Moreover, the rates of mass transfer are always high in the first few minutes due to the higher driving force of concentration difference at the solid-liquid interface. At later stages, the driving forces decrease and the pH level is stabilized.

3.4. Cr(III) Uptake Mechanism

The mechanism of Cr(III) uptake by zeolite tuff can be explored in the light of the chemistry of Cr(III) aquo-species which is strongly dependent on pH. Like many metal ions, the chromium cation Cr^{3+}, which is obtained from the ionization of hydrous chromium chloride salt in water, undergoes hydrolysis by reactions with water molecules to give different hydrated ions at different pH levels. The following equations represent the hydrolysis reactions (Rai, *et al*., 1987; Leyva-Ramos *et al*., 2004); the pK value for each is provided below (K is the ionic equilibrium constant):

$$Cr^{3+} + H_2O \leftrightarrow Cr(OH)^{2+} + H^+ \ (7)\ pK_1 = 3.83 \quad (7)$$

$$Cr^{3+} + 2\ H_2O \leftrightarrow Cr(OH)_2^{+} + 2\ H^+ \ (8)\ pK_2 = 10.06 \quad (8)$$

$$Cr^{3+} + 3H_2O \leftrightarrow Cr(OH)_3^{0} + 3H^+ \ (9)\ pK_3 = 18.70 \quad (9)$$

$$Cr^{3+} + 4H_2O \leftrightarrow Cr_3(OH)_4^{5+} + 4\ H^+ \ (10)\ pK_4 = 8.40 \quad (10)$$

The mechanism of Cr(III) uptake by zeolite tuff can be explored in the light of the chemistry of Cr(III) aquo-species which is strongly dependent on pH. Like many metal ions, the chromium cation Cr^{3+}, which is obtained from the ionization of hydrous chromium chloride salt in water, undergoes hydrolysis by reactions with water molecules to give different hydrated ions at different pH levels. The following equations represent the hydrolysis reactions (Rai, 1987; Leyva-Ramos *et al*., 1995); the pK value for each is provided below (K is the ionic equilibrium constant):

Fig. 11 is the speciation diagram of Cr(III) in dilute aqueous solutions(Leyva-Ramos *et al*., 1995; Bradl, 2004). This is a plot of percent molar concentration of each aquo-species versus pH indicating which species is dominant at a given pH. Fig. 10 indicates that the pH range investigated in this work was from 4.0 to 7.0 and thus two regions in Fig. 11 are of particular interest:

i) Region of pH 4.0 to 6.0: The chromium species $Cr(OH)_2^+$produced by the first hydrolysis reaction represented by equation 8 is dominant (50% at pH 4.0 rising to 70% at pH 4.5-5.0 then decreasing to 40% at pH 6.0). The co-existing Cr^{3+}cation has strong tendency to form stable complexes with H_2O molecules and ligands (particularly Cl^-, the counter ion of Cr^{3+} in chromium chloride) such as $[Cr(H_2O)_6]^{3+}$ which may further undergo hydrolytic polymerization to give more complicated complex ions with larger size and charge (Richens, 1997). Therefore, it is suggested that $Cr(OH)^{2+}$ is the ion mainly removed in this pH range by ion exchange as can be represented by the following chemical equation:

$$Cr(OH)^{2+}_{(aq)} + 2\ Na^+\ (Z) \rightarrow Cr(OH)^{2+}\ (Z) + 2\ Na^+_{(aq)} \ (11)$$

This does not, however, exclude the possibility of exchanging, to a lesser extent, other cationic species existing in this region for zeolite sodium ions.The average pore diameter of the investigated size cuts of zeolite is 1.75 Å (Table 1) indicating a microporous structure. According to Nightingale (1959) and Pauling (1970), the hydrated ionic radius of Cr(III) is estimated to be 9.0 Å which is five times as large. Therefore, it can be concluded that these ions are attached to the external surface of zeolite particle and would not be able to penetrate inside the porous structure. This stage of metal uptake is very fast since the final pH exceeds 6.0 in less than 10 minutes as shown in Fig. 11.

ii) Region of pH > 6.0: The published data in many sources supports the event of chemical precipitation of trivalent

chromium as hydroxide at moderately acidic conditions. According to Leyva-Ramos *et al.* (2004), Cr(III) precipitates as $Cr(OH)_3$ at pH 6.4 from solutions having up to 20 mg/L. According to Lurie (1975), precipitation of $Cr(OH)_3$ starts at 4.9 from high concentration of Cr(III) of 0.01 M (equivalent to 520 mg/L). At the intermediate concentrations tested in this study's experiments (50-100 mg/L as C_o), chemical precipitation is likely to start around pH 6.0 which is an intermediate value of acidity.

The above discussion reveals that two main mechanisms of uptake are plausible: (a) ion exchange of cations species especially $Cr(OH)^{2+}$ in the initial stage before reaching pH 6.0; and (b) adsorption on external particle surface of fine $Cr(OH)_3$ particles formed by chemical precipitation at pH > 6.0. The total monolayer coverage deduced from Langmuir isotherm fitting would should include all Cr(III) species removed by both mechanisms.

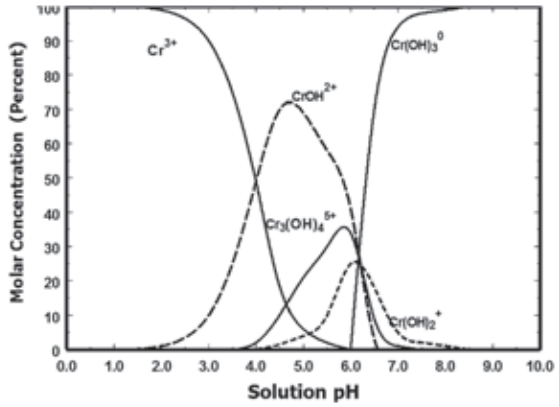

Figure 11: Speciation of chromium in aqueous solutions at 25°C

4. Conclusions

Based on data analysis and discussion of the experimental results of this study on Cr(III) removal by Jordanian NaCl-activated natural zeolite, it can be concluded that trivalent chromium is possibly removed from aqueous solutions up to 99% using phillipsite-rich zeolitetuff which appears to be a cost-effective adsorbent.The zeolite dose and initial Cr(III) ion concentration are key factors influencing equilibrium uptake.Equilibrium pH increased linearly with zeolite dose at a given initial Cr(III) concentration.Breakthrough curves demonstrated the applicability of the tested zeolite mineral in continuous fixed-bed column operation and breakpoint times up to 2.5 hours were obtained at 5% breakpoint.

Nomenclature

A_R: Redlich-Peterson parameter (mg/L)

B_R: Redlich-Peterson parameter (L/mg)

b: Langmuir isotherm parameter related to adsorption energy (L/mg)

C_o: Initial Cr ions concentration (mg/L)

C_e: Equilibrium Cr ions concentration (mg/L)

g: Exponent of Redlich-Peterson isotherm

H: Height of fixed-bed of zeolite, cm

K_F: Freundlich isotherm parameter related to adsorption capacity (L/mg)

n: Freundlich isotherm parameter related to adsorption intensity (dimensionless)

q_e: Equilibrium adsorption capacity (mg Cr(III)/g zeolite)

Q_L: Langmuir isotherm parameter related to adsorption capacity (mg/g)

R^2: Correlation coefficient obtained from linear regression

u: Solution velocity (flow rate divided by column cross-sectional area) (cm/min)

Z: Symbol representing active sites on the zeolite surface.

References

[1] Adriano, B.C., 2001. Trace Elements in Terrestrial Environments: Biogeochemistry, Bioavailability and Risks of Metals. Springer-Verlag, Berlin.

[2] Al-Haj-Ali, A. and Al-Hunaidi, T., 2004. Breakthrough Curves and Column Design Parameters for Sorption of Lead Ions by Natural Zeolite, Environmental Technology, 25:1009- 1019.

[3] Al-Haj-Ali, A. and El-Bishtawi, R., 1997. Removal of Lead and Nickel Ions Using ZeoliteTuff, Journal of Chemical Technology and Biotechnology, 69: 27- 34.

[4] Alvarez-Ayuso, E., Garcia-Sanchez, A. and Querol, X., 2003. Purification of Metal Electroplating Wastewaters Using Zeolites, Water Research, 37: 4855- 4862.

[5] Baker, H.M.,Massadeh, A.M. and Younes, H. A., 2009. Natural Jordanian Zeolite: Removal of Heavy Metal Ions from Water Samples Using Column and Batch Methods, Environmental Monitoring and Assessment, 157(1-4):319-30.

[6] Bradl, H. B., 2004. Adsorption of Heavy Metal Ions on Soils and Soils Constituents. Journal of Colloidal and Environmental Geology, 277:1-18.

[7] Ibrahim, K. and Jbara, H., 2009. Removal of paraquat from synthetic wastewater usingphillipsite–faujasite tuff from Jordan, Journal of Hazardous Materials, 163, 82-86.

[8] Ibrahim, K., 2001. Evaluation of Jordanian faujasite tuff by comparison with other natural and synthetic zeolite, Environmental Geology, 40 (4-5): 440-445

[9] Ibrahim, K., Nasser Ed-Deen, T. and Khoury, H., 2002. Use of Natural Chabazite- PhillipsiteTuff in Wastewater Treatment from Electroplating Factories in Jordan, Environ Geology, 41: 547- 551.

[10] Karatas, M., 2012. Removal of Pb(II) from Water by Natural ZeoliticTuff: Kinetics and Thermodynamics, Journal of Hazardous Materials, 199–200: 383–389.

[11] Kirk-Othmer. 2007. Kirk-Othmer Encyclopedia of Chemical Technology, 5th Ed, John Wiley, New York.

[12] Leyva-Ramos, R.; Fuentes-Rubio, L; Maria Guerrero-Coronado, R. and Mendoza-Barron, J., 2004. Adsorption of Trivalent Chromium from Aqueous Solutions onto Activated Carbon, Journal of Chemical Technology andBiotechnology, 62:64-67.

[13] Luri, J., 1975. Handbook of Analytical Chemistry. Mir Publishers, Moscow.

[14] Malamisa, S and Katsou, E., 2013. A Review on Zinc and Nickel Adsorption on Natural and Modified Zeolite, Bentonite and Vermiculite: Examination of Process Parameters, Kinetics and Isotherms, Journal of Hazardous Materials, 252–253: 428–461

[15] Natural Resources Authority of Jordan, 2006. Mineral Status and Future Opportunity: Zeolitic Tuff, prepared by Nawasreh, M. K.; Yasin, S.M. and Zurquiah, N.A., pp. 21, available athttp://www.nra.gov.jo,Accessed April, 9th, 2014.

[16] Nightingale, E. R., 1959. Phenomenological Theory of Ion Solvation: Effective Radii of Hydrated Ions, the Journal of Physical Chemistry, 63(9)1381- 1387.

[17] Obiri-Nyarko, F., Grajales-Mesa, F. G., Malina, G., 2014. An Overview of Permeable Reactive Barriers for In-situ Sustainable Groundwater Remediation, Chemosphere, 111: 243–259

[18] Pauling, P., 1970. General Chemistry. W H Freeman, New York.

[19] Rai, D., Sass, B. M. and Moore, D. A., 1987. Chromium (III) Hydrolysis Constants and Solubility of Chromium (III) Hydroxide, Inorganic Chemistry, 26: 345- 349.

[20] Redlich, O. and Peterson, D. L., 1959. A Useful Adsorption Isotherm, Journal of Physical Chemistry, 63: 1024-1024.

[21] Reynolds, T., Richards, P., 1996. Unit Operation and Process in Environmental Engineering, 3rd Ed., PWS, Boston, USA.

[22] Richens, D.T., 1997. The Chemistry of Aqua Ions. John Wiley, Chichester, UK.

[23] Stumm, W. and Morgan, J.J., 1996. Aquatic Chemistry: Chemical Equilibria and Rates in Natural Waters. 3rd Ed., John Wiley, New York.

[24] Taamneh, Y. and Al Dwairi, R., 2013.The Efficiency of Jordanian Natural Zeolite for Heavy Metals Removal, Applied Water Science, 3:77–84.

[25] Wang, S. and Peng, Y., 2010. Natural Zeolites as Effective Adsorbents in Water and Wastewater Treatment, Chemical Engineering Journal, 156 (1): 11-24.

[26] WHO, 2011. Guidelines for Drinking Water Quality.4thEd. World Health Organization, Geneva.

JJEES
Jordan Journal of Earth and Environmental Sciences

Volume 6, Number 2, December, 2014
ISSN 1995-6681
Pages 53- 59

Evaluation of Beach Volume Along the Tsunami Affected Coast, Southern East Coast of India

Sakthivel Saravanan* and Nainar Pandiyan Chandrasekar

Centre for GeoTechnology, Manonmaniam Sundaranar University, Tirunelveli – 627 012, Tamilnadu, INDIA

Received 7 August, 2014; Accepted 27 October, 2014

Abstract

To comprehend the impact of 26 December 2004 tsunami on beach environment, an assessment of the beach sediment volume in respective zones of the beach profile has been done by comparing the pre-event and post-event beach profile data. In spite of the considerable accretion in some of the beaches, rest of the beaches had suffered erosion. The coastal configuration, bathymetry, component of the beach, etc. had played a key role in determining the extent of change in the beach sediment volume. Erosion had occurred mostly in dune and berm while littoral zone favoured accretion of sediments eroded from the dune, berm and also the 'fresh' sediments brought in by the tsunami surge from the continental shelf. River inlets and other water passages had greatly influenced the degree of erosion by facilitating the seismic waves to inundate much of the coastal zone. The degree of erosion ranges between 1.84 m^3 and 0.34 m^3 with a maximum at Manappad and with a maximum at Periyathalai, the accretion amount varies from 1.36 m^3 to 0.06 m^3. Apart from Manappad, Kulasekaranpattinam, Alanthalai and Kayalpattinam, Tuticorin-2 was the heavily eroded beach whereas the beaches like Periyathalai, Tiruchendur and Veerapandianpatinam had the benefit of accretion. Erosion and accretion had played one and the same in the beach of Tuticorin-1.

Keywords: India, Tsunami, Beach, Accretion and Erosion Estimation, GIS.

1. Introduction

Tsunami is one of the coastal hazards that generates in the deep ocean due to an earthquake, volcanic activity, submarine landslide etc. and would then propagate to its maximum coverage across the ocean and will transform into a gigantic wave to bring disaster on the coastal regions. It is a frequent phenomenon in the Pacific and Atlantic coast but absolutely a rare phenomenon in the Indian Ocean. 26 December 2004 – a dark day in the earth's history because of the occurrence of tsunami – generating earthquake measuring more than 9 on the Richter Scale focused along the Sumatra Island near Indonesia resulting after the collision of Indian Plate with the Burma Micro Plate (Park *et al.*, 2005) which claimed not only thousands of lives, properties but also altered the shoreline, coastal geomorphology, beach configuration, etc. along the coastal regions of Southeast Asia including India, Sri Lanka, Indonesia, Malaysia, Thailand and part of Africa (Raval, 2005).

Koji Minoura *et al.* (1994) studied the tsunami deposits of lacustrine sequence of the Sanriku coast, northeast Japan and attempted to draw out the probable source of it. Minoura *et al.* (2001) studied the 869 Jogan tsunami deposit on the Pacific coast of northeast Japan and inferred the inundation extent of that tsunami surge. Gelfenbaum *et al.* (2001) studied about the sedimentary deposits of 17th July 1998 Papua New Guinea Tsunami and estimated the impact of that tsunami based on the sedimentation it induced. Fuminori Kato *et al.* (2001) brought out the grain-size effects on scour around a cylinder due to tsunami run-up. Jaffe and Gelfenbaum (2002) insisted on using tsunami deposits to create a geologic record of that particular tsunami and also obtaining a geologic record of past tsunamis using the tsunami deposits thereby, assessing the future risks. Barbara Keating *et al.* (2004) investigated the tsunami deposits at Queens beach, Oahu, Hawaii and deciphered the nature of it. Ramasamy (2005) reported the scenario of Indian coast after the 26 December 2004 with certain issues and strategies. Kumanan (2005) presented the global scenario of tsunamis mentioning the frequency of tsunamis in the Pacific and Atlantic coast and the rarity of tsunamis along the Indian coast. Radhakrishna (2005) reported the destructions rendered by the 26 Dec 2004 tsunami along the coast of India. Narayana *et al.* (2005) deciphered that the tsunami surge had carried huge amount of sediments from the continental shelf and deposited them in the beaches along the Kerala coast of India. Mruthyunjaya Reddy (2005) reported about the accretion and erosion due to tsunami in the beaches along the coast of Andhra Pradesh, India. Chandrasekar *et al.* (2006) classified the beaches of South India based on the inundation extent with respect to the coastal geomorphic features. Saravanan and Chandrasekar (2010) studied the potential littoral sediment transport along the coast of South Eastern Coast of India.

Though several works have been done on the 26 Dec 2004 tsunami, the research is still in the emerging stage since it is rare coastal hazard as far as the Indian Coast is concerned. Mujabar *et al.* (2007) and Saravanan et al. (2009) studied the impact of 26 December 2004 tsunami in beach morphology and post tsunami assessment along the Coast between Ovari and Kanyakumari. Almost all the works done by the previous world-wide researchers were based on the post-tsunami survey. Previous works of evaluating the impact

* Corresponding author. e-mail: geosaravanan2000@yahoo.co.in

of the tsunami surge on the beach volume by comparing the beach profile data prior to and subsequent to the tsunami event has been found to be nil since acquiring of the beach profile data before any tsunami event is not possible. But we obtained the pre-event data since we have been monitoring the beach morphology along the study area for quite a long period as a component of one of our research project and as a result we obtained, coincidentally, the beach profile along the study area prior to the tsunami event and subsequently we profiled those same beaches after the event. Accordingly, the impact of the tsunami in the beach pattern and in turn, on the sediment volume has been evaluated. Despite the fact that the majority of the consequences of that disaster could not be totally evaluated, a trustworthy inference could be done about the impact of tsunami on beach sediment volume by the application of advanced scientific techniques, GIS (Geographic Information System), in particular. In this paper, we would like to draw out a panoramic scrutiny of sediment dynamics induced by the tsunami event in no time.

2. Study Area

The study area (Fig. 1) encompasses of eight beaches and therein eleven profile stations along the southern east coast of India (between N 77^0 98' E 08^0 34' and N 78^0 16' E 08^0 79'). The majority of the beaches are depositional in nature with low to medium wave energy condition (Angusamy and Rajamanickam, 2000). Most of the beaches contain vegetated sand dunes with prolonged berm and gentle beach slope. There are two headlands along the study area one at Manappad and another at Tiruchendur. Observably, there are four bays between Periyathalai – Manappad; Manappad – Tiruchendur; Tiruchendur – Kayalpattinam and between Kayalpattinam – Tuticorin. Manappad is the only rocky coast along the study area situated at an elevated level from the mean sea level (~ 25 m) due to tectonic uplift with an emergent beach (Loveson *et al.*, 1996). Besides erosional features, Manappad coast displays also typical depositional features like sandspit, lagoon, baymouth bar etc. There is a notable Tombolo in Tuticorin which connects the Hare Island with the mainland on which the Port of Tuticorin has been constructed. The study area encompasses two river inlets one of the River Karamanayar and other of the River Tambraparani. These coastal geomorphologic features had played a key role in the accretion and erosion of coastal landforms along the study area. Even though, the study area falls on the 'shadow zone' (Fig. 2) due to the presence of Sri Lanka and had experienced mostly the refracted waves, the tsunami waves had altered the beach configuration, coastal landform, etc.

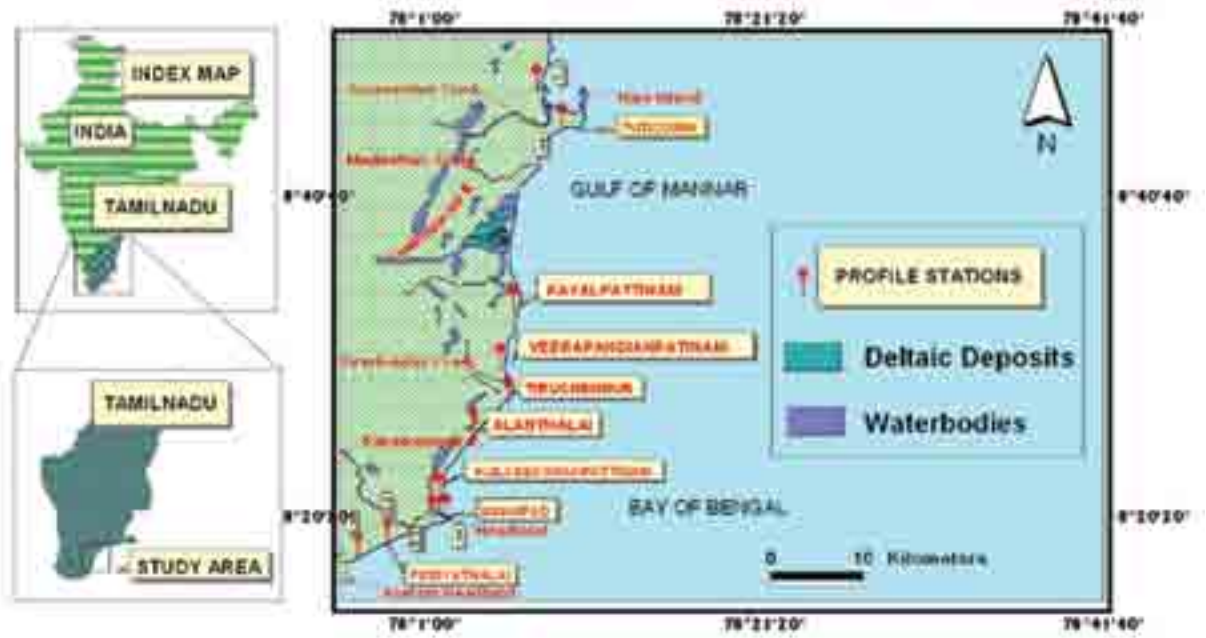

Figure 1: Location map of the study area

3. Methodology

Beach profile survey has been carried out along the study area prior to and subsequent to the tsunami event using levelling and measuring tools following Stack and Horizon method speculated by Lafond and Prasada Rao (1954) which was later simplified by Emery (1961). Transect between each profiling site ranges from many metres to few kilometres but care has been taken to profile the beaches along the study area with possible regular interval. Profiling in each beach starts from a fixed reference point usually near the coastline or beyond the interdune and covers the backshore, littoral zone and continues up to lowtide zone or near the inner breaker zone with a regular interval of 5 m. The levelling above mean sea level (MSL) and below sea level data are adjusted to MSL datum using fixed benchmark of known elevation, located behind the beach during the lowest-low water level period so that maximum length of the beach section was exposed.

The volume of sediments at each zone of the beach before and after the tsunami event has been calculated by means of the documented beach profile data using standard statistical package. The alteration induced by the tsunami surge in the beach volume was then interpreted using GIS software package – Arc View (3.2a) and other statistical packages. Chart map has been generated using GIS for each respective zone of the beach profile by inputting the sediment volume data. Every beach was divided into different zones namely the dune (if present), berm (backshore), hightide zone, midtidezone and lowtide zone. The hightide zone is the part of the beach immediately from the beach face to the margin of the midtide zone. The midtide zone is the intermediate zone between hightide zone and lowtide zone. The lowtide zone is the area from the swash zone to the inner breaker zone. Separate chart map has been prepared for each zone

and finally the impact of the tsunami surge in sediment volume of all the zones were incorporated which resulted in the map showing the overall evaluation of the beach volume along the study area.

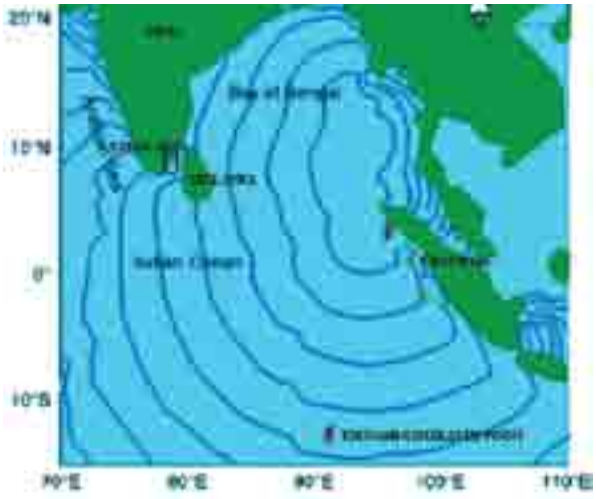

Figure 2: Map showing the nature and angle of the tsunami approached the study area.

4. Results and Discussion

4.1. Evaluation of Dune

Impact of the tsunami event in the coastal dunes along the study area is shown in Fig. 3 and given in Table 1. It reveals that almost all the beaches have suffered erosion in dune especially in Periyathalai and Kulasekaranpattinam ranging between 0.68 m^3 and 0.16 m^3, as it is the only reliable feature along the beach to resist the overwhelming seawater and thereby limiting the extent of inundation. Moreover, the vegetations on the dunes were also not left unaffected. The dunes of Kayalpattinam have experienced accretion of 0.06 m^3 sediments which may be due to the refracted waves from the Tiruchendur promontory (Chandrasekar, 2005). Kulasekaranpattinam was the foremost loser of dunes of 0.68 m^3 which may due to the convergence of the waves at the Manappad headland as it falls awfully next to it. Accordingly, Periyathalai-1 has too lost notable magnitude of dunes of 0.59 m^3 due to the similar phenomenon likely to be prevailed at the Kuttam headland, south of Periyathalai (Nobuo Shuto, 2001; Guy Gelfenbaum *et al.*, 2001).

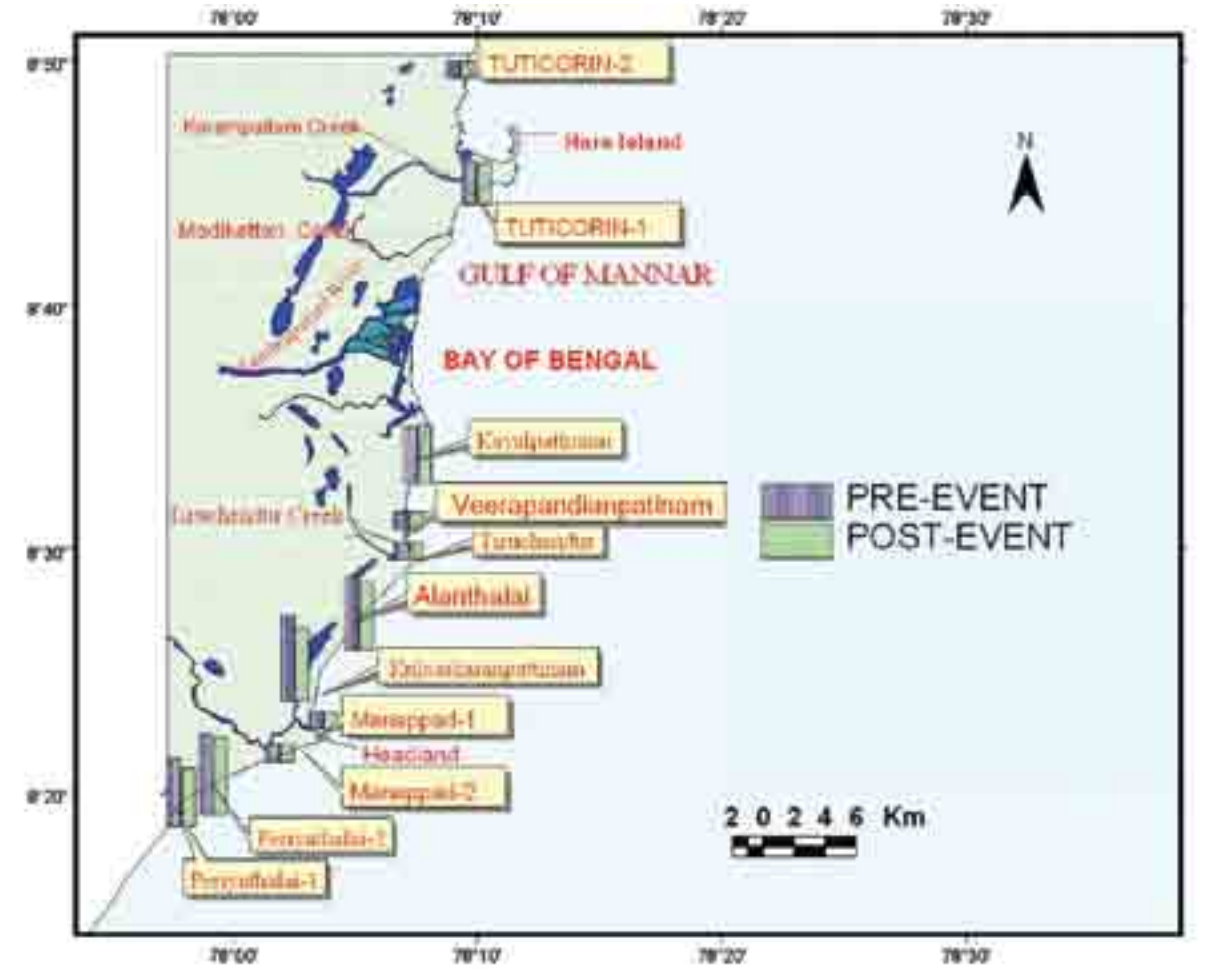

Figure 3: Evaluation of dune along the study area.

4.2. Evaluation of Berm

The assessment done in the berm is shown in Fig. 4 and Table 1. It is well evident that half of the beach has experienced erosion ranging from 0.95 m^3 to 0.04 m^3 with maximum at Tuticorin-2 and with a maximum at Periyathalai-2 accretion resulted in the rest of the beaches with values ranging between 0.15 m^3 and 0.003 m^3. There is not any noteworthy amendment in the beaches like Kayalpattinam and Tuticorin-1. It has been observed that the sediments eroded from the dunes are being deposited at the berm during backwash due to the loss in

the velocity of the receding water due to the sediment load as in the case of Periyathalai-2, Alanthalai (Barbara Keating *et al.*, 2004). The tsunami-borne sediments also might have deposited in the berm along with the sediments eroded from the dunes as it is the area which supported deposition for the retreating seawater (Koji Minoura *et al*., 1994; Narayana *et al*., 2005). But Manappad could not experience accretion due to the coastline shape (Raval, 2005) and the existence of headland. Furthermore, it is and emergent beach elevated well above the mean sea level and hence the retreating seawater during backwash could be the result of erosion.

Table 1: Beach Volume (in Cubic Metres) from the MSL at various parts of the beach.

Location	DUNE		BERM		HIGH TIDE		MID TIDE		LOW TIDE	
	PRE	POST	PRE	POST	PRE	POST	PRE	POST	PRE	POST
PET-1	2.84	2.25	2.10	1.92	0.60	1.35	0.10	0.50	-0.30	0.10
PET-2	3.46	3.29	2.17	2.29	0.90	1.30	0.35	1.00	0.15	0.50
MNP-1*	0.00	0.00	2.43	2.07	0.60	0.35	0.30	-0.50	-0.10	-0.60
MNP-2*	0.00	0.00	4.81	4.58	1.95	1.45	1.32	0.97	0.65	0.35
KUP	3.83	3.15	2.26	2.03	1.30	1.40	0.60	0.50	0.20	0.10
ALT	3.06	2.77	2.32	2.47	0.92	0.80	0.54	0.50	0.17	0.12
TUR*	0.00	0.00	0.69	2.75	1.2	1.5	0.85	1.05	0.60	0.52
VEP*	0.00	0.00	2.13	1.96	1.1	1.5	0.90	1.20	0.60	0.70
KAP	2.16	2.22	1.49	1.49	0.80	0.55	0.35	0.20	0.15	0.10
TUN-1	1.48	1.28	0.95	0.90	0.55	0.60	0.30	0.30	-0.50	-0.25
TUN-2*	0.00	0.00	2.05	1.12	1.00	0.48	0.70	0.35	0.30	0.25

Figure 4: Evaluation of berm along the study area.

4.3. Evaluation of HighTide Zone

Fig. 5 and Table 1 show the evaluation of sediment volume at hightide zone. Periyathalai-1, after successive erosion, has experienced significant amount of accretion in hightide zone followed by Periyathalai-2, Kulasekaranpattinam, Tiruchendur, Veerapandianpattinam and Tuticorin-1. The amount of accretion varies between 0.75 m^3 and 0.05 m^3. The degree of accretion has been determined by the gradient of the beach face and the rapidity of the backwash. As in other zones, Tuticorin-2 had suffered maximum amount of erosion and similar condition had prevailed in the beaches of Manappad, Kayalpattinam and Alanthalai. The quantity of erosion, as in the case of accretion, depends upon the similar aspects as for accretion mentioned above (Chandrasekar, 2005; Glenda Besana *et al*., 2004). The quantity of erosion ranges from 0.52 m^3 to 0.12 m^3.

Figure 5: Evaluation of hightide zone along the study area.

4.4. Evaluation of MidTide Zone

The accretion in the Periyathalai beach, as in high tide zone, continued in the midtide zone as shown in Fig. 6 and Table 1. Accretion, though not considerable, has also occurred in the beaches of Veerapandianpatinam and Tiruchendur. The magnitude of accretion varies between 0.65m^3 and 0.20 m^3. In this zone, the beach of Manappad-1 had undergone erosion higher than the beach of Tuticorin-2 accompanied by the beaches of Kayalpattinam, Kulasekaranpattinam and Alanthalai (Fig. 6). Tsunami has not induced much change in the mid tide zone of Tuticorin-1 beach as the change in the sediment volume seemed to be insignificant. The amount of erosion ranges from 0.80m^3 to 0.04m^3.

Figure 6: Evaluation of midtide zone along the study area.

4.5. Evaluation of Low TideZone

From Fig. 7 and Table 1, it is well evident that erosion had dominated at low tide zone in most of the beaches, excluding the beaches of Periyathalai, Tuticorin-1 and Veerapandianpatinam. The degree of erosion ranges from 0.50 m^3 to 0.05 m^3. Despite the fact that Manappad had endured high quantity of erosion, Tuticorin-2 had not experienced as much of erosion when compared with its other foreshore and backshore zones. A large amount of accretion has resulted in the Periyathalai beach followed by the beaches of Tuticorin-1 and Veerapandianpatinam. Accretion ranges from 0.40 m^3 to 0.25 m^3. Endurable amount of erosion had occurred on the beaches of Kulasekaranpattinam, Tiruchendur, Alanthalai and Kayalpattinam.

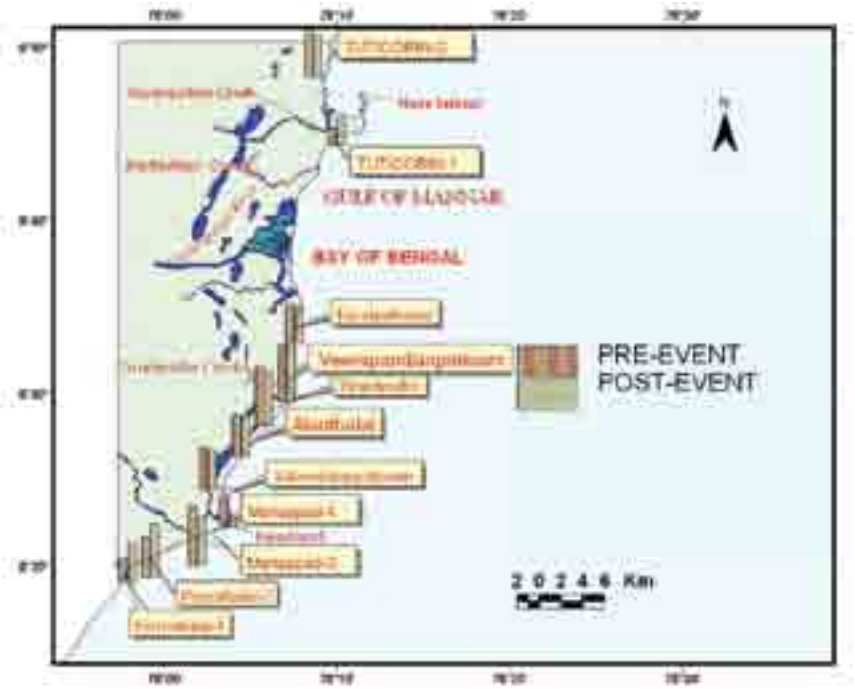

Figure 7: Evaluation of lowtide zone along the study area.

4.6. Overall Evaluation

The overall consequence of the tsunami surge in the beach sediment volume has been depicted in Fig. 8 and the total change in the beach volume has been tabulated in Table 2. It is well noticeable that substantial accretion had occurred in Periyathalai along with Veerapandianpatinam, Tiruchendur and Tuticorin-1. The quantity of accretion varies between 0.78 m^3 to 0.06 m^3 with the maximum at Periyathalai-2 and Tuticorin-1 had experienced the minimal accretion. The degree of erosion ranges between 1.91m^3 and 0.34 m^3. Manappad had endured the utmost erosion followed by Tuticorin-2, Kulasekaranpattinam, Kayalpattinam and Alanthalai, comparatively, with the minimum erosion. On the sum total, Periyathalai experienced the maximum amount of accretion and Tuticorin-1 with the lesser amount of accretion. As far as erosion is concerned, Manappad and Tuticorin-2 has suffered the maximum erosion with negligible erosion at Alanthalai.

Figure 8: Evaluation of lowtide along the study area.

Table 2: Overall Evaluation of the Beach Volume (in Cubic Metres).

LOCATION	EROSION	ACCRETION	OVERALL RESULT
PERIYATHALAI -1	0.77	1.55	+ 0.78
PERIYATHALAI - 2	0.16	1.52	+ 1.36
MANAPAD - 1*	1.91	0.00	- 1.91
MANAPAD – 2*	1.38	0.00	- 1.38
KULASEKARANPATTINAM	0.91	0.10	- 0.81
ALANTHALAI	0.49	0.15	- 0.34
THIRUCHENDUR*	0.07	0.56	+ 0.48
VEERAPANDIANPATINAM*	0.17	0.80	+ 0.63
KAYALPATTINAM	0.45	0.06	- 0.38
TUTICORIN – 1	0.24	0.30	+ 0.06
TUTICORIN – 2*	1.84	0.00	- 1.84

+ Accretion; - Erosion; * Habitually Devoid of Dunes

Since the study area was well protected by the 'barrier island' – Sri Lanka which reduced the intensity of the seismic waves approaching the study area, the beaches could not experience neither high accretion nor high erosion as the tsunami surge lost its potential to carry large amount of sediments from the continental shelf. Likewise, it could not implement heavy erosion since the inundation was not much higher when compared to other coastal regions of India where inundation was much high because they were directly exposed to the seismic waves propagated from the generation point (Raval, 2005). Moreover, the general nearshore bathymetry of the study area is around 50 m. The change in bathymetry from 50 m to around 200 m is observed far beyond the shoreline. Hence, the seismic waves would have felt the shoaling effect far before the shoreline. Hence, the uprushing wall of water would have both the potential of carrying sediments from the near continental shelf to deposit on the beach which is quite not feasible for the customary waves and tides and also to erode and redistribute the sediments in the beach during backwash (Ram Mohan, 2005). The redistribution of sediments on the beach had mainly occurred in the backshore and dunes. The sediments from the dunes have been redistributed in the backshore and the sediments in the littoral zone might have also redistributed at the berm during swash and backwash.

5. Conclusion

The evaluation of the beach volume at the various regions of the beach profile, along the study area, unveils scores of features of the tsunami event. At the outset, sand dune may be described as the *'natural beach fence'* since it has performed the unswerving task in reducing the extent of erosion. Regardless of the fact that dunes could not prevent erosion, it trims down the pace of the invading waves and favours the accretion of the dune-eroded and tsunami-borne sediments in berm and in the littoral zone as well.

Further, the elevation of the beach and the gradient of the beach face are also the deciding features of the beach sediment redistribution. Based upon the above evaluation it has been deducted that the coastal geomorphology, components of the beach, and bathymetry played a key role in the scale of accretion and erosion.

This evaluation could be possible in any other computer package but GIS grant a *bird's eye vision* of the alteration induced by the tsunami event on the beach dimension and the panoramic appraisal of the beach volume is made simple by the application of GIS. Further studies on the grain size analysis

of the sediments would shed light on the precise redistribution of the sediments along the beach and the sediments brought in by the tsunami surge from offshore.

Acknowledgement

The authors wish to thank the National Resource Data Management System (NRDMS) Division of the Department of Science & Technology (DST), Government of India for supplying the necessary equipments and financial assistance to carry out the study.

References

[1] Angusamy, N., and Victor Rajamanickam, G., 2000. Distribution of Heavy Minerals along the beaches from Mandapam to Kanyakumari, Tamilnadu, Journal of the Geological Society of India, 56(8), 199-211.

[2] Barbara Keating, Franziska Whelan and Julie Bailey Brock., 2004. Tsunami Deposits at Queen's Beach, Oahu, Hawaii – Initial Results and Wave Modelling, Science of Tsunami Hazards, 22(1), 23- 43.

[3] Chandrasekar, N. (2005). Tsunami of 26th December 2004: Observation on inundation, sedimentation and geomorphology of Kanyakumari Coast, South India. Proc. 22nd IUGG International Tsunami Symposium, Chania, Greece, pp. 49–56.

[4] Chandrasekar, N., Saravanan, S., Loveson Immanuel, J., Rajamanickam, M. and Rajamanickam, G.V., 2006. Classification of Tsunami Hazard along the Southern Coast of India: An Initiative to Safeguard the Coastal Environment from Similar Debacle. Science of Tsunami Hazards, 24(1), 03-24.

[5] Emery, K.O., 1961. A Simple Method of Measuring Beach Profiles, Limnology and Oceanography, 6(1), 90-93.

[6] Fuminori Kato, Susan Tonkin, Harry Yeh, Shinji sato and Kenichi Torii., 2001. 'The Grain-size Effects on Scour around a Cylinder due to Tsunami Runup, Proceedings of International Tsunami Symposium, pp.905-918.

[7] Gelfenbaum, G., Jaffe, B., Nongkas, M., and Davies, H., 2001. Sedimentary deposits from the July 17, 1998 Papua New Guinea tsunami International Tsunami Symposium, pp.449-452.

[8] Glenda Besana, M., Masataka Ando and Hannah Mirabueno, M., 2004. The May 17, 1992 Event: Tsunami and Coastal Effects in Eastern Mindanao, Philippines, Science of Tsunami Hazards, 22(2), 61-68.

[9] Jaffe, B. and Gelfenbaum, G. 2002. Using tsunami deposits to improve assessment of tsunami risk solutions to Coastal Disasters '02, ASCE, 836-847.

[10] Koji Minoura, Shu Nakaya and Masao Uchida., 1994. Tsunami Deposits in a lacustrine sequence of the Sanriku coast, northeast Japan, Sedimentary Geology, 89(1-2), 25-31.

[11] Kumanan, C.J., 2005. Global Scenario of Tsunamis, In: Ramasamy and Kumanan (eds) Tsunami: The Indian Context, Allied Publishers, India, pp.15-26.

[12] Lafond, E.C. and Prasada Rao, R., 1954. Beach Erosion Cycles near Waltair on the Bay of Bengal, Andhra Univ., India. Memoir in Oceanography, 1, 63-77.

[13] Loveson, V.J., Angusamy, N. and Rajamanickam, G.V., 1996. Usefulness of Identifying Different Geomorphic Blocks along the Coast of Southern Tamilnadu, Indian Journal of Geomorphology, 1(1), 97-110.

[14] Minoura, K., Imamura, F., Sugawara, D., Kono, Y. and Iwashita, T., 2001. The 869 Jogan Tsunami Deposit and Recurrence Interval of Large-scale Tsunami on the Pacific Coast of Northeast Japan, Journal of Natural Disaster Science, 23(2), 83-88.

[15] Mruthyunjaya Reddy, K., Nageswara Rao, A. and Subba Rao, A.V., 2005. Recent Tsunami and its Impact on Coastal Areas of Andhra Pradesh, in Ramasamy and Kumanan (eds), Tsunami: The Indian Context, Allied Publishers, India, pp.129-138.

[16] Mujabar, S., Chandrasekar, N., Saravanan, S. and Immanuel, J., 2007. Impact of 26 December 2004 Tsunami in Beach Morphology and Sediment Volume along the Coast between Ovari and Kanyakumari, South India, Shore and Beach, 75(2), 1-8.

[17] Narayana, A.C., Tatavarti, R. and Mudrika Shakdwipe., 2005. Tsunami of 26th December 2004: Observations on Kerala Coast, Journal of the Geological Society India, 65(2), 239-246.

[18] Nobuo Shuto., 2001. 'Tsunami Induced Topographical Change Recorded in Documents in Japan', presented at the International Tsunami Symposium, pp.513-522.

[19] Park, J., Anderson, K., Aster, R., Butler, R., Lay, T. and Simpson, D., 2005. Global Seismographic Network Records the Great Sumatra-Andaman Earthquake, EOS, Transactions, American Geophysical Union, 86(6), 57-64.

[20] Radhakrishna B. P. 2005. Devastating tsunami strikes coastline of India, Jounrnal of the Geological Society ofIndia, 65 (2), 129-134.

[21] Ram Mohan, V., 2005. December 26, 2004 Tsunami: A Field Assessment in Tamilnadu, in Ramasamy and Kumanan (eds). Tsunami: The Indian Context, Allied Publishers, India, pp.139-153.

[22] Ramasamy, S.M. 2005. Tsunamis in the Indian Context – Certain Issues and Strategies, in Ramasamy and Kumanan (eds), Tsunami: The Indian Context, Allied Publishers, India, pp.01-14.

[23] Raval, U., 2005. Some Factors Responsible for the Devastation in Nagapattinam Region due to Tsunami of 26th December 2004, Journal of the Geological Society of India, 65(5), 647-649.

[24] Saravanan, S, N. Chandrasekar, C.Hentry, M. Rajamanickam, J.Loveson Immanuel and P. Sivasubramanian (2009). Post-Tsunami Assessment along the beaches between Ovari and Kanyakumari, Southern TamilNadu Coast, India, Earthscience Frontiers, 16(6), pp.129-137.

[25] Saravanan, S., and N. Chandrasekar (2010). Potential littoral sediment transport along the coast of South Eastern Coast of India. Earth Science Research Science Journal, 15(1), 24-31.

JJEES

Volume 6, Number 2, December, 2014
ISSN 1995-6681
Pages 61- 66

Jordan Journal of Earth and Environmental Sciences

The Characteristics of Cement Mortars Utilizes the Untreated Phosphogypsum Wastes Generated From Fertilizer Plant, Aqaba- Jordan

Nafeth A. Abdelhadi[1], Monther A. Abdelhadi[2] and Tayel M. El-Hasan[3]*

[1] Department of Civil Engineering, Faculty of Engineering Technology, Al-Balqa Applied University, Amman-Jordan.
[2] Department of Civil Engineering, Faculty of Engineering, Al-Ahliyya Amman University, Jordan.
[3] Department of Chemistry, Faculty of Science, Mu'tah University, 61710, Al-Karak – Jordan.

Received 15 May, 2014; Accepted 20 November, 2014

Abstract

Huge amounts of phosphogypsum (PG) are produced as by-products of phosphoric acid manufacture process in Jordan. Millions of tones of PG wastes are stockpiled over open areas. Major negative environmental impacts are highly expected due to dissolution of various hazardous chemicals the stockpiled contains. This will cause a serious threat to the soil, surface and groundwater bodies. X-Ray Fluorescence revealed that the main oxides were SO_3 and CaO with 39% and 31.9%, respectively. What reflected its mineralogy were gypsum, as main phase, and calcite, quartz and apatite, as minor. Two PG samples were used, first dried to 60°C (PG1) and then heated up to120°C (PG2). Both samples were used in sand-clinker and clinker–sand-pozzolanic tuff mortars to investigate compressive strength, setting time, consistency and other physical properties. The results showed that the addition of 2-4% of PG1 gave an average of 52 N/mm^2 and 46.4 N/mm^2 at 28 days for the two mixing ratios, respectively. Meanwhile, PG2 showed lower compressive strength values. Moreover, lower consistency was achieved with PG1 more than with PG2 samples, due to the fact that PG2 contains more anhydrite. Setting time is higher and shows an increasing trend in PG1, which contradicts PG2 samples. The result approves the possibility for the utilization of raw untreated PG wastes instead of expensive pure gypsum in cement industry, because it showed good setting time, minimizes the W/C ratio, and increases the compressive strength of the mortars. Besides, it will decrease the production cost and convert these wastes into useful industrial material.

Keywords: Phosphogypsum, Clinker, Compressive strength, Setting time, LE-CHATE, Pozzolana

1. Introduction

Natural materials are usually targeted as a replacement of ordinary cement past in order to attain a high compressive strength, longer workability, lower water consumption, better soundness, etc. El-Hasan and Al-Hamaideh (2012) used Tripoli as a partial replacement of OPC, and they reported that increasing the replacement ratio of Tripoli did not affect the setting time or soundness; however, it increased the volume of the required water to produce the past. Smadi *et al.* (1999) studied the behavior of the compressive strength of cement with different replacement ratios of purified PG and calcined temperature up to 900 °C, finding an increasing trend in compressive strength which improved the initial and final setting time. Bhadauria & Thakare (2006) utilized the phosphogypsum wastes in cement additive as past or mortar in concrete. They carried these applications after purifying the phosphogypsum. They found it suitable for concrete in terms of workability and 28 days compressive strength. PG is also known worldwide for its applications as a binder or cement. Therefore, it was also studied by many researchers (e.g. Gutt 1978; Ouyang *et al.* 1978; Ghafoori, 1986; Akın & Yesim, 2004; Degirmenci, 2008; Lysandrou & Pashalidis, 2008; and Yang *et al*., 2009).

According to the European Fertilizer Manufacturing Association (EFMA), there are two phosphoric acid production processes; the first, at temperature 70 -80 °C that yields 26-32% P_2O_5, and gives acid and dehydrated phase ($CaSO_4.2H_2O$); the second, at temperature 90 - 110 °C, which yields 40-52% P_2O_5, and gives acid and Hemihydrate phase ($CaSO_4.1/2H_2O$) (EFMA 2000). The Phosphogypsum is found to be radioactive due to the presence of naturally occurring uranium and radium in the phosphate ore (Dippel, 2004). The PG is known for having some chemical impurities like its source rock (i.e., phosphates). Thus, PG is classified as a hazardous waste and is currently being disposed and stockpiled on sandy soil (Berish, 1990; Azouazi *et al*., 2001; Dueñas *et al*., 2007). The PG is supposed to be treated for these impurities; therefore, PG without treatment is referred to here as raw or impure PG.

There are various storage processes of PG wastes, such as ocean disposal (Wissa, 2001), dry stacking on land, which is the common practice (EPA 1999), and wet stacking on basins (Anon, 1998), as well as the use of PG as mine backfill disposal as suggested by (Dippel, 2004).

At the industrial complex at Aqaba, south of Jordan, a daily average of 900-1310 tons of phosphoric acid are produced (http://www.jpmc.com.jo/?q=node/166). For every ton of phosphoric acid produced, about 5 tons of PG are generated, depending on the quality of the phosphate ore (http://ardaman.com/waste.php3). Therefore, about 5000 tons of (PG) are produced each day. Al-Hwaiti *et al.* (2005) reported that heavy elements concentrations in the PG stacks are stable with age, which indicated that trace elements were not leached from the stacks in any significant amount. Whereas, Abed (2011) suggested that Uranium is concentrated in the phosphoric acid

* Corresponding author. e-mail: tayel.elhasan@gmail.com

then into Di-Ammonium Phosphate (DAP) in the fertilizer industry and not in the phosphogypsum.

The possible use of PG as a major constituent in construction materials is vital in order to solve the serious negative environmental impacts caused by the dispersion of the harmful chemicals contained in PG into surrounding environment. Several studies were carried out on purifying the PG by washing it with water to minimize the impurities content before utilizing it in various industrial aspects (Smadi *et al*., 1999).

To enlighten the environmental concerns of the huge PG stockpiled at the industrial complex at Aqaba, this study aims to examine the possible utilization of these untreated PG wastes replacing the expensive pure gypsum in cement industry, presenting the best scenario and mixing ratios to attain the best cement mortar properties.

Cement – Phosphogypsum mixes

In case of cement phosphogypsum mixes, the materials used were untreated phosphogypsum, clinker, tap water, and pozzolana.

Phosphogypsum

Phosphogypsum, used in this study, was obtained from the industrial complex at Aqaba, south of Jordan. Its chemical composition and mineralogical constituents are illustrated in Table (1) and Fig. (1).

Clinker

The Clinker used here is obtained from Fuhais Cement Factory located at Amman city; its code is (OPC type 1). The Clinker was procured from local market and in one lot to maintain uniformity throughout the investigation.

Pozzolana

Tuff as pozzolanic material was obtained from Tal-Hassan which is located about 120 km northeast of Amman.

Water

Ordinary tap water was used for mixing and curing operation.

2. Analytical procedures and equipments

Ordinary Portland Cement type-1 (OPC), from Lafarge Cement Factory at Al-Fuhais area, was mixed with sand to prepare reference standard mortar following ASTM C109. Two samples of PG were heated separately up to 60°C (PG1) and 120°C (PG2) using automatically controlled electrical oven. Grounded clinker (OPC Type-1) was used to produce different mortars of clinker-sand-phosphogypsum and tested following ASTM C109.

The 5*5*5 cm cubes were cured at laboratory temperature for 2, 7 and 28 days. Compressive strength of samples was tested using Digital Compression Machine (Type: ADR- Auto manufactured by ELE); a computerized compression machine was used to determine the compressive strength of multi size concrete cubes. The initial and final setting time for clinker-phosphogypsum mortar was tested using the Vicat needle according to ASTM C191.

The chemical composition of PG was investigated through X-Ray Fluorescence analysis. It was done using the machine (XRF-Pioneer F4), manufactured by Broker at the labs of Natural Resources Authority (NRA), Amman. The machine comes with an attached 72-position sample changer. Pellets were made by fusing 0.8 g of sample powder and 7.2 g of $L_2B_4O_7$ in Au/Pt crucible using a flexor machine (Leco 2000) for 3 – 4 minutes at 1200 ºC. The melt was poured in a mold and left to cool to form a glass disc; trace elements were analyzed. The machine was calibrated with international standards, particularly the Geological Survey of Japan (GSJ) geochemical standards (i.e., Japanese slate JSl-1 and JSl-2). The analytical error was within 5%.

Moreover, mineral constituents were determined using X-Ray Diffraction analysis. It was executed using the machine (XRD-Philips Expert MPD) at the labs of Natural Resources Authority (NRA), Amman. The samples were scanned between 2º and 65º 2θ, using Ni-filtered Co K α radiation, 40 kV/40mA, divergent and scattering slits of 0.02ºmm, a receiving slit of 0.15mm, with stepping of 0.01º and scanning speed of 3º/min.

3. Results and Discussion

3.1. Phosphogypsum chemistry and mineralogy

The chemical composition of the Jordanian PG is shown in Table (1). CaO and SO_3 formed about 71.1 wt %, Loss On Ignition (LOI) (24.4 wt %) with some SiO_2 and P_2O_5. It is well known that PG contains a lot of impurities inherited from its parent phosphatic rocks, such as U, Cr and Ni (Jiries *et al*., 2004; El-Hasan, 2006; Abed *et al*., 2008, Batarseh & El-Hasan, 2009; and Abed, 2011). Therefore, it is considered as an environmental waste (Dippel, 2004; and Bhadauria & Thakare, 2006). It is clear from Table (1) that the main mineral will be gypsum, which is suitable for being used as a blinder or cement past.

Table 1: The chemical composition of the Jordanian Phosphogypsum (wt%).

Oxides	Concentrations (wt%)
SiO_2	4.11
Al_2O_3	0.087
Fe_2O_3	0.068
TiO_2	0.016
Na_2O	0.21
K_2O	0.48
MgO	0.002
CaO	31.9
MnO	0.001
P_2O_5	0.95
SO_3	39.2
Cl	0.001
LOI	24.4

The chemical composition confirms the mineral constituents of PG which was revealed from the X-Ray diffraction, the main phase is gypsum, with minor calcite quartz, apatite and montmorrillonite (Fig. 1). This is in agreement with the findings of Al-Hwaiti *et al.* (2005). As have been reported by Taylor (1990), between 100 -150ºC the gypsum is converted into the metastable phase Hemihydrates ($CaSO_4.1/2H_2O$), and above 170ºC it changed into the Anhydrite ($CaSO_4$). Therefore, in our experiment, cold PG (i.e., 60ºC) represents gypsum and heated PG (i.e., 120ºC) represents the hemihydrates phase, sometimes called bassanite. Because this phase is metastable, it reacts quickly with normal tap water and returns to its complete hydrated form (gypsum), with an exothermic reaction.

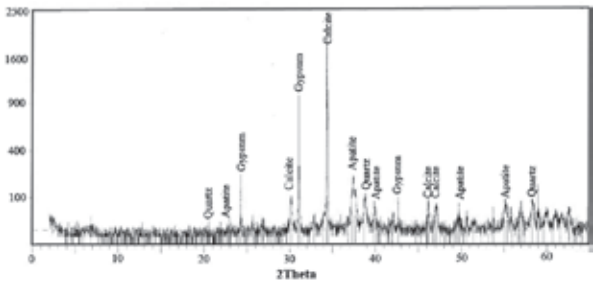

Figure 1: X-Ray diffraction chart for the Jordanian Phosphogypsum used in the mixtures.

3.2. Cement mortar without Pozzolana

3.2.1. Blaine and pH

The Blaine and pH results of produced mortars of both (PG1) and (PG2) resemble those of OPC, Tables (2, 3, 4 and 5). The Blaine was high enough to provide a larger surface area relative to grain size, which caused an acceptable setting time and compressive strength. Moreover, pH of cement water paste was similar to OPC, which facilitates the alkali-pozzolanic reaction, where, clinker compounds react with water through hydration reaction to produce calcium silicate hydrate (C-S-H) and calcium alumina silicate hydrate (C-A-S-H). The time and intensity of these reactions depend on the pH.

3.2.2. Setting time

The setting time for cold raw PG shows a higher initial and final setting time at PG% (4%). Meanwhile, at lower ratios (2%), the heated (PG2) has a higher initial and final setting time. However, at 3%, they show similar initial and final setting time (Fig. 2). Thus 3% may illustrate the optimum mixing ratio of both PG1 & PG2. This can show that at a higher mixing ratio of PG1, more workability can be attained. On the contrary, a lower mixing ratio of PG2 can give better workability behavior of cement mortar.

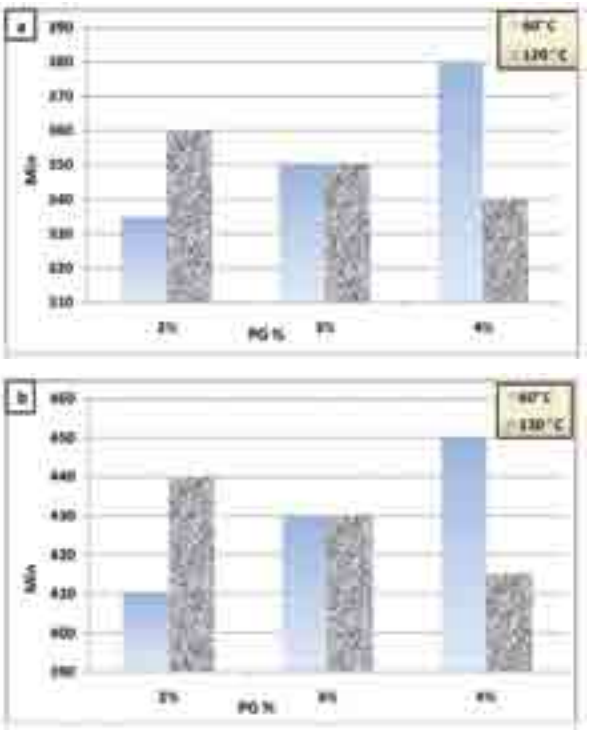

Figure 2: Initial (a) and Final (b) Setting Time (Minutes) difference between PG1 & PG2 for the three PG mixing ration.

3.2.3. Consistency

Water/cement ratio was found increase with increasing the PG replacement percentages for both PG1 & PG2 in the produced mortars, Fig. (3). PG2 has higher percentages than PG1. This might be attributed to the fact that PG2 converted into anhydrite, which needs more water than gypsum, thus PG1 mixing ratio shows lower water/cement (W/C) %, which is a good advantage of cement mortar. The increase in W/C is very small (21.1 - 22%) for PG1 mixed mortars Fig. (3), this may be due to the fact that the PG replacement percentages are small. However, the PG1 shows larger W/C% (21-22.5%), and the highest was in PG1 mixing ratio of (4%) due to anhydrite higher water demand. Bhadauria & Thakare (2006) found that at PG replacement percentage of 5%, the consistency was very near to standard OPC. Furthermore, any further addition causes W/C % to increase rapidly. Both PG1 and PG2 mixing ratios have consistency, lower than OPC standard value (Tables 2 and 4).

Table 2: Generalized table showing complete measurements for unheated raw PG (PG1) mixtures (up to 60°C) without Pozzolana.

Sample No.	Samples components			Blaine	pH	Compressive Strength (N/mm2)			Consist.	Setting time (Minutes)		LE-CHAT	
	K	PG1	Pozz	cm^2/g		2 days	7 days	28 days	(W/C)%	Initial	Final	(mm)	
2%	98	2	-	3377	13	21.7	41.8	53.3	21.2	335	410	1	Lab
3%	97	3	-	3356	13	24.3	42	52.3	21.8	350	430	1	Lab
4%	96	4	--	4404	13	22.3	41.9	53	22	380	450	1	Lab
OPC	-	-	-		13	27.2	41.7	53	25	165	215	1	Lab

Table 3: Generalized table showing complete measurements for unheated raw PG mixtures (PG1) (up to 60°C) with Pozzolana; SO_3 = 2.8%.

Samples No.	Samples components			Blaine	pH	Compressive Strength (N/mm^2)			Consist.	Setting Time (Min)		LE- CHAT.	
	K	PG1	Pozz	cm^2/g		2 days	7 days	28 days	(W/C)%	Initial	Final	(mm)	
1	96.3	3.7	-	3412	13	22.6	41.7	52.1	22.6	375	455	1	Lab
2	86.3	3.7	10	4200	12	20.1	39	47.7	23.2	365	445	1	Lab
3	96.3	3.7	-	3412	13	22.6	41.7	52.1	22.6	160	210	1	Sun
4	86.3	3.7	10	4200	12	20.1	39	47.7	23.2	145	195	1	Sun

Table 4: Generalized table showing complete measurements for heated raw PG mixtures (PG2) (heated up to 120°C) without Pozzolana.

Sample No.	Samples			Blaine	pH	Compressive Strength (N/mm²)			Consist.	Setting Time (Min)		LE-CHAT	
	K	PG2	.Pozz	cm²/g		days 2	days 7	days 28	(W/C)%	Initial	Final	(mm)	
2%	98	2	-	3410	13	19.9	39.3	49.1	21.6	360	440	1	Lab
3%	97	3	-	3385	13	20.5	39	46.6	22.4	350	430	1	Lab
4%	96	4	-	3369	13	19.7	37	43.9	22.6	340	415	1	Lab
OPC	-	-	-	-	13	27.2	41.7	53	25	165	215	1	Lab

Table 5: Generalized table showing complete measurements for heated raw PG mixtures (PG2) (heated up to 120°C) with Pozzolana; SO3 = 2.8%.

Sample No.	Samples			Blaine	pH	Compressive Strength (N/mm²)			Consist.	Setting Time (Min)		LE-CHAT.	
	K	PG2	.Pozz	cm²/g		days 2	days 7	days 28	(W/C)%	Initial	Final	(mm)	
1	95.5	4.5	-	3387	13	21.2	40.5	49.1	22.4	370	450	1	Lab
2	86.3	3.7	10	4218	13	17.8	36.7	44.3	23.4	355	435	1	Lab
3	95.5	4.5	-	3387	13	21.2	40.5	49.1	22.4	155	205	1	Sun
4	86.3	3.7	10	4218	13	17.8	36.7	44.3	22.4	135	185	1	Sun

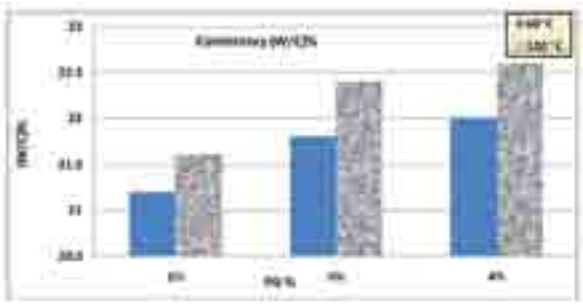

Figure 3: Consistency (W/C)% differences between PG1 & PG2, for the three PG mixing ratios.

3.2.4. Compressive Strength

Obviously, PG1 showed a higher compressive strength than PG2, Fig. (4). Also, PG1 showed an increasing compressive strength starting from 2 days up to 28 days, Fig. (4a). They showed very near compressive strength values to the OPC; the only difference was at 2 days curing time, as shown in Table (2). On the contrary, PG2 showed a decreasing trend in compressive strength, the lowest compressive strength was in the 4% mixing ratio, Fig. (4b). They showed different compressive strength values compared to those of OPC; all mixing ratios have lower values than those of OPC at all curing times, Table (4). This might be due to the increased demand of mixing water and hence higher W/C %.

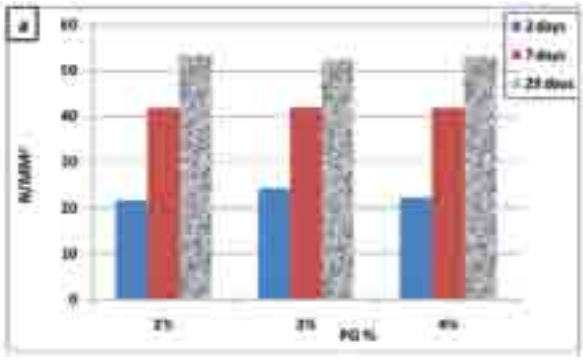

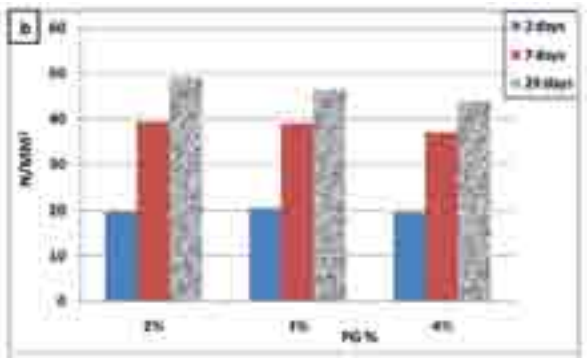

Figure 4: Plotting showing the Compressive Strength (N/mm2) differences between used PG (a) cold at 60°C (PG1) and (b) heated at 120°C (PG2), for the three PG mixing ratios.

3.2.5. Soundness (LE-CHAT)

The LE-CHAT values are shown in Tables (2, 3, 4 and 5); it maintained its value at 1 mm, which means that no volume changes were noticed, be it an expansion or a shrinkage. This is similar to LE-CHAT value of the OPC, which is an additional advantage of the suitability of using raw PG in cement mortar. This shows that the produced mortars show a perfect soundness with either PG1 or PG2 mixes. This is in agreement with the results reached by Bhadauria & Thakare (2006).

4. Cement mortars with Pozzolana

4.1. Setting time

In the second experiment that includes the addition of Pozzolana (10%) to the PG-clinker past, the addition of Pozzolana (Mixture No. 2) slightly lowered the initial and final setting time than the mixture without Pozzolana (Mixture No. 1). The effect of temperature was clear, when the same mixture was done under Sun (Mixtures 3 & 4), where the setting time dropped sharply, compared with those under room temperature (Mixtures 1 & 2), as shown in Fig. (5). Again the PG1 mixtures showed higher initial and final

setting time in all mixtures. A very slight decrease in initial and final setting time for PG2 was noticed; this might be due to the dehydration of PG2 to anhydrite.

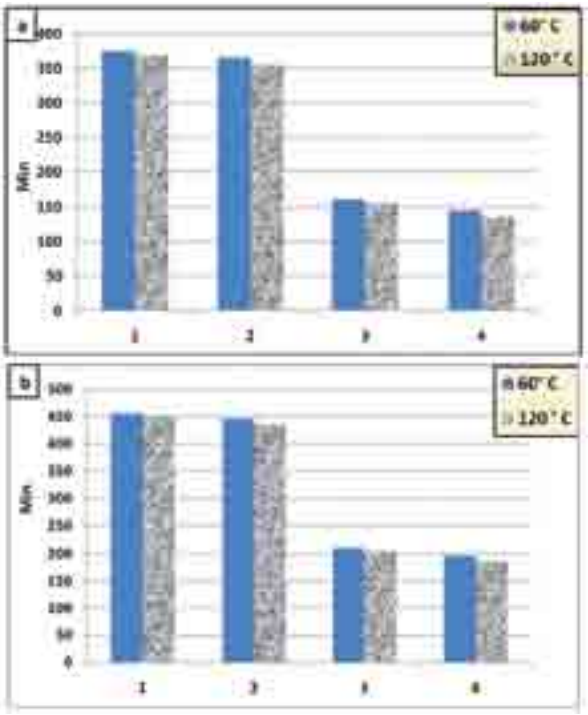

Figure 5: Plotting showing Initial (a) and Final (b) Setting Time (Minutes) difference between PG1 and PG2 for samples (1): Clinker 96.3 + PG 3.7 under room temperature (2): Clinker 86.3 + PG 3.7 + Pozzolana 10 under room temperature (3): Clinker 96.3 + PG 3.7 under Sun (4) Clinker 86.3 + PG 3.7 + Pozzolana 10 under Sun.

4.2. Consistency

The water consumption was also higher in the mixture that used Pozzolana (Mixture No. 2), and the PG2 has the higher (W/C%), as shown in Fig. (6). This behavior changed under the Sun temperature (mixture No. 4). Meanwhile, the mixture with Pozzolana showed the opposite behavior where PG1 (mixtures 1&3) had a higher (W/C%), whether at room temperature or under the sun. In general, the addition of Pozzolana (10%) is too large that decreases the clinker to (86.3%). Pozzolana addition to the mixture slightly increased the W/C% in PG2 that mixed at room temperature (No. 2). However, under the sun, pozzolanic mixture sharply dropped in W/C% as in mixture (No. 4), which might be due to the utilization of heated (PG2), as shown in Fig. (6).

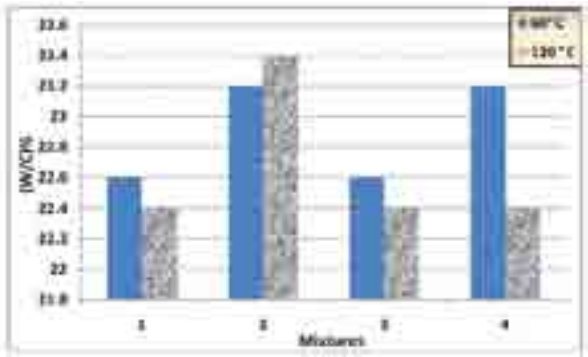

Figure 6: Consistency (W/C)% differences between PG1 & PG2, for mixtures (1): Clinker 96.3 + PG 3.7 under room temperature (2): Clinker 86.3 + PG 3.7 + Pozzolana 10 under room temperature (3): Clinker 96.3 + PG 3.7 under Sun (4) Clinker 86.3 + PG 3.7 + Pozzolana 10 under Sun.

4.3. Compressive Strength

Clearly, the addition of Pozzolana (10%) decreased the compressive strength of 2, 7 and 28 days for PG1 & PG2, Fig. (7). The same trend was noticed for mixtures solidifying either under room temperature or under the sun, as shown in Fig. (7). This might be due to the addition of more Pozzolanic materials (i.e., 10%), which sharply decreased the clinker share in the mortar, causing a decrease in the compressive strength.

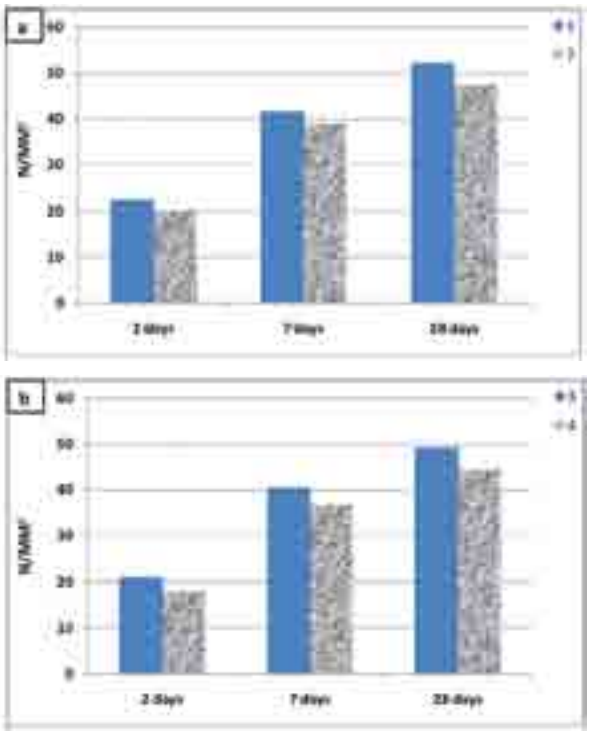

Figure 7: Plotting showing the Compressive Strength (N/mm2) differences between PG1 & PG2, for mixtures (1): Clinker 96.3 + PG 3.7 under room temperature (2): Clinker 86.3 + PG 3.7 + Pozzolana 10 under room temperature (3): Clinker 96.3 + PG 3.7 under Sun (4) Clinker 86.3 + PG 3.7 + Pozzolana 10 under Sun.

5. Conclusions

Colder phosphogypsum (PG1) can easily and successfully replace gypsum in the production of ordinary cement. The setting time (i.e., workability), consistency and compressive strength showed an acceptable value. On the contrary, heated phosphogypsum (PG2) showed an imperfect setting time, consistency and compressive strength. The addition of 10% pozzolana showed a negative impact because of its large mixing ratio. In general, pozzolanic material is added with certain percentages as mineral admixtures to cement in order to increase the compressive strength of the concrete. In our case. Pozzolana was added on the expense of clinker, which resulted in decreasing the compressive strength of the tested samples. The cement mortars using PG had similar Blaine and pH values to OPC. Moreover, they showed perfect soundness values.

Experimental results recommend the use of raw PG without treatment (heating) in cement production. This will eliminate a serious environmental source of pollution; besides, it will decrease the cost of cement production. It is also recommended that further investigations be executed to explore the possibility of extracting gypsum from PG that can be used directly in cement industry.

Acknowledgment

Thanks are due to the Fuhais Cement Factory for the execution of these experiments at their labs and for providing the clinker (OPC type 1) and the Pozzolana.

References

[1] Abed, A.M. 2011. Review of Uranium in the Jordanian Phosphorites: Distribution, Genesis and Industry. Jordan Journal of Earth and Environmental Sciences. Volume 4 (2): 35- 45.

[2] Abed, A.M. Sadaqah, R. and Al-Kuisi, M. 2008. Uranium and Potentially Toxic Metals during the Mining, Beneficiation, and Processing of Phosphorite and their Effects on Groundwater in Jordan. Mine Water Environ. 27: 171-182.

[3] Akın, A.I., Yesim, S., 2004. Utilization of weathered phosphogypsum as set retarder in Portland cement. Cement and Concrete Research 34 (4): 677-680.

[4] Al-Hwaiti, M.; Carney, V.; Ranville, J. F. and Ross, P. E. 2005. Heavy Metal Assessment of Phosphogypsum Waste Stockpile Material from Jordan. National Meeting of the American Society of Mining and Reclamation. 19-23.

[5] ANON 1998. Gypsum disposal and the environment. Phosphorus and Potassium. 215:35-38.

[6] ASTM C 109/C 109M, Standard Test Method for Compressive Strength of Hydraulic Cement Mortars (Using 2-in. or [50mm] Cube Specimens).

[7] ASTM C191, Standard Test Method for Time of Setting of Hydraulic Cement by Vicat Needle.

[8] Azouazi, M., Ouahibi, Y., Fakhi, S., Andres, Y., Abee, J.C.H., Benmansour, M., 2001. Natural radioactivity in phosphates, phosphogypsum and natural waters in Morocco. Journal of Environmental Radioactivity. 54:231-242.

[9] Batarseh, M., and El-Hasan, T. 2009. Toxic Element Levels in the Phosphate Deposits of Central Jordan. Soil & Sediment Contamination. 18:205-215.

[10] Berish, C.W., 1990. Potential environmental hazards of phosphogypsum storage in central Florida. In: Proceedings of the third international symposium on phosphogypsum, Orlando, FL, FIPR Pub. No. 01060083; 2, 1–29.

[11] Bhadauria, S. S.; Thakare, R. B. 2006. Utilization of Phosphogypsum in cement mortar and concrete. 31st Conf. OUR WORLD IN CONCRETE & STRUCTURES, Singapore.

[12] Degirmenci, N., 2008. Utilization of phosphogypsum as raw and calcined material in manufacturing of building products. Construction and Building Materials. 22: 1857-1862.

[13] Dippel, S.K. 2004. Mineralogical and geochemical characterization of phosphogypsum waste material and its potential for use as backfill at WMC Fertilizers' Mine site, Phosphate Hill, N-W Queensland. Masters thesis, James Cook University. P336.

[14] Dueñas, C., Liger, E., Cañete, S., Pérez, M., Bolívar, J.P. 2007. Exhalation of 222Rn from phosphogypsum piles located at the Southwest of Spain. Journal of Environmental Radioactivity. 95: 63-74.

[15] El-Hasan, T., 2006. Geochemical dissociation of major and trace elements in bed and suspended sediment phases of the phosphate mines effluent water, Jordan. Environmental Geology. 51(4):621-629.

[16] El-Hasan, T.; Al-Hamaideh, H. 2012. Characterization and Possible Industrial Applications of Tripoli Outcrops at Al-Karak Province. Jordan Journal of Earth and Environmental Sciences. Volume 4 (2): 63- 66.

[17] Environmental Protection Agency (EPA). 40 CFR Part 61. 1999. National emission standard for hazardous air pollutants; National Emission standards for Radon emissions from phosphogypsum stacks, Federal register, Vol.64(2): 5574 – 5580.

[18] European Fertilizer Manufacturers Association (EFMA) 2000. Production of Phosphoric Acid. Best Available Technique for pollution Prevention and control in the European Fertilizers Industry. Booklet No. 4, EFMA, Brussels, Belgium

[19] Ghafoori, N. 1986. Phosphogypsum based concrete: Engineering characteristics and road applications, Ph. D. thesis, University of Miami, Corel Gables, Florida.

[20] Gutt, W. 1978. The use of by-product in concrete (CP 53/ 74), BRE research series, Concrete: Practical studies from BRE, The construction press, Volume 1:47 – 66.

[21] Jiries, A., El-Hasan, T., Al-Hiwati, M., and Seiler, K. P. 2004. Evaluation of the Effluent Water Quality Produced from Phosphate Mines in Central Jordan. Mine Water and the Environment. 23 (3): 133-137.

[22] Lysandrou, M., Pashalidis, I. 2008. Uranium chemistry in stack solutions and leachates phophogypsum disposed at a coastal area in Cyprus. Journal of Environmental Radioactivity. 99: 359-366.

[23] Ouyang, C.; Nanni, A. and Chang. W. 1978. Sulfate attack resistance of Portland cement mixtures containing phosphogypsum, Proceedings of Katherine and B. Mather International conference, Concrete durability, Vol. II, P100–102, American Concrete Institute, Detroit, 2007 – 2015.

[24] Smadi, M.M.; Haddad, R.H. and Akour, A.M. 1999. Potential use of phosphogypsum in concrete. Cement and Concrete Research. 29(9):1419–1425.

[25] Taylor, H.F.W. 1990. Cement Chemistry. Academic Press. London. Pages 459.

[26] Wissa, A.E.Z. 2001. Phosphogypsum disposal & the Environment. http://www.ardaman.com/pubs/phosphogypsum_disposal.htm. Acc. 13/09/2001.

[27] Yang, J., Liu, W., Zhang, L., Xiao, B. 2009. Preparation of load-bearing building materials from autoclaved phosphogypsum. Construction and Building Materials 23, 687-693.

[28] (http://ardaman.com/waste.php3

[29] (http://www.jpmc.com.jo/?q=node/166)

JJEES
Jordan Journal of Earth and Environmental Sciences

Volume 6, Number 2, December, 2014
ISSN 1995-6681
Pages 67- 75

Effect of Oil Shale Ash on Static Creep Performance of Asphalt-Paving Mixtures

Qahir N. Al-Qadi[1], Arabi N. Al-Qadi[2*], and Taiser S. Khedaywi[3]

[1] *Department of Earth Sciences and Environment, the Hashemite University, Zarqa, Jordan.*
[2] *Corresponding Author: Department of Civil Engineering, AL Hussien Bin Talal University, Ma'an.*
[3] *Department of Civil Engineering, Jordan University of Science and Technology, Irbid, Jordan.*

Received 2 May, 2014; Accepted 4 December, 2014

Abstract

The objectives of the present study are to evaluate the effect of oil shale ash on the rutting of flexible pavement and to find the optimum percentages of ash, which will give the best properties of flexible pavement. Oil shale ash was used as an additive in an asphalt concrete mix. Specimens, with five-ash content (0%, 5%, 10%, 15% and 20%) by volume of binder, were made by Marshall Moulds. Then they were exposed to creep tests (static) through the Universal Testing Machine (UTM). Three testing temperature levels (5°C, 25°C and 40°C) resembling relatively cold, moderate and high levels of temperature were considered. Oil shale ash is an air and water pollutant by product of oil shale rock. This research attempt to recycle oil shale ash by using it as an additive to hot mix asphalt (HMA). Furthermore, it will decrease the economic costs of constructing asphalt mix. The optimum percentage (12.5%) of oil shale ash addition it will increase the quality and performance of asphalt mix by reducing rutting. Statistical models analysis of the data provided by the UTM, consequently, this increased stiffness, resilient modulus and the accumulated strain of the asphalt concrete mix. Moreover, rutting depth and air voids were decreased.

Keywords: Static creep; Universal testing machine; Oil shale ash; Flexible pavement; Marshall Test.

1. Introduction

One of the Oil Shale rocks spreading in Jordan is the Sultani deposit located near Amman with 100 Km the south direction. The use of oil shale as a source of energy in Jordan will lead to environmental hazardous oil shale ash coming to the surface. Most of the forecast of the world energy demand agree that conventional energy resources are not sufficient to meet the energy requirement of an expanding world economy beyond the year 2020. (Ministry of energy and mineral resources, 1995); hence the need for benefiting from this ash in asphalt constructions.

This study will investigate methods that will help reducing the pollution of the environment in Jordan, when oil shale is used as a major source of energy in the future. In addition, oil shale ash, as an additive substance to asphalt cement pavement forming a binder; is available and of low cost. Characteristics of asphalt mixtures can be evaluated using conventional tests, such as Marshall and Hveem tests. In addition, many studies were undertaken to improve the properties of asphaltic concrete mixtures by additives.

Several studies (Van de loo, 1976 and1974) indicate that the conventional bituminous mixture tests cannot provide information about the rutting potential of paving mixtures. The use of oil shale ash in road construction materials, on the long run, focusing on static creep test, were investigated to demonstrate the effect of ash content on accumulated strain, stiffness, resilient modulus and rutting (permanent deformation) by using UTM.

Young-Chan *et al*. (2011) studied the Accelerated Pavement Testing (APT) with temperatures and air void ratio factors. These are the most important factors that influence rutting (permanent deformation). The purpose was to use APT results to calibrate and develop a laboratory rutting models for asphalt concrete mixtures. The layer of asphalt concrete tested was of 30cm, and sub-base 30cm, and sub-grade of 180cm, at temperature 50°C and air voids (7.31% to 10.57%) measurement of the plastic and resilient strain.

Gui-ping and Wing-gun (2007) investigated the effects of bitumen grade, the content of Reclaimed Asphalt Pavement (RAP) material and the aging of RAP. The study presents the evaluation of permanent deformation of Foamed Asphalt (FA) mixes by using the dynamic creep test. The mix design of WC-20 was conducted based on the graduation requirement of FA mix and RAP aggregate size. Three factors, namely Creep Strain Slope (CSS), Intercept, and Secant Creep Stiffness Modulus (SCSM), were used to analyze the test results. Mean comparison and multiple analyses of variance (ANOVA) reveal that bitumen grade significantly affects CSS, whilst content and aging of RAP would have an insignificant effect on CSS. High bitumen grade also helps FA mixes on the reduction of susceptibility to permanent deformation. Test results reflect that variances of CSS, Intercept, and SCSM are large and they also lead to the conclusion that there is a good exponential relationship between CSS and SCSM. However, no correlation between CSS and air void is found. The comparison between the test results of FA mixes and those of hot asphalt mixes exhibits that susceptibility and creep strength of FA mixes are better than those of the selected hot asphalt mixes.

Biligiri *et al.* (2007) studied several mathematical models to be used in calculating the onset of tertiary flow for asphalt

* Corresponding author. e-mail: arabi.alqadi@gmail.com

mixtures. The Flow Number (FN) indicates the onset of shear deformation in asphalt mixtures, which is a significant factor in evaluating rutting in the field. They found that the FN is obtained from the Repeated Load Permanent Deformation (RLPD) laboratory test. The current modelling techniques in determining the FN use a polynomial model fitting approach, which works well for most conventional asphalt mixtures. Biligiri *et al.* (2007) offered an analysis and some observations on the use of this polynomial model for rubber-modified asphalt mixtures, showing that the problems lie in identifying the true FN values. Their scope were to collect and analyze more than 300 RLPD test data files, which comprised more than 40 mixtures, a wide range of test temperatures, and several stress levels. A new comprehensive mathematical model was recommended to accurately determine the FN. The results and analyses were evaluated through manual calculations and they found them accurate, rational, and applicable to all mixture types.

Carpenter and Vavrik (1999) recognized the need for a simple test that can be preferably performed on a super pave gyratory compactor (SGC) samples during mix design that would rank the performance potential of the mixtures. They proved of the difficulties of finding one test that can rate mixture potential for rutting, fatigue cracking and modulus. They used Illinois mixtures that provide evidence that a simple test performed during mix design has the potential of predicting a diverse set of performance characteristics. Their results are presented for 10 Illinois dense-graded mixtures of surface and binder (9.5mm and 12.5mm) gradations that were tested in an Asphalt Pavement Analyzer (APA) and subjected to flexural beam fatigue, unconfined repeated load permanent deformation, and diametric resilient modulus testing. The mixtures were subjected to a rapid triaxial test procedure using SGC compacted samples, as taken from the SGC machine, and tested at 50°C in a triaxial stress reversal mode. The triaxial testing provides data that predict resilient modulus, APA rutting results, fatigue coefficients, and permanent deformation characteristics of accumulated strain at tertiary failure, loads to tertiary failure, and the exponent to the standard logarithmic permanent deformation curve. The excellent correlations obtained from this study provide direct evidence that this test protocol may provide a structural evaluation procedure to supplement the volumetric mix design process.

Vacin *et al.* (1999) used samples of one polymer-modified asphalt mixing with fine filler (mastic), and one HMA prepared with the same modified asphalt as binders were tested in the Dynamic Ahear Rheometer (DSR) and the Bending Beam Rheometer (BBR). The materials were tested to characterize discrete relaxation and retardation spectra (under the condition of small deformations). DSR testing was performed in the plate–plate and the torsion bar geometry. From the obtained relaxation and retardation spectra, the shear compliance, J(t), was calculated and compared with the tensile creep compliance, D(t), measured in BBR. A simple relationship between J(t) and D(t) was found for the asphalt binder and the asphalt mastic. In the case of HMA, the bulk compliance, B(t), contributes to D(t) at short and long times. Both the Boltzmann superposition principle and the time–temperature superposition principle hold very well for all the tested materials at low temperatures. They conclude that there are qualitative differences in the rheological behaviour of the asphalt binder and the asphalt mastic on one side and the HMA on the other. These differences can be seen in dynamic (DSR) as well as in transient (BBR) experiments.

Abo-Qudais and Shatnawi (2007) tried to predict the number of the cycles causing a fracture in Hot Mix Asphalt (HMA) with the slope of accumulated strain turn from decreasing to increasing mode of failure. Furthermore, they studied the effect of aggregate gradation and temperature on the fatigue behaviour of HMA. They used Marshall Test to find the optimum asphalt content. The material they used were crushed lime stone, penetration of asphalt 60/70, and three gradation of aggregate with maximum nominal size of 12.5mm, 19mm, and 25mm; five magnitude of loading (1.5KN, 2.0KN, 2.5KN, 3.0KN, and 3.5KN) were studied. Temperatures 10°C, 25°C, 45°C, and 60°C were used to evaluate the load at 3.5KN. They concluded that the slope of accumulated strain decreases until the number of the cycles loading reach 44% of fracture cycles of HMA, and the stiffness increases as the applied load increases and the gradation maximum nominal size decreases.

Oil shale ash, as a by-product of oil shale burning, causes serious environmental problems; but using it in flexible pavement material decreases the cost of road constructions.

The present study aims at:

- investigating the feasibility of using oil shale ash as an additive to the asphalt bituminous paving mixtures to achieve economic advantage and good performance;
- determination the effect of oil shale ash on static creep of flexible pavement by studying the responses (stiffness, accumulated strain, and rutting) ; and
- finding the optimum percentage of ash, thus giving the best properties via reducing rutting and air voids

2. Approach of the Study

To achieve the objectives of this study, Hot Mix Asphalt (HMA) specimens were prepared at optimum asphalt content using Marshal mix design procedure (MS-2, 1976). Marshal compactor was used to compact the HMA specimens. Limestone aggregate, asphalt with 60/70 penetration, Oil shale were used as an additive to the asphalt cement composed of oil shale ash burned at 600°C, which passed a #200 sieve, was tested as an additive to asphalt cement. In preparing ash-asphalt binders, ash and asphalt contents were heated and maintained at a temperature between 145°C and 150°C (293°F and 302°F) (Al-Massaid *et al*., 1989). Tests include the characteristics of the materials used in the research, preparation of binders, and optimum asphalt determination. Also, the present study presents a static creep test on asphalt-ash concrete specimens.

3. Materials Used

Aggregate

One type of aggregate was used in the study; it was brought from Al-Halabat quarries in Jordan. Gradation was according to the Ministry of Public Works and Housing (MPWH) specification in Jordan (1991). Table (1-A) shows the aggregate properties while Table (1-D) lists the aggregate gradation.

Asphalt

One penetration grade of asphalt cement (60–70) was used in this study. Asphalt was obtained from the Jordan Petroleum Refinery Company in Zarqa, Jordan, and it is widely used in flexible pavement constructions. Table 1-B summarizes the physical properties of the asphalt used in this study.

Table 1: A, B, C, D. Properties of the materials used in this study*

A. Aggregate Properties Used in Research				
Aggregate Type (Limestone)	ASTM Test Designation	Bulk Specific Gravity	Apparent Specific Gravity	Absorption (%)
Coarse Agg.	C127	2.426	2.618	3.0
Fine Agg.	C128	2.460	2.628	3.6
Mineral Filler	C128	2.485	2.485	5.0
B. Physical Properties of Asphalt				
Test		Methods		Results
Ductility, 25 ^{0}C,Cm		ASTM D 113		110
Penetration, 25 ^{0}C, 100 g, 5 s, 0.1 mm		ASTM D 5		65
Softening Point, ^{0}C		ASTM D 36		50
Flash Point (Cleveland Open Cup), ^{0}C		ASTM D 92		330
Fire Point, ^{0}C		ASTMD92		335
Specific Gravity, 25 ^{0}C		ASTM D 70		1.014
C. Properties of Oil Shale Ash				
Properties		ASTM Designation		Test Result
Specific Gravity		C188		2.842
Color				Brown To Black
D. Aggregate Gradation Used				
Sieve Size		Specification Limits* (% Passing)		%Passing (Midpoint)
1» (25 mm)		100		100
¾» (19 mm)		90-100		95
½» (12.5 mm)		71-90		80.5
3/8» (9.5 mm)		56-80		68
No. 4 (4.75 mm)		35-56		45.5
No. 8 (2.35 mm)		23-38		30.5
No. 20 (850 µm)		13-27		20
No. 50 (300 µm)		5-17		11
No. 80 (180 µm)		4-14		9
No. 200 (75 µm)		2-8		5
*Ministry of Public Works and Housing (MPWH), Specification Sec. 4.01, Table 4.1 Wearing Mix (11)(1991).				

Oil Shale Ash

Oil shale was obtained from the Sultani deposit. Ash was produced by grinding the shale then burning it at 600^{o}C in an oven. It was then passed through a # 200 sieve to be used as an additive in the asphalt cement. The specific gravities of the binder (asphalt-ash) at 0%, 5%, 10%, 15%, and 20% by volume were 1.014, 1.089, 1.103, 1.216, and 1.325, respectively. Table 1-C presents the physical properties of the oil shale ash.

Determination of Optimum Asphalt Content for Conventional Mixes

To determine the optimum asphalt content by weight of total mixture, the procedure indicated by the standard Asphalt Institute MS-2 Manual (1976) and ASTM D1559 (1990) was determined using Marshal Mix design of 50 blow procedures (represent medium traffic). Three samples from each asphalt level (4.0%, 4.5%, 5.0%, 5.5%, and 6%) of the total weight of the mix were prepared. Specimens were extruded from the Marshall moulds after 24 hours. Height and weight measurements were conducted to determine the unit weight of each specimen, and specimens were submerged in water at 60^{o}C for 40 minutes before testing. A total of 15 specimens were tested for flow, stability, unit weight, air voids, and voids in mineral aggregate. The optimum asphalt content was measured as the average of asphalt contents that meet maximum stability, maximum unit weight, and 4.0% air voids; then the measured optimum asphalt contents were checked to figure out whether they are within the specification limits of the factors (flow, stability, air voids unit weight, and voids in mineral aggregate). The optimum asphalt content was found to be 5.4% by total weight of mixture.

4. Static Uniaxial Loading Strain Test

The method for the determination of resistance to permanent deformation of bituminous mixtures subject to unconfined uniaxial loading involves the application of a static load to a sample for 3600 second loading at different temperatures (5^{o}C, 25^{o}C, and 40^{o}C). It is performed by Universal Testing Machine (UTM). This test was conducted in accordance with UTM Reference Manual (1996) and BSI standards. The Marshall specimens with different percentages of ash (0%, 5%, 10%, 15%, and 20%) by volume of binder were tested using the UTM. Specimen heights with six measurements were taken and if the difference between the smallest and the largest of the six thickness measurements was more than 2% of the nominal diameter of the specimens, the specimen was levelled. Specimens were placed in a cabinet with a suitable force air circulation, in which the specimen gains the test temperature for 24 hour, and then the test was performed for different level of temperatures (5^{o}C, 25^{o}C, and 40^{o}C). Grease was spread evenly and thinly over the ends of the specimen to minimize friction. Surplus grease was removed with a cloth to leave surface with a damp appearance to minimize the friction at the platen-to-specimen interface.

Conditioning was made by the use of a software program in a stress of 10 KPa for 20 second. Specimen was subjected to static loading for 3600 second with a stress of 100 KPa. Then levelling was made in Linear Variable Displacement Transformers (LVDTs), data of accumulated strain, creep stiffness, slope of accumulated strain and temperature were measured by the assistance of a computer. Fig. 1 shows the testing setup.

Figure 1: Specimen in the static creep frame of a UTM.

5. Results and Discussion

5.1. Effect of Static Creep Test

Static creep test was developed to estimate the rutting potential of asphalt mixtures. This test was conducted by applying a static load to a HMA ash specimen and measuring the resulting permanent deformation with time. The most common creep test is the static unconfined. This test involves application of a static load to a sample for specified time and temperature and the measurement of deformation as the sample deforms (BSI, 1996).

Test of static uniaxial loading strain conforms to the requirements issued by the British Standards Institute (BSI part 111, 1995) for determination of resistance to permanent deformation of bituminous mixtures subjected to unconfined uniaxial loading. The tests initially apply conditioning stress to the specimen and measure the resulting accumulating strain. The magnitude and applied time duration of conditioning stress have present default values of 10 KPa and 120 second, and then the specimen was subjected to static loading for 3600 second with default s tress level of 100 KPa. During the full static loading stage, the accumulated strain is measured and displayed as a plot with linear scale axis.

Test proceeds; plotted data are displayed with linear vertical and horizontal axis. The output of this test is the selection of:

- accumulated strain (creep or permanent strain);
- derivative of accumulated strain (slope);
- applied stress;
- creep stiffness (modulus); and
- core temperature of a dummy specimen.

Static creep test was performed in order to obtain the accumulated strain, mix stiffness, creep compliance, and permanent deformation (rutting) for different oil shale ash contents. The recorded deformation, as a function of time of loading, was used to calculate accumulated strain, stiffness, and permanent deformation at three levels of temperature 5°C, 25°C, and 40°C.

5.2. Accumulated Strain

Accumulated strain is the ratio of the total deformation to the original height of the specimen at any instant of time during the test. Axial micro-strain was calculated according to the following formula in Eq. (1):

$$Єct = (L2t - L1)/G \quad (1)$$

Єct = is the accumulated axial strain (creep) at time t

L1 = is the initial zero reference displacement of the transducers before the full loading stress is applied.

L2t = the displacement level of the transducers at time t.

G = is the initial specimen length.

The axial micro-strain was calculated for different temperature levels (5°C, 25°C, and 40°C) and different oil shale ash content with the same asphalt content. The axial micro-strain was calculated for different temperature levels (5°C, 25°C, and 40°C) and different oil shale ash content with the same asphalt content (UTM 2 Manual, 1996). The relationship between accumulated strain and time at different temperature levels and percent of oil shale ash are shown in Fig. 2. Accumulated micro-strain versus time for (a) 0%, (b) 5%, (c) 10%, (d) 15%, and (e) 20% oil shale ash at different temperatures levels. This figure shows that there is a decrease in axial strain at low temperature, while at high temperature there is a certain increase.

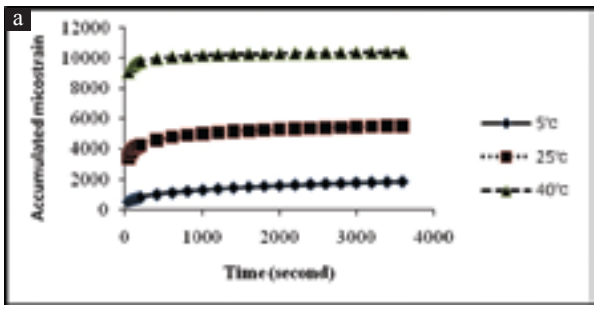

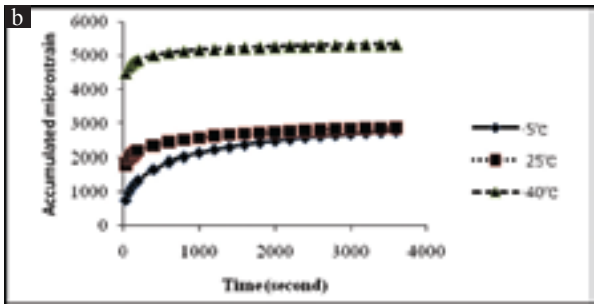

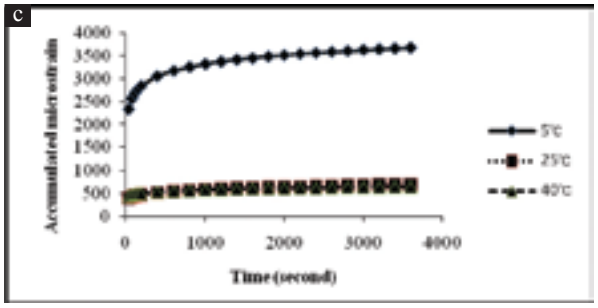

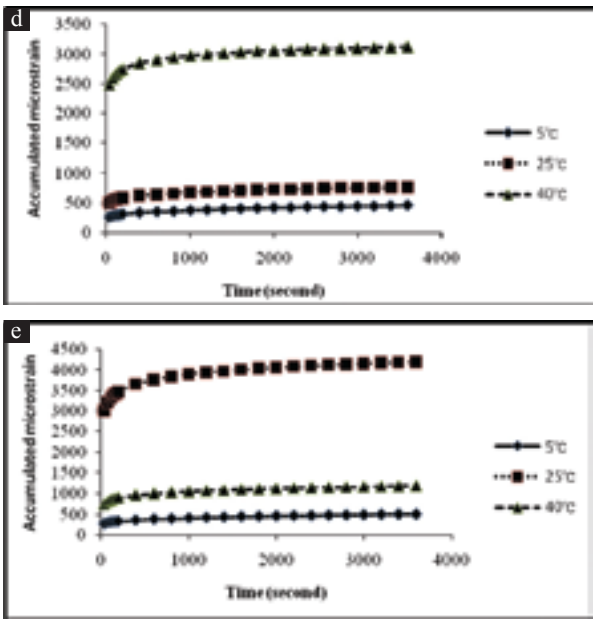

Figure 2: Accumulated micro-strain versus time for (a) 0 %, (b) 5%, (c) 10%, (d) 15%, and (e) 20% of oil shale ash at different temperature levels.

In Fig. 3 accumulated micro-strains versus time for different % of oil shale ashes contents at (a) 5°C, (b) 25°C, and (c) 40°C are shown, in a logarithmic scale, that as ash content increases the axial micro strain decreases; this is due to the fact that the adhesive forces between particles become relatively weak.

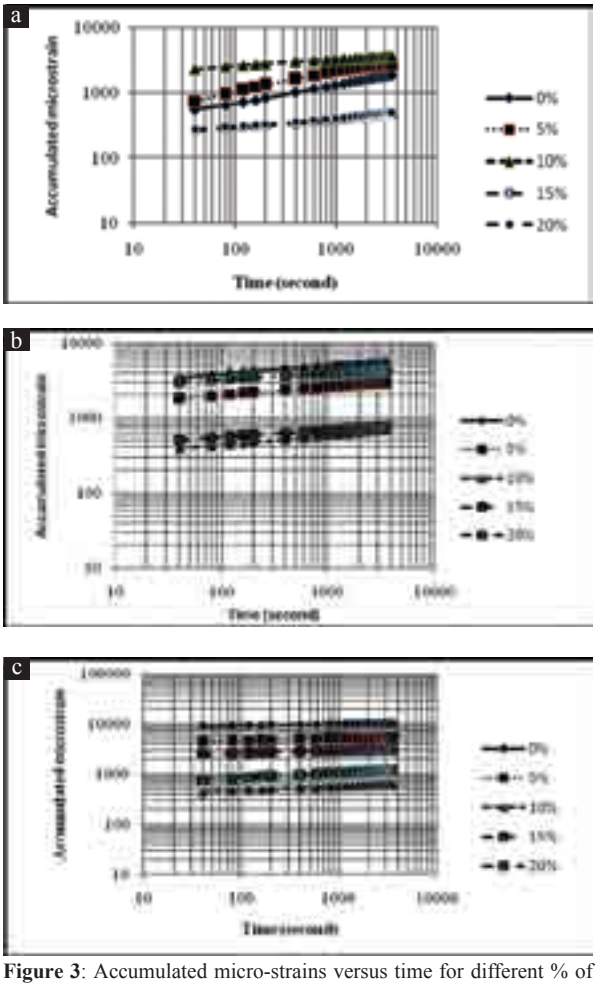

Figure 3: Accumulated micro-strains versus time for different % of oil shale ash content at (a) 5°C, (b) 25°C, and (c) 40°C.

5.3. Creep Stiffness

Stiffness (S_{mix}) is defined as the ratio of applied constant load to deformation as a function of time and temperature. Stiffness was calculated according to the following Eq. (2):

$S_{mix} = \sigma/Є s(t,T)$ (2)

where

S_{mix} = is the static load stiffness modulus of the mixture at loading time t (in second) and loading temperature T (in °C).

Єs = Static strain

σ = is the applied stress (in KPa).

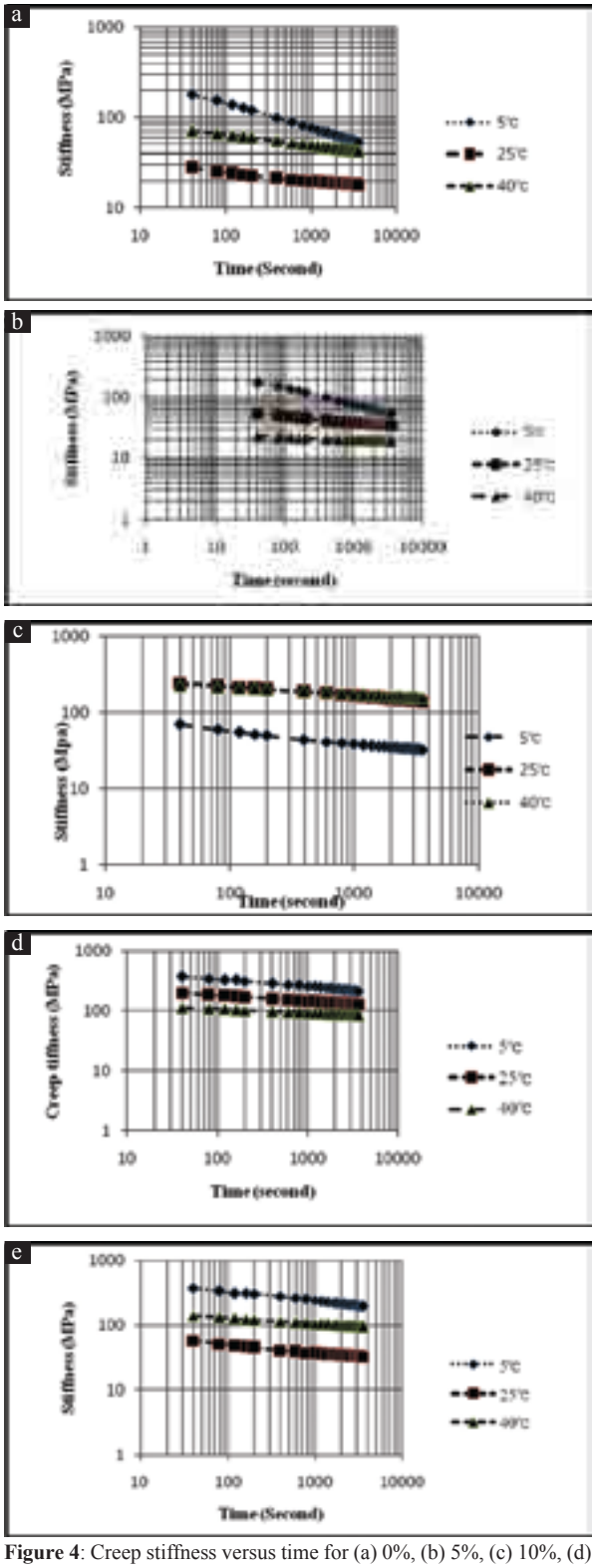

Figure 4: Creep stiffness versus time for (a) 0%, (b) 5%, (c) 10%, (d) 15%, (e) 20% of oil shale ash at different temperatures.

The stiffness values were calculated for different temperature levels and ash contents. Fig. 4 shows the creep stiffness versus time for (a) 0%, (b) 5%, (c)10%, (d) 15%, (e) 20% oil shale ashes at different temperatures, and Figs. 4(a) through (e) show the relationship between stiffness (S_{mix}) and time at different temperature and oil shale ash contents. As observed from the Figs. 4 (a-e), the highest stiffness in 0%, 5%, 15%, and 20% ash are seen at 5°C curve, and the lowest stiffness at 25°C for Figs. 4(a), and (e), and at 40°C in Figs. 4(b) and (d). In Fig. 4(c) the stiffness is high in 10% ash at 25°C and 40°C while it is low at 5°C. This implies that the 10% ash fraction can stand better than the other fraction in different climatic conditions, moderate and high temperatures; these are the ideal percentages; in fact this is the optimum.

At different ash content, stiffness versus time at different temperature, as shown in Figs. 5(a), (b), and (c), the stiffness decreases with the decrease in ash contents, while stiffness modulus for different ash content at different temperature 5°C, Fig. 5(a), the highest stiffness was seen in 20% and 0% and the lowest in 10% ash. In Fig. 5 (b), at 25°C the highest stiffness was observed in 10% and 15%, while the lowest at 0% ash. Also, in Fig. 5(c) at 40°C, the highest stiffness modulus at 10% ash was seen and the lowest in 5% ash.

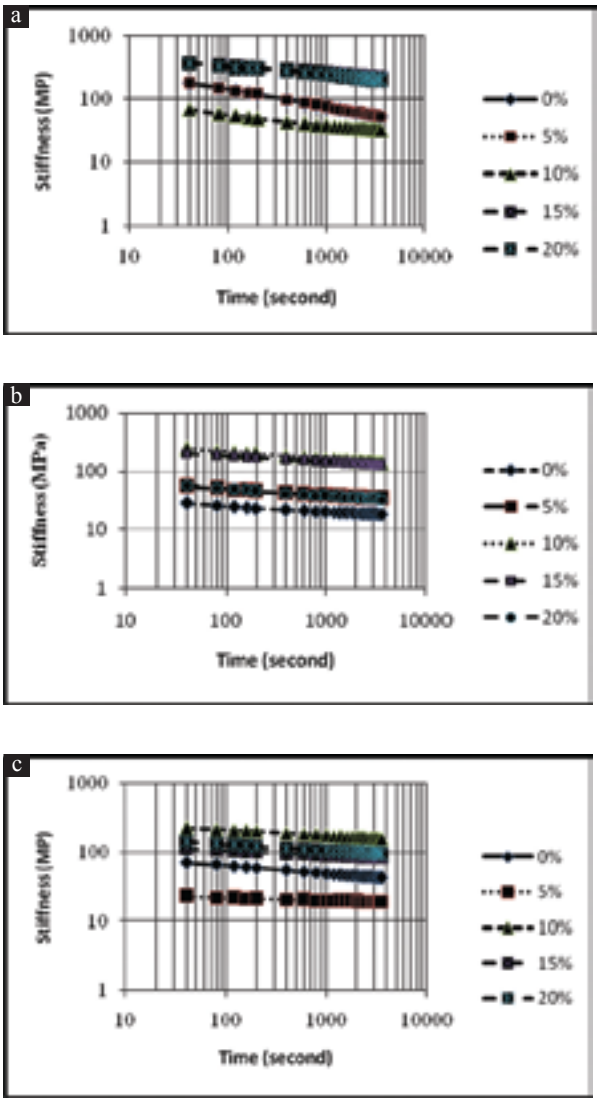

Figure 5: Stiffness versus time for different % of ash contents at (a) 5°C, (b) 25 °C, and (c) 40 °C.

6. Statistical Models for Air Voids, Stiffness Modulus and Accumulated Strain

To achieve the objectives of this study, 60 specimens were prepared for one type of aggregate (Limestone) with five levels of oil shale ash content. Static creep was carried out at three temperature levels. Graphical and statistical approaches were followed to investigate the effect of the oil shale ash additive on accumulated strain, stiffness, and air voids.

Tables 2, 3 and 4 contain a more realistic data set; the *X* represents the percentages of volume fraction (0%, 5%, 10%, 15% , and 20%) of oil shale ash in flexible pavement mixture, and *Y* represents the measured accumulated micro-strain and stiffness modulus at different temperatures (5°C, 25°C, and 40°C). These points do not clearly fall along a fitted line. These lines are shown in Figs. 5, 6 and 7 which provide a good fit to the data. The quadratic model assumes that the dependent or response variable, represented by Y_1 at 5°C, Y_2 at 25°C, and Y_3 at 40°C , are related to an independent variables, represented by *X*, by the relation as shown in the pure quadratic formula (3):

$$Y = \beta_o + \sum_{i=1}^{\kappa} \beta_o \chi_i + \sum_{i=1}^{\kappa} \beta_i \chi_i^2 + \Xi \qquad (3)$$

Where *Y* represents response variable, *βo* is the interception coefficient, *βi*, coefficient of the linear effect, and *βii*, the coefficient of quadratic effect. Where y represents an accumulated strain, and stiffness modulus for the pure quadratic model. The error term, Ξ is a normally distributed random variable with mean equal to 0.0 and standard deviation equal to σ. The error sum of square (SSE) was measured by the sum of squaring the residuals. A residual is a measure of the deviation of the data from the predicted or estimated regression line. SSE equal to 0.0 if all the data fitted perfectly in the line of regression and this indication for checking the data as the SSE increase means that the data more variable from the fitted line. The total sum of squares (SST) reveals, after the estimation of the mean number of accumulated strain, air voids and stiffness modulus at different percentages of oil shale ash, which percent is the optimum; our best estimate is the mean of micro-strain, air voids (%), and stiffness (MPa) by % of ash. The accuracy of the estimate is related to the variation of *Y* values around the mean. The sum of square about the mean is called the total sum of squares (SST).

Regression sum of squares (SSR) is when there is still some unexplained variation about the regression line. This implies that the regression line demonstrates an amount of variation equal to SST-SSE.

Coefficient of determination (R^2) is when all the data fall perfectly on a regression line, SSE=0.0, and SST=SSR. The value of R^2 is equal to 1.0. When there is no explanation for the variation of *Y*, SSR=0.0 then the R^2=0.0. When R^2 is expressed in percentages, it is related to SST which can be explained via using the predicted regression equation.

As seen in Figs. 6 through 8 and Tables 2, 3 and 4, the values of R^2 are equal to 0.999, 0.996, and 1.0 at 5°C, 25°C, and 40°C for measuring air voids, 0.996, 0.979, and 0.969 for stiffness modulus and 1.0, 0.999, and 0.999 for accumulated strain with a good fitness for representing the data. Also, the standard deviation of the errors for air voids equal to 0.0096, 0.122, and 0.176, stiffness modulus are 2.22, 6.15, and 1.91, and accumulated strain 2.58, 28.87, and 133.68 at 5°C, 25°C, and 40°C. These show that the lowest standard deviations of errors are cited at 5°C and in measurement of air voids (*Av*) with volume fraction of the oil shale ash percentages (*Vf*).

Table 2: Comparison of predicted, effectiveness and measured values and errors air voids of asphalt pavement mixtures with and without ash percents

Ash (%)	Air voids (%)											
	Measured			Predicted			Residual			Error Sum of Square(SSE)		
	5°C	25°C	40°C	5°C	25°C	40°C	5°C	25°C	40°C	5°C	25°C	40°C
0	4.8	4.1	3.5	4.811	4.034	3.762	-0.011	0.066	-0.262	0.000121	0.004356	0.068644
5	7.55	7.02	6.7	7.546	7.059	6.687	0.004	-0.039	0.013	1.6E-05	0.001521	0.000169
10	8.57	8.1	7.8	8.581	8.234	7.762	-0.011	-0.134	0.038	0.000121	0.017956	0.001444
15	7.92	7.7	7.1	7.916	7.559	6.987	0.004	0.141	0.113	1.6E-05	0.019881	0.012769
20	5.55	5	4.46	5.551	5.034	4.362	-0.001	-0.034	0.098	1E-06	0.001156	0.009604
	Measured-Mean			Predicted-Mean			Residual Error (%)*			Air void- Effectiveness (%)		
0	4.32	5.22	5.82	4.32	5.17	5.73	-0.23	1.64	-6.96	-	-	-
5	0.45	0.40	0.62	0.45	0.36	0.53	0.05	-0.55	0.19	57.29	70.73	91.43
10	2.86	2.94	3.56	2.86	2.90	3.47	-0.13	-1.63	0.49	78.54	97.56	122.85
15	1.086	1.73	1.41	1.09	1.69	1.32	0.051	1.87	1.62	65.00	87.80	102.85
20	1.764	1.92	2.11	1.76	1.87	2.02	-0.02	-0.68	2.25	15.63	21.95	31.43
	Total Sum of Square(SST)			Regression Sum of Square (SSR)			Coefficient of Determination (R^2)			Standard deviation of errors(S)		
	10.482	12.213	13.523	10.482	12.168	-119.48	0.999	0.996	1.0	0.0096	0.122	0.176

* Residual error (%) = ((measured value- residual value) / (residual value)) x100%

Table 3: Comparison of predicted, effectiveness and measured values and errors for stiffness modulus of asphalt pavement mixtures with and without ash percents of asphalt.

Ash (%)	Stiffness modulus (MPa)											
	Measured			Predicted			Residual			Error Sum of Square(SSE)		
	5°C	25°C	40°C	5°C	25°C	40°C	5°C	25°C	40°C	5°C	25°C	40°C
0	50	27	17	49	24.4	15.88	1	2.6	1.12	1.00	6.76	1.254
5	98	76	60	100.8	80.2	62.43	-2.8	-4.2	-2.43	7.84	17.64	5.905
10	129	107	90	126.6	110	89.28	2.4	-3	0.72	5.76	9.00	0.518
15	126	122	98	126.4	113.8	96.43	-0.4	8.2	1.57	0.16	67.24	2.465
20	100	88	83	100.2	91.6	83.88	-0.2	-3.6	-0.88	0.04	12.96	0.774
	Measured-Mean			Predicted-Mean			Residual Error (%)*			Stiffness- Effectiveness (%)		
0	2560.36	3249	2766.76	2545.56	3135.4	2755.843	2.04	10.66	7.05	-	-	-
5	6.76	64	92.16	-8.04	-49.6	81.243	-2.78	-5.24	-3.89	96	181	253
10	806.56	529	416.16	791.76	415.4	405.243	1.90	-2.73	0.81	158	296	429
15	645.16	1444	806.56	630.36	1330.4	795.643	-0.32	7.21	1.63	152	352	476
20	0.36	16	179.56	-14.44	-97.6	168.643	-0.20	-3.93	-1.05	100	226	388
	Total Sum of Square(SST)			Regression Sum of Square (SSR)			Coefficient of Determination (R^2)			Standard deviation of errors(S)		
	4019.2	5302	4261.2	4004.4	5188.4	4128.2	0.996	0.979	0.969	2.22	6.15	1.91

* Residual error (%) = ((measured value- residual value) / (residual value)) x100%

Table 4: Comparison of predicted, effectiveness and measured values and errors for accumulated strain pavement mixtures with and without ash percents.

Ash (%)	Accumulated micro-strain											
	Measured			Predicted			Residual			Error Sum of Square(SSE)		
	5°C	25°C	40°C	5°C	25°C	40°C	5°C	25°C	40°C	5°C	25°C	40°C
0	4081.9	5540	10412	4085	5551	10335	-3.1	-11	77	9.61	121	5929
5	2384.9	2894	6106	2382.4	2859	6288	2.55	35	-182	6.50	1225	33124
10	1175	1170	3587	1176.4	1203	3491	-1.4	-33	96	1.96	1089	9216
15	468.1	591	2000	467.2	583	1944	0.95	8.0	56	0.90	64	3136
20	255.6	1000	1600	254.6	999	1647	1.0	1.0	-47	1	1	2209
	Measured-Mean			Predicted-Mean			Residual Error (%)*			Accumulated strain-Effectiveness (%)		
0	5802317	10896601	32160241	5802297	10894101	32106627	-0.076	-0.198	0.745	-	-	-
5	506659.2	429025	1863225	506639.3	426525	1809611	0.107	1.224	-2.894	-41.57	-47.76	-41.36
10	248103.6	1142761	1331716	248083.6	1140261	1278102	-0.119	-2.743	2.750	-71.21	-78.88	-65.55
15	1452025	2715904	7513081	1452005	2713404	7459467	0.203	1.372	2.881	-88.53	-89.33	-80.79
20	2009306	1535121	9865881	2009286	1532621	9812267	0.393	0.100	-2.854	-93.74	-81.95	-84.63
	Total Sum of Square(SST)			Regression Sum of Square (SSR)			Coefficient of Determination (R^2)			Standard deviation of errors(S)		
	10018412	16719412	52734144	10018392	16716912	52734011	1.0	0.999	0.999	2.58	28.87	133.68

* Residual error (%) = ((measured value- residual value) / (residual value)) x100%

6.1 Air Voids Models

The improvements, as the air voids in Fig. 6 and Table 2, were 57.29, 70.73, and 91.43 for 5, 25, 40°C at 5% fraction; 78.54, 97.56, and 122.85 for 5°C, 25°C, and 40°C at 10% fraction, 65, 87, and 102.85 for 5°C, 25°C, and 40°C at 15 fraction, and reduced to 15.63, 21.95, and 31.43 at 20% fraction, being a reduction small compared to the maximum improvement at 10% fraction. The air voids improvement of fixable pavement mixture ranged from 57.29 to 78.54 for 5°C, 70.73 to 97.56, at 25°C, and 91.43 to 122.85 for 40°C to 20% fraction. The predicted models for air voids are as presented in Eqs. (4), (5), and (6):

$$Av = 4.070 + 0.776\ Vf - 0.036\ Vf^2 \quad (4)$$

$$Av = 3.522 + 0.816\ Vf - 0.038\ Vf^2 \quad (5)$$

$$Av = 4.802 + 0.718\ Vf - 0.034\ Vf^2 \quad (6)$$

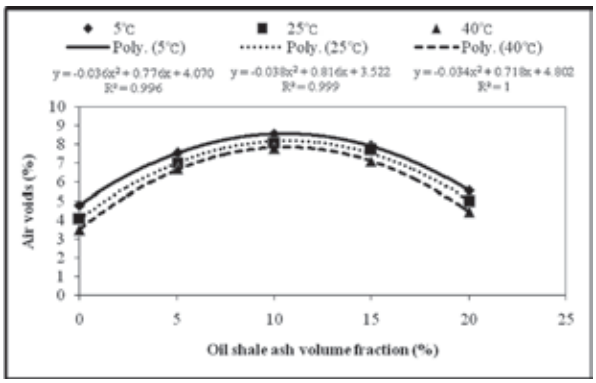

Figure 6: Effect of oil shale ash volume on air voids of asphalt pavement mixtures.

The air voids prediction using the above equations agreed favourably with the test results, as shown in Table 2. The production error runs below are 0.13%, 1.63%, and 6.96% at 5°C, 25°C, and 40°C, respectively.

6.2 Stiffness Modulus Models

The improvements, as the stiffness modulus in Fig. 7 and Table 3, were 96, 181, and 253 for 5% fraction, 158, 296, and 429 for 10% fraction, 152, 352, and 476 for 15% fraction, and 100, 226, and 388 for 20% fraction at 5°C, 25°C, and 40°C temperatures, and reduced at 20% fraction, being a reduction small compared to the maximum improvement at 15% fraction. The stiffness modulus improvements of fixable pavement mixture ranged from 96 to 158 for 5°C, 181 to 352, at 25°C, and 253 to 476 for 40°C to 20% fraction. The regression models of the stiffness modulus(*Sm*) are measured as seen in Eqs. (7), (8), and (9):

$$Sm = 49 + 12.96\ Vf - 0.52\ Vf^2 \quad (7)$$

$$Sm = 24.4 + 13.76\ Vf - 0.52\ Vf^2 \quad (8)$$

$$Sm = 15.88 + 11.28\ Vf - 0.394\ Vf^2 \quad (9)$$

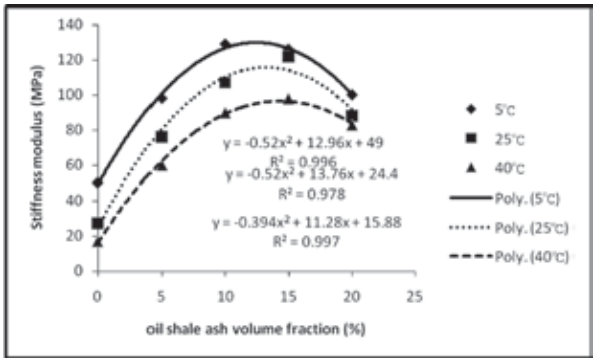

Figure 7: Effect of oil shale ash volume on stiffness modulus of asphalt pavement mixtures.

The air voids prediction using the above equations agreed favourably with the test results, as shown in Table 3. The production error runs below are 2.78%, 5.24%, and 3.89% at 5°C, 25°C, and 40°C, respectively.

6.3 Accumulated Strain Models

The reductions as the accumulated strain in Fig. 8 and Table 4 were 41.57, 47.76 and 41.36 for 5% fraction71.21, 78.88, and 65.55 for 10% fraction, 88.53, 89.33, and 80.79 for 15% fraction, and 93.74, 81.95, and 84.63 for 20% fraction at 5°C, 25°C, and 40°C temperatures, and increase at 20% fraction, being a reduction small compared to the maximum improvement at 5% fraction. The accumulated strain reduction of fixable pavement mixture ranged from 41.57 to 93.74 for 5°C, 47.76 to 81.95, at 25°C, and 41.36 to 84.63 for 40°C to 20% fraction. Models of accumulated strain (*As*) are shown below in Eqs. (10), (11), and (12):

$$As = 4085 - 390.2\ Vf + 9.934\ Vf^2 \quad (10)$$

$$As = 5552 - 642.3\ Vf + 20.73\ Vf^2 \quad (11)$$

$$As = 10336 - 934.2\ Vf + 24.98\ Vf^2 \quad (12)$$

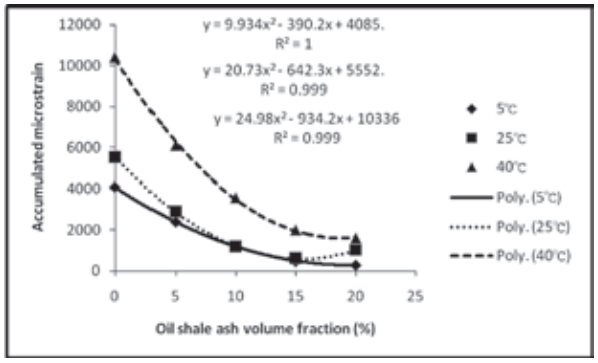

Figure 8: Effect of oil shale ash volume on accumulated strain of asphalt pavement mixtures.

The air voids prediction using the above equations agreed favourably with the test results, as shown in Table 4. The production error runs below are 0.119%, 2.743%, and 2.854% at 5, 25, and 40°C, respectively.

7. Conclusions

The following conclusions were drawn:

- The addition of a certain percentage of oil shale ash (10 – 15%) improves the stiffness of bituminous mixtures because it increases the adhesive forces between the asphalt and the aggregate. Thus, the mechanical interlocking between the aggregate particles is improved by this treatment.
- Temperature has a significant effect on resilient modulus and creep stiffness, so as temperature decreases, resilient and stiffness modulus increase. Accumulated strain increases if the oil shale ash is within the optimum, then decreases with the increase in oil shale ash content above the optimum.
- Stiffness decreases with time for different oil shale ash contents at different levels of temperature. Maximum stiffness was found at 5oC and ash was at 10%.
- The predictive model is statistically significant with a coefficient of multiple determinations R2 of 0.715; also, the model and the included variables had a high level of significance (0.002); there is a decrease in the rutting potential of the asphaltic-ash mixtures as the amount of ash increases.

Acknowledgment

Authors sincerely thank The Founder Professor of Engineering Imad L. AL-Qadi, PhD, PE, Dist. M. ASCE, Illinois Center for Transportation, Director, Advanced Transportation Research and Engineering Lab, Director, for his constructive encouragement and support to carry this experimental investigation.

References

[1] Al-Massaid, H., Taiser Khedaywi, and Mohammed Smadi. 1989. Properties of Asphalt-Oil Shale Ash Bituminous Mixtures under Normal and Freeze-Thaw Condition. Transportation Research Record (TRB), National Research Council, Washington, D.C, Vol. 1228, PP.54-62.

[2] Annual Book of ASTM Standards, (ASTM D1559) 1990. Road and paving materials. Vol.4.03, pp. 206-211.

[3] Biligiri Krishna P., Kaloush Kamil E., Mamlouk Michael S., and Witczak Matthew W., 2007. Rational Modeling of Tertiary Flow for Asphalt Mixtures. Transportation Research Record: Journal of the Transportation Research Board, No. 2001, Transportation Research Board of the National Academies, Washington, D.C., pp. 63–72. DOI: 10.3141/2001-08.

[4] Carpenter Samuel H. and William R. Vavrik,1999. Repeated Triaxial Testing During Mix Design for Performance Characterization", Transportation Research Record 1767, Paper No. 01-3219, Paper No. 01-3219

[5] Gui-ping He a,b, Wong Wing-gun, 2007. Laboratory study on permanent deformation of foamed asphalt mix incorporating reclaimed asphalt pavement materials. Construction and Building Materials, Vol. 21, PP.1809–1819.

[6] Khashayer Hadipour and Kenneth O. Anderson. 1972. An Evaluation of Permanent Deformation and Low Temperature Characteristics of Some Recycled Asphalt Concrete Mixtures. Association of Asphalt Paving Technologists, PP. 615-644.

[7] Krishna P. Biligiri, Kamil E. Kaloush, Michael S. Mamlouk, and Matthew W. Witczak, 2007. Rational Modeling of Tertiary Flow for Asphalt Mixtures. Transportation Research Record: Journal of the Transportation Research Board,No. 2001, Transportation Research Board of the National Academies, Washington, D.C., pp. 63–72. DOI: 10.3141/2001-08.

[8] Method for Determination of Resistance to Permanent Deformation of Bituminous Mixtures Subject to Unconfined Universal Loading (BSI), 1995. BSI, Part111, PP. 1-8.

[9] Method for Determining Resistance to Permanent Deformation of Bituminous Mixtures Subject to Unconfined Dynamic Loading. 1996. DD226, PP. 1-6.

[10] Ministry of Energy & Mineral Resources., 1995. Natural Resources Authority (Basic Information on Oil Shale in Jordan), Amman-Jordan, Feb., pp 3-13.

[11] Ministry of Public Works & Housing Directorate of Planning & Development Specification. 1991. Highway and Bridge Construction., Sec. 4.01, Table 4.1, Amman, PP.4-5.

[12] Mix Design Method for Asphalt Concrete and Other Hot Mix Types. 1976. Asphalt Institute, MS-2, PP. 17-32.

[13] Saad Abo-Qudais and Ibrahem Shatnawi., 2007. "Prediction of bituminous mixture fatigue life based on accumulated strain", Construction and building Materials, Vol. 21, PP. 1370-1376.

[14] Universal Testing Machine (UTM) 2 Manual, 1996.Test no: 036. Static Uniaxial Loading Strain Test. K B de Vos, Oct.-99. BSI, PP.1-23.

[15] Vacin Ota J., Stastna Jiri, and Zanzotto Ludo, 1999. Creep Compliance of Polymer-Modified Asphalt, Asphalt Mastic, and Hot-Mix Asphalt. Transportation Research Record 1829, Paper No. 03-3152.

[16] Van de Loo P. J., 1974. Creep Testing, A Simple Tool to Judge Asphalt Mix Stability. Association of Asphalt Paving Technologists (AAPT), PP. 253-284.

[17] Van de Loo P. J., 1976. Practical Approach to the Prediction of Rutting in Asphalt Pavements: The Shell Method. Koninklijke / Shell-Laboratorium, Anesterdam,pp.15-21.

[18] Young-Chan Suh, Nam-Hyun Cho, Sungho Mun, 2011. "Development of mechanistic–empirical design method for an asphalt pavement rutting model using APT.", Construction and Building Materials, Vol.25, pp. 1685–1690.

JJEES
Jordan Journal of Earth and Environmental Sciences

Volume 6, Number 2, December, 2014
ISSN 1995-6681
Pages 77- 83

Late Cretaceous Muwaqqar Formation Ammonites in Southeastern Jordan

Amani M. Khrewesh, Abdullah Abu Hamad and Abdulkader M. Abed*

Department of Geology, University of Jordan, Amman, Jordan

Received 27 January, 2014; Accepted 25 October, 2014

Abstract

Three Maastrichtian ammonite species belonging to two families, were recorded in the upper part of Muwaqqar Formation (MCM). Two planispiral species belong to the family, namely, Sphenodiscidae, Sphenodiscus lobatus and Libycoceras ismaeli while the third, straight species, belongs to Baculitidae family; Baculites sp. The Paleocene strata are represented by 6 m in the measured section below the Rijam Formation. This might indicate a long erosional unconformity at the end of the MCM which was documented by other workers several tens of kilometers west of the study area. The erosional unconformity is also supported by the presence of tree trunks at the Muwaqqar-Rijam formations contact. Microfacies analysis indicates that the upper Muwaqqar Formation in the Jebal Khuzayma area was deposited in an offshore, open marine conditions affected by upwelling currents. This is evidenced by the abundant planktonic fauna exceeding benthic fauna, the abundant matrix represented by lime mudstone, and the relatively high phosphate particles and organic matter.

Keywords: Ammonites, microfacies, Muwaqqar Formation, Jebal Khuzayma, southeastern Jordan.

1. Introduction

The Muwaqqar Formation (MCM) crops out extensively towards the eastern parts of the Jordanian plateau and covers wide areas east of the Desert Highway, the Risha area and the extreme northern Jordan (Bender, 1974; Powell, 1989; Abed, 2000). It consists of a uniform soft chalk - marl material throughout its thickness all over the country where the famous oil shale deposits of Jordan occupy its lower part. The age of the MCM is Maastrichtian – Paleocene (Yassini, 1979; Powell, 1988).

During the deposition of the MCM, the Jordan and the adjacent areas witnessed a major marine transgression transforming the area into the outer continental shelf (Powell and Moh'd, 2011). Thus, the MCM was deposited in a pelagic environment evidenced by the abundant planktonic foraminifera especially in northern Jordan (e.g. Yassini, 1979). The formation of the oil shale seems to have been associated with cold, deep upwelling currents from the Neo-Tethys onto the area which fertilized the photic zone water with nutrients and enhanced bioproductivity and thus organic matter deposition (Abed and Amireh, 1983; Almogi-Labin et al, 1993; Abed, 2013).

Ammonite studies in Jordan are rather limited. Al-Harithi and Ibrahim (1992) had studied four cephalopod species from the Maastrichtian of Wadi Usaykhim outcrop section, Al Azraq area in east Jordan. One species is new: *Eutrephoceras azraqensis*. The other three taxa are *Sphenodiscuss* cf. *lobatus*, *Libycoceras ismaeli* and *Baculites ovatus*. Nazzal and Mustafa (1993) had studied the Upper Cretaceous ammonites from north Jordan. They described the genera *Acanthoceras*, *Neolobites*, *Baculites*, *Pseudoshloenbachia*, *Pachydiscus* and *Libycoceras* from the Wadi Shueib, Wadi As Sir Limestone, Wadi Umm Ghudran, Amman Silicified Limestone and Muwaqqar formations. Makhlouf et al. (1996) had studied the Ajlun group in three sites in Jordan; they found some ammonites species in two sites, Ras en Naqab section: aff *Metoiceras* sp., and Wadi ben Hammad section: *Vascoceras* aff. Cf. *cauvini,* aff *Schloenbachia* spp., aff *Tropitiodes* sp., *Neolobites* sp., aff *vascoceras* spp. These ammonites are older than those of the study area because they all belong to the Ajlun Group.

The study area is located at Jebal Khuzayma, (30 ° 33` N, 36 ° 20` E) in south eastern Jordan (Fig. 1). The study area is situated 160 km (aerial) south east of Amman and some 40 km SW of Bayer. Jebal Khuzayma can be reached from Amman via the Desert Highway, Suwaqa-Tuba road then Azraq –Jafr Highway.

Figure 1: Location map of the study area in southeastern Jordan. The inset map is a geological map of the study area. (Modified from Kherfan, 1987).

* Corresponding author. e-mail: *amabed43@gmail.com*

The aim of this work is a) try to identifying and classifying the ammonites in the Muwaqqar Chalk Marl Formation (MCM), b) determine the age of MCM in SE Jordan, and c) to deduce the depositional environment of the MCM through its microfacies.

2. Geological setting

By the onset of the Cenomanian, early Late Cretaceous, a global marine transgression took place, and almost all the Eastern Mediterranean, including Jordan, was flooded (Sharland et al. 2001; Haq and Qahtani, 2005; Powell and Moh'd, 2011). Jordan became part of the shallow, epeiric, tropical Neo-Tethys continental shelf and consequently, the scene for carbonate production and deposition. This essentially carbonate regime continued from the Cenomanian throughout the Eocene, a duration of around 65 million years with the deposition of more than 1000 m of carbonates and associated sediments in north Jordan decreasing to the south and southeast (Powell, 1989; Abed 2000; Powell and Moh'd, 2011).

This regime has been subdivided into two groups: lower or Ajlun Group and upper or Belqa Group (Burden, 1959). Both groups were further subdivided into formations especially by Masri (1963) as shown in Table (1). The Ajlun Group is of Cenomanian - Turonian age. It consists of alternating limestone/dolomite and marl horizons of varying thicknesses. Some of these horizons are highly fossiliferous with ammonites especially in the Hummar through Wadi As Sir Limestone Formations (Bender, 1974).

Table 1: Nomenclature of the Upper Cretaceous rock units in Jordan using the geographic names of the formation without the lithology (Masri, 1963; El-Hiyari, 1985; Powell, 1989).

Age		Group	Formation Member	
Tertiary	Eocene	Belqa	Shallala (WSC)	
			Rijam (URC)	
	Paleocene		Muwaqqar (MCM)	
Late Cretaceous	Paleocene - Maastrichtian		Al-Hisa (AHP)	Qatrana Phosphorite
				Bahiyya Coquina
				Sultani Phosphorite
	Campanian – Santonian		Amman (ASL)	
	Coniacian		Ghudran	Dhiban Chalk
				Tafila
				Mujib chalk
	Turonian	Ajlun	Wadi As Sir	
			Shueib	
	Cenomanian		Hummar	
			Fuheis	
			Na'ur	
Early Cretaceous	Aptian - Albian	Kurnub (Hathira) Sandstone Group		

The Belqa Group overlies the Ajlun Group and extends from the Coniacian through the Eocene. It consists of chert, phosphorite, and oil shale with limestone, marl, and chalk. The deposition of chert, phosphorite, and oil shale was taken to indicate prevailing of cold upwelling currents from the Neo-Tethys proper in the north onto its southern continental shelf, which led to the deposition of these rocks (Abed et al., 2005; Abed, 2013). These conditions remained the same until about the upper Eocene when the Neo-Tethys Ocean regressed due to the start of continent-continent collision between the Afro-Arabian Plate in the south and the Eurasian Plate in the north. (Powell, 1989; Abed and Sadaqah, 1998; Sharland et al.,, 2001; Haq and Qahtani, 2005; Abed, 2013).

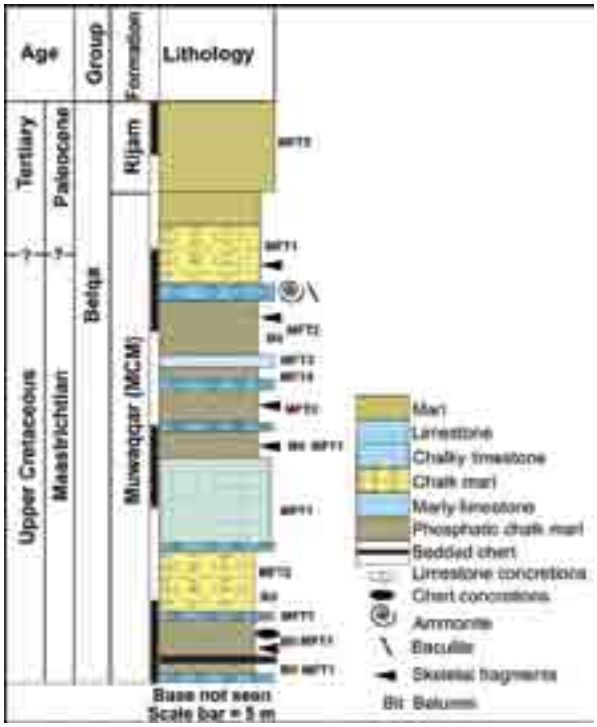

Figure 2: Columnar section measured in the study area showing the upper Muwaqqar Formation with overly base of the Rijam Formation.

The Belqa Group consists of the following formations from older to younger (Table 1): Ghudran, Amman, Al-Hisa, Muwaqqar, Umm Rijam and Shallala Formations. The Muwaqqar Formation (MCM) is made essentially of chalk - marl with varying thicknesses decreasing form the northern parts of Jordan to its south. It is characterized by the abundant organic matter at its lower part known locally as the "oil shale horizon" giving it a black to dark colors.

Jebal Khuzayma are the product of uplift along the Karak-Faiha Fault zone running from just east of the Dead Sea into a southeastern direction into Saudi Arabia (Fig. 1). Jebal Khuzayma consists of the Muwaqqar Formation at their base and ending up with the Rijam Formation. However, the base of the Muwaqqar Formation is not exposed in the study area and only the upper part is cropping out overlain by Rijam Formation. Fig. 2 shows the columnar section measured in the study area. Its lithology consists of phosphatic bituminous chalk marl, bituminous chalk marl, marly limestone, limestone, chalk marl and marl with abundant concretions.

3. Material and methods

Forty nine (49) ammonite samples were collected from the study area during the field work during the year 2010. The collected samples include well preserved, complete shells as well as fragments of shells. All the ammonite samples were found within the uppermost part of the MCM as shown in Fig. 2. Fig. 3 Is a field photo showing the position of the ammonite locality within the columnar section. The samples were treated with a soft brush and water to remove any material adhering to it. They were then stored at the Department of Geology, the University of Jordan.

Twelve samples were collected from the cropping part of the MCM for microfacies analysis. The samples were chosen to represent the variations in the lithology along the measured section (Fig. 2).

Figure 3: Field photo showing the position of the ammonite samples within concretion level sex towards the top of the Muwaqqar Formation. Amani for scale = around 1.65 m

Ammonite systematic paleontology:

The ammonite specimens were assessed on the base of preserved morphological characters which include the most frequently used features: the suture line, shell coiling, whorl cross section and shell ornamentation (Arkell, 1990; Miller et al. 1990). The paleontological study of the ammonite fauna led to identify three species belonging to two families. The taxonomic list, including a description of the taxa, is as follows;

Order Ammonoidea Zittel, 1884
Suborder Ammonitina Hyatt, 1889
Superfamily Acanthocerataceae Hyatt, 1900
Family Sphenodiscidae Hyatt, 1900
Genus *Sphenodiscus* Meek, 1871
Sphenodiscus lobatus (Tuomy, 1856).
Fig. 4a and b, Fig. 5a

Table 2: Dimensions of three samples representing Sphenodiscus lobatus

Sample no.	Diameter (mm)	Whorle Height (mm)	Whorle Width (mm)
1	105	55	?
2	150	45	40
3	195	80	50

Occurrence: Masstrichitian of Africa, Europe, both Americas and Jordan (Al-Harithi and Ibrahim, 1992; Ifrim et al. 2010).

Synonyms:

1852*Ammonites lenticularis* Owen. - Owen : p.579 pl. 8, fig. 5
1854 *Ammonites lobata* Tuomey. - Tuomey : p.168
1995 *Sphenodiscus lobatus* Tuomey. - Cobban & Kennedy : p.12 figs. 6.2-6.3, 8.4, 8.6-8.11, 12.18-12.19, 16.16-16.17
1996 *Sphenodiscus lobatus* Tuomey. - Kennedy & Cobban : p.802 figs. 2.4-2.6, 2.13-2.14, 2.19-2.21
1997 *Sphenodiscus lobatus* Tuomey. - Kennedy et al. : p.4 figs. 3-8,9a-i,10
2005 *Sphenodiscus lobatus* Tuomey. - Ifrim et al. : 54, 55, 57, 59 figs. 4d-g; 5a-d, 6a-e, 7d-f

Material: One well preserved external shell and four well preserved internal moulds (three entire samples and two fragmented) found in the final concretion level of Jebal Khuzayma section.

Description: The specimens are involute. The whorl section is triangular; the ventral side is thinner than the umbilicus. The whorl height is greater than the whorl width. The shell is smooth (there is no ornamentation). The suture line is well preserved (belongs to pseudoceratites suture), the saddles are entire and elongated and the lobes are highly teethed. The saddles and lobes tend to become smaller from the venter toward the umbilicus.

Dimensions: specimens differing in size, but height of the whorl generally exceed 4.5cm; width 4-5cm, diameter 10-20cm (Table 2).

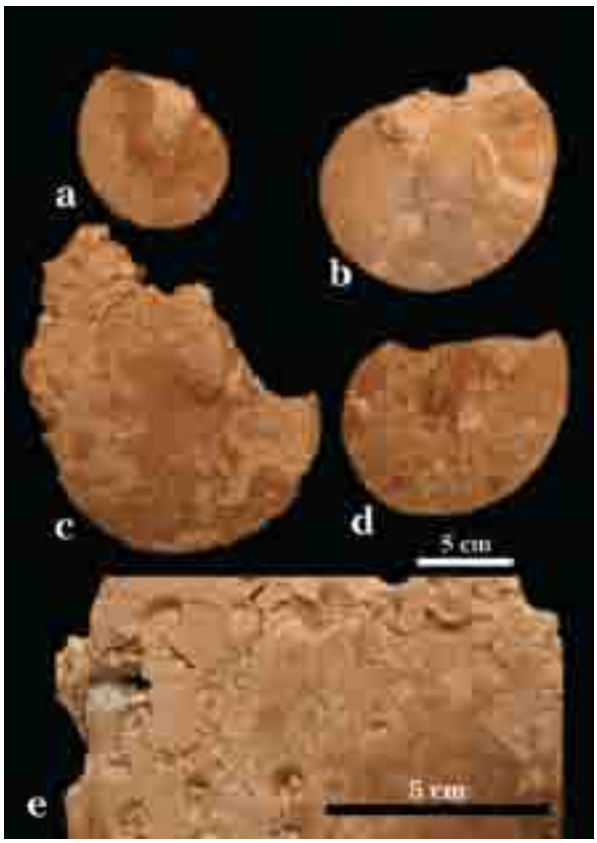

Figure 4: a and b Sphenodiscus lobatus (Tuomy, 1856) lateral view; c and d *Libycoceras ismaeli* (Zittel, 1895) lateral view; e) *Sphenodiscus lobatus* (Tuomy, 1856) close view to show the suture line. The photos are smaller than the natural size which is shown in Table 2.

Genus Libycoceras Hyatt, 1900
Libycoceras cf. ismaelis (ZITTEL 1884)
Fig.4c and d, Fig.5b and c.

Synonyms:

cf. 1884 Sphenodiscus ismaelis - ZITTEL, p. 451; fig. 63 1.
cf. 1902 Libycoceras ismaeli ZITTEL - QuAs, p. 302; Plate 29, figs. 3-7; Plate 30, figs. la-b.
cf. 1996 Libycoceras ismaelis (ZITTEL) - WIESE et al., p. 109; Plate 2, fig. 1 (and synonymy).
cf. 1999 Libycoceras ismaelis (ZITTEL) var. soudanense PEREBASKINE, ZABORSKI & MORRIS, text-figs. 4/9-10.

Material: two samples with external shell and 6 well preserved internal moulds (three entire samples and five fragmented)

Description: the specimens are involute. The whorl section is triangular, the ventral side is thinner than the umbilicus. The whorl height is greater than the whorl width. The shell is smooth (there is no ornamentation) the suture line is well preserved (belongs to pseudoceratites suture), the saddles are entire and rounded and lobes are highly teethed. The saddles and lobes tend to become smaller from the venter toward the umbilicus.

Dimensions: specimens differing in size, height of the whorl range from 5-6cm; width 3-4cm, diameter 14-15.5cm (Table 3).

Table 3: Dimensions of three samples representing *Libycoceras ismaeli*

Sample no.	Diameter (mm)	Whorle Height (mm)	Whorle Width (mm)
1	105	55	?
2	150	45	40
3	195	80	50

Occurrence: Masstrichtian of Africa, Europe, Americas, Nigeria, Libya and Jordan (Zaborski, 1982; Al-Harithi and Ibrahim, 1992; Amard, 1996; Ifrim and Stinnesbeck, 2010).

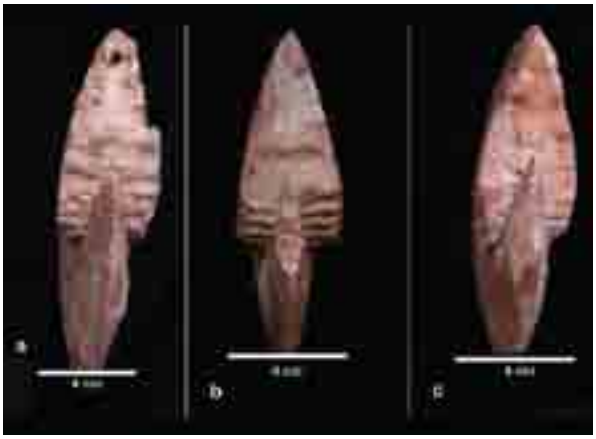

Figure 5: a Sphenodiscus lobatus (Tuomy, 1856) ventral view; b and c) Libycoceras ismaeli (Zittel, 1895) ventral view. The natural size of the specimens can be seen in Table 3.

Suborder Lytoceratina Hyatt, 1889
Superfamily Turrilitaceae Meek, 1876
Family Baculitidae Meek, 1876
Genus Baculites (Lamark, 1799)
Baculites sp. Lamark, 1799.
Fig. 6 a and b

Synonyms:

1786 Homaloceras Hubsch, 1786 (non. binom.), p. 110.
1861 Baculites faujasi Lamarck. – Binkhors, 1861, p. 33
1925 Baculites vertebralis Lamarck. – Diener, 1925, p. 40
1993 Baculites cf. vertebralis Lamarck. - Ward & Kennedy, 1993, p. 114, pl. 7
1995 Baculites sp. C . - Cobban & Kennedy : p. 22, 24 fig. 15.1, 15.5, 16.1-16.6, 16.10-16.12, 16.25-16.27, 16.31-16.38

Material: two large and thirteen small, incomplete samples.

Description: the specimen is a part of a fragmented phragmocone. The cross section is ovate, smooth surface, some samples have arcuate ribs. The ammonitic suture line is moderately complex, the saddles and lobes are teethed.

Occurrence: Masstrichtian of Jordan. Baculites were recorded from Egypt, Mexico, Palestine and North America; it indicates Campanian-Maastrichtian age (Ifrim et. al., 2010). They were recorded in Jordan in Wadi Usaykhim, Al Azraq area as of Maastrichtian age (Al-Harithi and Ibrahim, 1992).

Age of the section studied

Sphenodiscidae ammonites were widespread during the Maastrichtian, with records from localities in Africa, Europe and both Americas (Turekian and Armstrong, 1961; Kennedy and Cobban, 1996; Landman et al., 2004).. Outside North America, however, their record is rather scattered. The genus is known from Maastrichtian sediments in Western Europe (Hancock, 1967; Bandel, Landman and Waage, 1982; Kennedy, 1986), in the lower Maastrichtian of India and in the upper Maastrichtian of Poland and Bulgaria, Madagascar and West Africa. The most widespread species of Sphenodiscus is, however *Sphenodiscus lobatus*. Zaborski (1982) suggested that the Sphenodiscidae originated in the African epicontinental seas from unknown ancestor of Campanian age. Sphenodiscids dispersed and radiated during the latest Campanian and Maastrichtian, until they went extinct at or near the Cretaceous-Paleogene boundary (Ifrim and Stinnesbeck, 2010). *Libycoceras ismaeli* (Zittel) has been reported from the upper Maastrichtian of the Algerian Sahara, North Africa and Niger, and it has been reported from the upper Campanian in the Middle East and the Eastern desert, Egypt (Amard, 1996). The two species were recorded in Jordan in Wadi Usaykhim, Al Azraq area as Maastrichtian age (Al-Harithi and Ibrahim, 1992).

Figure 6: a, b: Baculites sp. (Lamark, 1799). Lateral view.

Baculites were recorded from Egypt, Mexico, Palestine and North America indicating Campanian-Maastrichtian age (Ifrim et. al., 2010). They were recorded in Jordan in Wadi Usaykhim, Al Azraq area as of Maastrichtian age (Al-Harithi and Ibrahim, 1992).

Microfacies analysis

Twelve samples representing the nearly 30 m measured section in Jebal Khuzayma in southeastern Jordan. It should be mentioned that almost all these facies, in varying proportions, are matrix (micrite) supported.

MFT1: Phosphatic foraminiferal wackestone

This microfacies represents several horizons (Fig. 2) with different thickness. It consists of phosphate particles (peloids, intraclasts and skeletal fragments) and foraminiferal tests and fragments supported by lime mudstone (matrix) stained dark because of the presence of organic matter (Fig. 7a, b and c). Depending on the horizon, the phosphate particles range is 4 – 13%, foraminiferal tests and fragments 22 – 39%, and the matrix 49 – 72%. The identified foraminifera belongs

to the following families Bulminidae, Heterohelicidae, Rotaliporidae, and others such as Trochospiral foraminifera. Champers are filled with micrite or sparite cement. Some benthic foraminifera tests are also found in at least one horizon at mid section within this microfacies. The abundant matrix as well as planktonic foraminifera would indicate the deposition of this microfacies in a calm, offshore, open marine conditions (Flugel, 2004). The presence of appreciable amounts of phosphatic material and organic matter might indicate that upwelling currents were still reaching the study area (Almogi-Labin et al, 1993; Abed 2013). However, the non transformation of these deposits into true phosphorites is possibly due to depth of water column which caused no reworking and winnowing of deposited sediments (Glenn et al., 1994; Abed and Sadaqah, 1998).

Figure 7: MFT1 Phosphatic foraminiferal wackestone. a) represents the lowest 4 m of the section Fig. 2, b) from the 4.5 m marly limestone, 10 m from the base, c) From the 60 cm limestone horizon mid section. p, phosphate particles; f. foraminiferal test; m, matrix. Plane polarized light (PPL).

MFT2: Laminated phosphatic foraminiferal packstone

MFT2 is essentially similar to MFT1 except that the constituent particles and the matrix are laminated (Fig. 8 a, b and c). Small fossils and phosphate particles have their longer axes nearly parallel to bedding. The foraminiferal tests can be up to 48% by volume of the thin section while the phosphate particles are up to 12%. Lamination most probably is due to compaction in a calm offshore environment without reworking.

MFT3: Lime mudstone

This microfacies consists of lime mudstone with less than 10% highly fragmented fossils and phosphate particles (Fig. 9a). This microfacies is restricted to one horizon only.

Figure 8: Laminated phosphatic foraminiferal packstone MFT2. Note long axis of the phosphate particles and some fossil tests are parallel to bedding. a) from the 4.5 m chalk marl, 6 m above the base, b) represents 3.5 m phosphatic marl horizon mid section, c) from a 4 m greyish, laminated phosphatic-rich, underlying the upper concretion horizon.
p, phosphate particles; f, foraminiferal tests; m, matrix. Plane polarized light (PPL).

MFT4: Phosphorite grainstone

This microfacies is also restricted to one horizon and is almost completely made of phosphate intraclasts with seldom fossils (Fig. 9b). The phosphate particles are of various sizes and shapes bounded by sparry calcite. Fossils and fossil fragments are rather rare. for these characteristics, this microfacies looks similar to the phosphorite grainstone of the Al-Hisa Phosphorite Formation (e.g. Abed and Sadaqah, 1998). The abundant phosphate intraclasts and the lack of matrix indicate a higher energy regime compared with the environments of previous microfacies. A higher energy regime is possibly needed to produce such concentrates of phosphorite through reworking and winnowing (Abed, 2013).

MFT5: Foraminiferal packstone

This microfacies represents the lowest five metres of the Rijam Formation overlying the MCM (Fig. 9c). It is composed of 26% micrite and 74% highly fragmented foraminifera belong to the following families: Heterohelicidae (pl.4f), Rotaliporidae? (pl.5f) and fragmented foraminifera belong to the Globigerinacea superfamily, with calcite cement filling the chambers. Other undefined foraminifera is also present. Please note the non presence of phosphate particles as compared with the microfacies of the MCM Formation. This microfacies is interpreted to have been deposited in a calm, offshore, open marine environment. The lack of phosphatic material might be explained by the waning upwelling current in this part of the eastern Mediterranean. The Rijam Formation, throughout Jordan, is known to contain very minor phosphorite especially in the eastern most parts of the country. For more details, see Abed (2013).

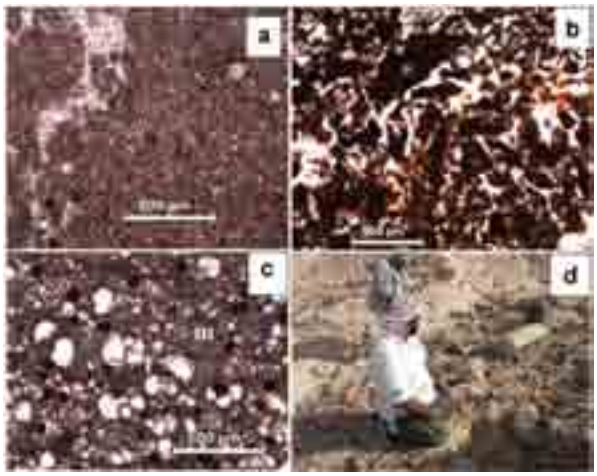

Figure 9: a) Lime mudstone MFT3, from the 4 m chalk marl towards the top of the section, b) Phosphorite grainstone MFT4, dominated by phosphate intraclast cemented by calcite at mid section. C) Foraminiferal packstone, with phosphate particles making the base of the Rijam Formation, black circles are air pubbles. f, foraminiferal tests; m, matrix. Plane polarized light (PPL). D) Field photo of the tree trunks (not in situ) in Jebal Khuzayma several metres below the MCM-URC formations contact, N. Hmaidan for a scale.

4. Discussion

The studied section represents the upper part of the MCM Formation because its base is not cropping out. However, the section is the best at Jebal Khuzayma in SE Jordan. The microfacies analysis shows a rise in sea level compared with the underlying Al-Hisa Phosphorite Formation (AHP). The AHP, in central and south central Jordan, is characterized by small basins in an essentially onshore environments indicated by the conspicuous oyster buildups and the rarity of planktonic fauna (e.g. Abed and Sadaqah, 1998). The AHP was then followed by a regional sea level rise documented throughout the eastern Mediterranean (e.g. Almogi-Labin et al. 1993; Powell and Moh'd, 2011, 2012). In the study area, this is indicated by the abundant planktonic foraminifera and the high percentage of lime mudstone in the rocks investigated (Wilson, 1975; Flugel, 2004). Consequently, the study area seemed to have formed part of the open shelf environment with relatively deeper water, thus differentiated it from the small basins in central Jordan such as El-Lajjun.

The presence of relatively higher content of organic

matter and phosphatic material, in the investigated section compared with upper MCM in central Jordan, might be taken to indicate the ongoing activity of upwelling currents onto the area. Upwelling currents spread deep, cold marine water on the sea surface of the continental shelf usually rich in nutrients bioproductivity in the photic zone, the upper 100-200 m of the sea water column. Under such upwelling conditions, higher than normal organic matter is deposited which consequently leads to the diagenetic formation of phosphatic material (Burnett, 1990; Almogi-Labin et al., 1993; Glenn et al, 1994). The non transformation of the phosphate material into high grade phosphorites can be explained by the absence of reworking and winnowing, very much like the recent phosphate deposits of the Peru-Chili shelf documented by Burnett (1990). The phosphate deposits in the Peru-Chili shelf consist of small and large phosphate nodules embedded in an organic rich lime mud.

Based on ammonites, a Maastrichtian, Late Cretaceous age is given to the studied section of the MCM in Jebal Khuzayma in southeastern Jordan. Other authors arrived to the same conclusion much earlier (e.g. Al-Harithi and Ibrahim 1992; Nazzal and Mustafa (1993). It is not possible, in this work, to assign a shorter age duration for the investigated section; e.g. Lower or Upper Maastrichtian. Fig. 2 clearly shows that studied section belongs to the upper part of the MCM immediately underlying the Rijam Formation of the Eocene. Moreover, the Maastrichtian ammonites are only 6 m below the contact with the Rijam Formation (Fig. 2), leaving, at best, 6 m of strata to represent the Paleocene. The MCM is well known, for a long time to be of Maastrichtian – Paleocene age (e.g. Bender, 1974; Yassini, 1980; Powell, 1989). So, how to solve this problem with Paleocene strata and the underlying upper Maastrichtian and the overlying Rijam Formation in this part of the country? Al-Mashagbah (2012), amongst others, documented the presence of at least two unconformities (gaps) in the MCM in southern Jordan (around 50 kilometers east of Jurf Ed Darawish), one at the base of the Paleocene and another at its top. Furthermore, abundant tree trunks are wide spread at the contact between the MCM and the Rijam Formation in Jebal Khuzayma area and further southeast (Fig. 9d and Ammar Khammash pers. Comm. 2012). The presence of the trees below the Rijam Formation indicates a long subaerial exposure towards the top of the MCM in southeast Jordan, thus supporting the findings of Al-Mashagbah (2012) and indicating that a considerable part of the Paleocene might have been eroded through this subaerial event. In the authors opinion, the Jebal Khuzayma and the area southeast of it needs a detailed micropaleontological investigation to solve the above discussed stratigraphic problems during the Maasrichtian-Eocene.

5. Conclusions

1. The paleontological study led to identify three ammonite species belonging to two families, recorded in the upper part of Muwaqqar Formation. Two planispiral species belong to the family Sphenodiscidae (Hyatt, 1900); Sphenodiscus lobatus (Tuomy, 1856) and Libycoceras ismaeli (Zittle, 1895).The third one (straight species) belongs to Baculitidae family (Meek, 1876); Baculites sp. (Lamark, 1799).
2. The age of the measured section is Maastrichtian and it was not possible to obtain a shorter duration age; i.e. lower or upper Maastrichtian.
3. The Paleocene strata are, at best, represented by 6 m in the measured section below the Rijam Formation. This might indicate a long erosional unconformity at the end of the MCM which was documented by other workers (e.g. Al-Mashagbah, 2012) several tens of kilometers west of the study area. The erosional unconformity is also supported by the presence of tree trunks at the Muwaqqar-Rijam formations contact.
4. Microfacies analysis indicates that the upper Muwaqqar Formation in the Jebal Khuzayma area was deposited in a calm, offshore, open marine conditions affected by upwelling currents. This is evidenced by the abundant planktonic fauna exceeding benthic fauna, the abundant matrix represented by lime mudstone, and the relatively higher than normal phosphate particles and organic matter.

Acknowledgment

The authors would like to thank Mr. Khaled Al-Momani of the NRA for his help and guidance in the field work, Prof. W. Mutterlose of Germany for his help in identifying the ammonites and foraminifera, Prof. Ghaleb Jarrar, Emad Al Kharabsheh, Ibtisam El Beik and Hind Ghanem for support during the field work. This article is part of the M.Sc thesis of the first author.

References

[1] Abed, A. M., Arouri, K. and Boreham, C., 2005. Source rock potential of the phosphorite-bituminous chalk-marl sequence in Jordan. Marine and Petroleum Geology, 22, 413-425

[2] Abed, A. M. and Amireh, B., 1983. Petrography and geochemistry of some oil shales from north Jordan. Jour. Petrol. Geol., 5, 261-274.

[3] Abed, A. M. and Sadaqah, R., 1998. Role of Upper Cretaceous oyster bioherms in the deposition and accumulation of high-grade phosphorites in central Jordan. Journal of Sedimentary Research, 68B, 1009-1020.

[4] Abed, A. M., 2000. Geology of Jordan, Jordanian Geologists Association: Amman. (In Arabic)

[5] Abed, A. M., 2013. The eastern Mediterranean phosphorite giants: interplay between tectonics and upwelling. Geoarabia, 18, 67-94.

[6] Al-Harithi, T., and Ibrahim, K., 1992. Some Cephalopoda from Maastrichtian outcrops of Wadi Usaykhim, Al Azraq area in East Jordan. Senckenbergiana lethaea. 71, 427-437.

[7] Al-Mashagbah, Habes, 2012. Micropaleontology and biostratigraphy of some oil shale deposits in Jordan. Unpublished Ph. D thesis. The University of Jordan, 239p.

[8] Almogi-Labin, A., A. Bein and E. Sass, 1993. Late Cretaceous upwelling system along the southern Tethys margin: Interrelationship between productivity, bottom water environments, and organic matter preservation. Paleoceanography, 8, p. 671-690.

[9] Amard, B., 1996. Occurrence of Libycoceras ismaeli (Zittel) in the Upper Maastrichtian of Eastern Tademait, Algerian Sahara. Journal of African Earth Sciences 22, 609-615.

[10] Arkell, W. J., 1990. Treatise on Invertebrate Paleontology, part L, Introduction to Mesozoic Ammoniodea, (5 ed). Geological society of America and the University of Kansas Press.

[11] Bandel, K., Landman, N. H. and Waage, K. M. 1982. "Micro-Ornament on Early Whorls of Mesozoic Ammonites: Implications for Early Ontogeny". Journal of Paleontology 56 (2): 386–391

[12] Bender, F., 1974. Geology of Jordan. Borntraeger: Berlin.

[13] Burdon, D. J., 1959. Handbook of the geology of Jordan. Government of the Hashimite Kingdom of Jordan: Amman.

[14] Burnett, W.C. 1990. Phosphorite growth and sediment dynamics in the modern Peru shelf upwelling system, In: Burnett, W. C., Riggs, S. (Eds), Phosphorite Deposits of the World, v. 3, Neogene to Modern Phosphorites. Cambridge University Press, Cambridge, p. 62-74.

[15] Cobban, W. A. and Kennedy,W.J.. 1995. Maastrichtian ammonites chiefly from the Prairie Bluff Chalk in Alabama and Mississippi . Journal of Paleontology Vol. 69(5) p. 1-40.

[16] El-Hiyari, M., 1985. The geology of Jabal Al-Mutarammil, Map sheets No 3252, III. National Mapping Project, Bulletin 1, Natural Resources Authority, Amman, Jordan.

[17] Flügel, E. 2004. Microfacies of carbonate rocks. Springer: Berlin.

[18] Glenn, C.R., K.B. Follmi, S.R. Riggs, G.N. Baturin, K.A. Grimm, J. Trappe, A.M. Abed, C. Galli-Oliver, R.E. Garrison, A.V. Ilyin, C. Jehl, V. Rohrlich, R. Sadaqah, M. Schidlowski, R. Sheldon and H. Siegmund, 1994. Phosphorus and phosphorites: Sedimentology and environments of formation. Eclogae Geologicae Helvetiae, 87, p. 747-788.

[19] Hancock, J. M. 1967. Some Cretaceous-Tertiary marine faunal changes. Geological Society, London, Special Publications 2: 91–104.

[20] Haq, B.U and A.M. Qahtani 2005. Phanerozoic cycles of sea-level changes on the Arabian Plateform. GeoArabia, 10, 27-160.

[21] Ifrim, C., and Stinnesbeck, W., 2010. Migration pathways of the late Campanian and Maastrichtian shallow facies ammonite Sphenodiscus in North America. Palaeogeography, Palaeoclimatology, Palaeoecology. 292, 96-102.

[22] Ifrim, C., Stinnesbeck, W., Garza, R. and Ventura, J., 2010. Hemipelagic cephalopods from the Maastrichtian (late Cretaceous) Parras Basin at LaParra, Coahuila, Mexico, and their implications for the correlation of the lower Difunta Group. Journal of South American Earth Sciences. 29, 597–618.

[23] Kennedy, W. J. 1986. "The Campanian-Maastrichtian ammonite sequence in the environs of Maastricht (Limburg, the Netherlands), Limburg and Liège provinces (Belgium)". Newsletters on Stratigraphy 16 (3): 149–168.

[24] Kennedy, W. J. and Cobban, W. A. 1996. "Maastrichtian Ammonites from the Hornerstown Formation in New Jersey". Journal of Paleontology 70 (5): 798–804.

[25] Kherfan, A., 1987. The geology of Jebal Khuzaymamap sheet No. 3251 II. . NRA, Geology Directorate, Geological Mapping Division, Bulletin 6: Amman.

[26] Landman, N. H., Johnson, R. O. and Edwards, L. E. 2004. "Cephalopods from the Cretaceous/Tertiary boundary interval on the Atlantic Coastal Plain, with a description of the highest ammonite zones in North America. Part 1, Maryland and North Carolina". American Museum novitates (3454). hdl:2246/2819.

[27] Makhlouf, I., Abu-Azzam, H. and El-Hiayri, A., 1996. Surface and subsurface lithostratigraphic relationships of the Cretaceous Ajlun Group in Jordan. NRA, Subsurface Geology, Bulletin No. 8.

[28] Masri, M., 1963. Report on the geology of the Amman-Zerqa area. Central Water Authority, (Unpublished Report): Amman.

[29] Miller, A. K., Furnish, W. M. and Schindewolf, O. H., 1990. Treatise on Invertebrate Paleontology, part L (5 ed), Geological Society of America and University of Kansas Press.

[30] Nazzal, J. and Mustafa, H., 1993. Ammonites from the Upper Cretaceous of north of Jordan, Abhath Al-Yarmouk, 2, 87-120.

[31] Powell, J. and B.K Moh'd, 2011. Evolution of Cretaceous to Eocene alluvial and carbonate platform sequences in central and south Jordan. GeoArabia, 16, 4, p. 29-82.

[32] Powell, J. H., 1988. The Geology of the Karak area, map sheet No. 3152 III. (Geology Directorate, Natural Resources Authority, Amman, Jordan) Bulletin 8, 171 pp.

[33] Powell, J. H., 1989. Stratigraphy and sedimentation of the Phanerozoic rocks in central and south Jordan, part B: Kurnub, Ajlun and Belqa Groups. (Geology Directorate, Natural Resources Authority, Amman, Jordan), Bulliten 11, 130 pp.

[34] Powell, J.H., and B.K. Moh'd, 2012. Early diagenesis of Late Cretaceous chalk-chert-phosphorite hardgrounds in Jordan; Implications for sedimentation on a Coniacian–Campanian pelagic ramp. GeoArabia, 17, 4, p 17-38.

[35] Sharland, P.R.,R. Archer, D.M. Casey, R.B. Davies, S.H. Hall, A.P. Heward, A.D. Horbury and M.D. Simmons 2001. Arabian plate sequence stratigraphy. GeoArabia Special Publication 2, Gulf PetroLink, Bahrain, 371p.

[36] Turekian, K. K.; Armstrong, R. L. 1961. "Chemical and mineralogical composition of fossil molluscan shells from the Fox Hills Formation, South Dakota". Geological Society of America Bulletin 72 (12): 1817–1828.

[37] Wilson, J.L., 1975, Carbonate facies in geologic history. Springer: New York. 471pp.

[38] Yassini, I., 1979. Maastrichtian-Lowe Eocene biostratigraphy and the planktonic foraminiferal biozonation in Jordan. Rev. Esp. Micropal., 11, 5-57.

[39] Zaborski, P., 1982. Campanian and Maastrichtian sphenodiscid ammonites from southern Nigeria. Bull. Brit. Mus. Nat. Hist. (Geol.) 36, 303-332.

JJEES
Jordan Journal of Earth and Environmental Sciences

Volume 6, Number 2, December, 2014
ISSN 1995-6681
Pages 85- 92

Effects of the Upgrading of Al-Ramtha - Northern Jordan, Wastewater Treatment Plant on Quality of the Effluent and Environment

Alaa A. Mayyas; Hakam A. Mustafa* and Nigem El-Deen Yusuf

Department of Earth & Environmental Sciences, Yarmouk University, Irbid, Jordan

Received 19 May, 2013; Accepted 4 December, 2014

Abstract

The present study concludes that the wastewater generated in Al-Ramtha wastewater treatment plant is classified as strong in terms of the total dissolved solids (TDS) content, the total suspended solids (TSS) content, and the chemical and biochemical oxygen demands (COD and BOD5). The efficiency of the plant in removing total dissolved solids (TDS) from wastewater is still low, while it is reasonably high in terms of suspended solids, COD and BOD removal. The upgrading which took place in 2003 added a significant improvement in the process of plant treatment regarding the selected parameters (COD, BOD and TSS). Regarding these parameters, the new plant effluent complies with Jordanian standards for irrigation parks, reuse for irrigation of cooked vegetables, fruits, and trees, and for fodder crops, but not with respect to TDS concentration of effluent used for irrigation purposes. The obtained concentrations of all analyzed metals indicate that the studied soils are uncontaminated with respect to Cd, Zn, Mn, Pb, Cu and Fe.

Keywords: Wastewater, Upgrading, Treatment Plant, Ramtha, Jordan.

1. Introduction

Wastewater is the water that carries the waste removed from residences, institutions, and commercial and industrial establishments. It can be subdivided on the basis of the levels of the major constituents into strong, medium and weak domestic wastewaters (Table 1) (FAO, 2008).

Table 1: Major constituents of typical domestic wastewater (FAO, 2008).

Major Constituents	Level of Major constituents and their concentration in mg/l		
	Strong	Medium	Weak
Total solids	1200	720	350
Dissolved solids (TDS)	850	500	250
Suspended solids	350	220	100
Nitrogen (as N)	85	40	20
Phosphorus (as P)	15	8	4
Chloride	100	50	30
Alkalinity (as $CaCO_3$)	200	100	50
Grease	150	100	50
Biochemical Oxygen Demand(BOD_5)	400	210	110

Currently available systems of treatment in Jordan need upgrades in capacity or supplementary systems. In the present study, Al-Ramtha wastewater treatment plant (WWTP) was selected to determine the effect of upgrading on the quality of effluent and whether the current effluent quality can be used in agriculture.

Al-Ramtha WWTP was constructed in 1988 on gently sloping plateau about 4km northwest of Al-Ramtha city, near the road leading to Turra (Fig. 1).

Wastewaters from homes, commercial buildings, hospitals (domestic sewage), etc. of about 70,000 people are collected via a collection system and flow to Al-Ramtha WWTP for treatment.

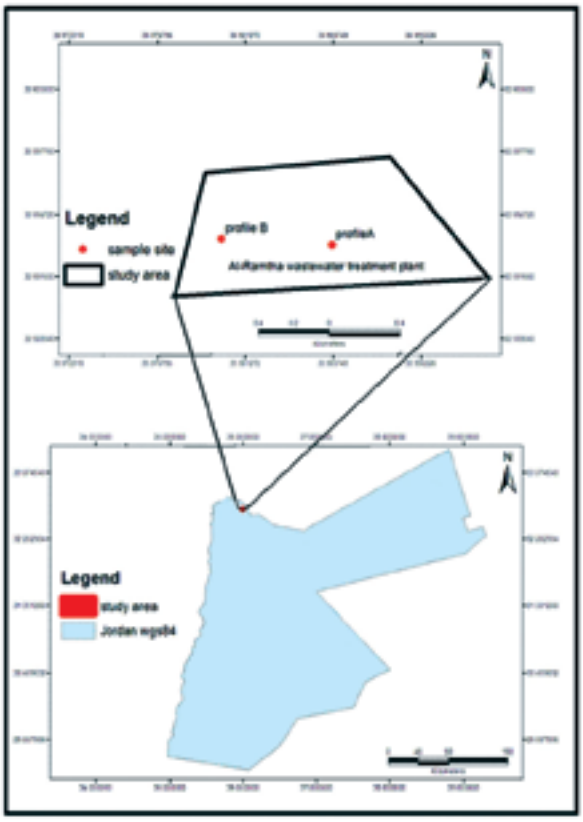

Figure 1: Location map of the study area.

In the old stabilization ponds plant, three stages were used. In the first stage, settable organic materials are accumulated as sludge in the bottom of anaerobic ponds and decomposed to produce inorganic matter. In the second stage,

* Corresponding author. e-mail: *haksawalha@yahoo.com*

facultative ponds which are divided into two zones upper aerobic and lower anaerobic, consumer and decomposer organisms mainly reduced organic material during two to three weeks to basic intracellular inorganic constituents. In the third stage, the shallow maturation ponds, where the water is light loaded with organic matter and contains dissolved oxygen; provide a high quality effluent (Parker, 1979; Rich 1980; Arceivala, 1981, and Gharaibeh *et al*., 2000). After the upgrading in 2003 an activated sludge process is in use. The treatment is divided into pretreatment, where coarse solids and other materials are removed using screens, aerated greave and grit chamber, in the secondary treatment activated sludge in the aeration tank is used, and in the tertiary treatment residual particles and parasites are removed.

The hydraulic design capacity for the new plant is 5400 m^3/d and operating capacity 3492 m^3/d. All effluent has to be reused throughout the year in order to eliminate effluent discharge to the wadi downstream of the plant.

Evaluation of several options for reuse of the reclaimed water showed that agricultural reuse was the most suitable alternative. The proposed agricultural lands irrigated with the reclaimed water are around 1 Km^2 located adjacent to the WWTP.

The present research aims to achieve the main following goals:

- Determining of the effects of upgrading that was finished in 2003 on the quality of Al-Ramtha wastewater treatment plant effluent by measuring chemical oxygen demand (COD), biological oxygen demand (BOD), total suspended solids (TSS), total dissolved solids (TDS) and comparing the results with data available before upgrading.
- Determining the new plant effluent suitability for agricultural irrigation and comparing the new plant effluent properties with Jordanian standards and the international standards.
- Investigating the environmental impact of effluent in its current quality on irrigated soil by measuring the concentration of some heavy elements (Cd, Fe, Cu, Pb, and Zn) and comparing it with soil samples from non- irrigated profile.

2. Methodology

A combination of both field and laboratory work were used to accomplish this study.

Field work

A) Sixteen water samples were collected from influent and effluent of the plant during the period from May to October 2009. The effluent samples used in analysis were taken from the plant after secondary treatment and before chlorination; the influent samples were taken from the plant inlet. The samples were preserved in bottles and transported to the laboratory for further analyses.

B) Soil samples were collected from two profiles: The first profile (Coordinates 35.985744° N and 32.593295° E) represents soil irrigated by effluent, and the second profile (Coordinates 35.98129° N and 32.593580° E) represents a reference from non-irrigated soil. Soil samples were preserved in polyethylene bags to minimize contamination then transported to the laboratory for further analysis.

Temperature**,** pH value and TDS were measured in the field by using thermometer, pH meter and conductivity meter, respectively.

Laboratory work

Laboratory work was carried out at the Faculty of Science at Yarmouk University and laboratories of the Ramtha Wastewater Treatment Plant.

A. Wastewater samples analyses

a) Suspended Solids (TSS)

A known volume of water sample was filtrated through a pre-weighed Whatman glass fiber filter (GFC), 47 mm in diameter. The filter was dried at 105ºC and reweighed. The amount of suspended solids was determined from the increase in weight of Whatman glass fiber filter.

b) Chemical Oxygen-Demand (COD)

The Chemical Oxygen Demand is used as a measure of the oxygen equivalent of the organic and inorganic matter content of a sample that is susceptible to oxidation by a strong chemical oxidant. The COD test was carried out by using Photolab S6 equipment (Fig. 2).

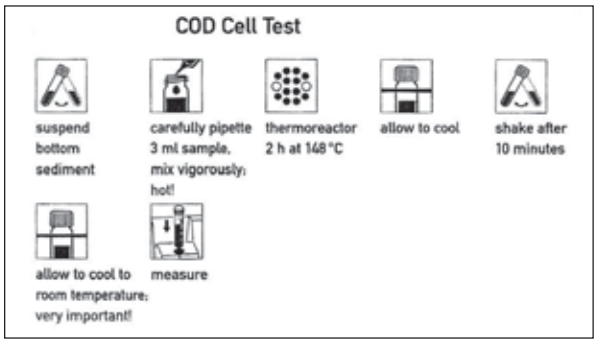

Figure 2: Process of measuring COD.

c) Biochemical Oxygen Demand (BOD)

BOD is a measure of the amount of oxygen used by microbes to decompose organic matter in a wastewater. The sample is kept in a sealed container fitted with a pressure sensor. A substance that absorbs carbon dioxide (typically sodium hydroxide) is added in the container above the sample level. The sample is kept at 20 °C in darkness to prevent photosynthesis (and thereby the addition of oxygen) for five days. Oxygen is consumed, and carbon dioxide is released. The total amounts of gas, and thus the pressure, decrease because carbon dioxide is absorbed. From the drop of pressure, the sensor electronics compute and display the consumed quantity of oxygen.

d) Heavy metals chemical analysis

The (Nov AA300 "Analytic Jena") atomic absorption spectrophotometer (AAS) was used for the determination of Cd, Pb, Cu, Fe, Zn and Cr content in all analyzed water and soil samples.

B. Soil samples analyses

All soil samples were dried at 110˚C, disaggregated, homogenized and sieved to discard coarse materials (>2mm). Representative subsamples were taken for each soil sample.

a) Heavy metals chemical analysis

The same as the analysis of heavy metals in wastewater.

b) Total Organic Matter Content (%TOM)

The percentage of organic matter in the soil samples was measured by titration method which is based on the oxidation of organic matter by potassium dichromate, followed by chemical titration with ferrous sulphate until the color flashes to green, as suggested by Loring and Rantala (1992).

3. Results and Discussions

- Properties of influent and effluent in the new plant

Data concerning Al-Ramtha WWTP were obtained from the Ministry of Water and Irrigation, and the chemical and physical analyses of the collected wastewater samples (Tables 5-7).

Data of chemical and physical analyses of the collected wastewater samples (Table 2) during the study period are divided into two groups (summer and winter).

- Physical properties of influent and effluent

The physical properties of interest here are the temperature and solids content of the wastewater. The waste water temperature is an important parameter because of its effects on type and rate of the biochemical reactions. The average influent wastewater temperatures in Al-Ramtha treatment plant is ranging from 15.4° to 20.4°C in winter, and from 21° to 26°C in summer (Table 2). The minimum temperature in winter is never less than 10°C. These temperature ranges are suitable for high bacterial activity. The temperature for optimal bacterial activity ranges from 25-35°C and this activity decreases to about the half when the temperature decreases by 10°C (Metcalf & Eddy1990).

The average effluent wastewater temperature ranges from 15.17° to 22.8 °C in winter and from 25.4° to 27.9°C in summer (Table 2). The effluent temperature is significant because it can affect aquatic life upon discharge, and the sustainability of the water for beneficial uses. Also, oxygen is less soluble in warm water than in cold water.

The other important physical property of wastewater is the solids content. The average studied influent total dissolved solids range from 916 mg/l to 1176 mg/l in winter and from 1068 mg/l to 2068 mg/l in summer (Table 2). The average effluent total dissolved solids contents for the winter and summer range from 826 mg/l to 1400 mg/l and 806 mg/l to 1533 mg/l, respectively (Table 2). Accordingly, the treated wastewater is classified as strong wastewater (Table 1). The low efficiency of the used technologies in removing dissolved solids from wastewater is of concern because it affects the reuse of wastewater for agriculture.

In winter, the average influent of total suspended solid content (Silt, clay, algae, zooplankton, bacteria) of the studied wastewater is 628 mg/l, and in summer 725.8 mg/l (Table 2). Accordingly, this wastewater is classified as strong wastewater (Table 1). But the percentage removed of TSS from treated wastewater is 95.8% (Table 2) because solid particles precipitate throughout the treatment process, causing the water to become clear when it flows down and enters a reservoir.

Table 2: Summary of statistical information of influent and effluent wastewater parameters of Al-Ramtha WWTP after upgrading.

Parameter	Unit	Season	Influent				Effluent			
			Ave.	Std.	Max.	Min.	Ave.	Std.	Max.	Min.
Qave.	M^3/day	___	3244	___	___	___	____	____	____	_____
Temp	°C	Winter	18	1.7	20.4	15.4	18.19	2.35	22.8	15.7
		Summer	24.5	1.5	26	21	26.8	0.8	27.9	25.4
pH		Winter	7.6	0.27	7.95	7.2	7.2	0.48	7.88	6.28
		Summer	7.4	0.26	7.75	6.96	7.74	0.25	8.21	7.34
TDS	mg/l	Winter	1088.9	84.36	1176	916	1182,8	159.4	1400	826
		Summer	1379.9	318.8	2068	1068	1143.9	251.2	1533	806
TSS	mg/l	Winter	628	341.7	1374	192	26.8	16.8	66	10
		Summer	725.8	226	958	324	30.46	16.75	84	13
BOD_5	mg/l	Winter	924.4	488	1708	229	11	4	20	5
		Summer	989	248	1310	580	13.45	5	20	5
COD	mg/l	Winter	1629.8	616.35	2590	799	58	34.6	156	24
		Summer	2259.6	849	3651	1156	69.38	33.4	121	25
COD/BOD ratio	____	Winter	1.76	1.26	3.48	1.5	5.3	8.65	7.8	4.8
		Summer	2.28	3.42	2.78	1.99	5.4	6.48	6.05	5

**** TDS: Total Dissolved Solids, TSS: Total Suspended Solids, BOD_5: Biochemical Oxygen Demand and COD: Chemical Oxygen Demand. Std: Standard Deviation

- Chemical and biochemical properties of influent and effluent

The wastewater properties of interest here are the pH and the organic matter content; which include the biochemical oxygen demand (BOD_5), the chemical oxygen demand (COD), and the ratio of COD to BOD_5. The pH is an important parameter. Most biological life dislike pH outside the range 4 – 9. The well-being of microorganisms in the aerated tanks is of concern. Most bacteria cannot tolerate pH outside the range 4.0 - 9.5. Generally, pH for optimum bacterial growth lies in the range 6.5 - 7.5 (Sincero, 1996). The pH reported for Al-Ramtha treatment plant ranges from 6.28 to 8.21, (Table 2) they are well within the range favored by the bacteria.

Special consideration must be given to the organic matter content of the wastewater; it is characterized in terms of the biochemical oxygen demand (BOD_5), the chemical oxygen demand (COD), and the ratio of the COD to the BOD_5. The BOD_5 by definition is the quantity of oxygen required for the stabilization of the oxidizable organic matter present after five days of incubation at 20°C. It is the amount of Oxygen used by microorganisms to decompose organic matter.

The average, studied influent BOD_5 concentrations range from 229 mg/l to 1708 mg/l in the winter time and from 580 mg/l to 1310 mg/l in the summer time (Table 2). These numbers indicate that the wastewater being treated is classified as strong wastewater (Table 1). The percentage

removals of BOD_5 obtained for plant selected for the study averaged 98%.

The COD test measures the total organic content of a wastewater which is oxidizable by dichromate in acid solution (Eckenfelder, 1989). Certain aromatics such as benzene and straight chain carboxylic acids are not completely oxidized in the reaction, and on the other hand reduced substances, such as sulfides, sulfates, and ferrous iron, will also be oxidized and reported as COD.

The average influent COD concentrations of the studied wastewater range from 799 mg/l to 2590 mg/l in winter and from 1156 mg/l to 3651 mg/l in summer (Table 2).

These numbers indicate that the studied wastewater is strong (Table 1). Because the five-day BOD will represent a different proportion of the total oxygen demand for raw wastewater than for effluents, the COD/BOD_5 ratio will frequently vary for effluents as compared with untreated wastes (Table 2). The influent wastewater of the plant is characterized as containing high percentage of nonbiodegradable organic matter; which can be concluded from the ratio of COD/BOD_5 (Table 2) which ranges from about 1.5 to about 3.48. These numbers are comparable to those presented by Metcalf and Eddy (1990) which state that the typical COD/BOD_5 ratio of domestic wastewaters is usually in the range 1.25 to 2.5. The COD/BOD_5 ratio becomes even more profound for treated effluents and ranges from 4.8 to 7.8. This indicates that the proportion of the nonbiodegradable content of treated effluent is relatively higher than that of raw wastewater and that the efficiency of BOD_5 removal is higher than that of COD removal.

Heavy Metals in influent and effluent in the new plant.

Cadmium (Cd) and Zinc (Zn)

The Cd and Zn concentration in all analyzed samples lies below the detectable limit of the atomic absorption spectrophotometer used. Thus, the effluent can be classified as uncontaminated with Cd and Zn.

Table 3: Mean and standard deviation of heavy metals concentration (ppm) in the influent and effluent of Al-Ramtha WWTP.

Heavy metals	Influent		Effluent	
	Mean of concentration	Stdev	Mean	Stdev
Cd	ND	ND	ND	ND
Zn	ND	ND	ND	ND
Pb	0.090	0.067	0.083	0.036
Mn	0.167	0.02	0.156	0.008
Cu	0.230	0.037	0.230	0.017
Fe	0.438	0.185	0.472	0.311

ND: not detect

Lead (Pb)

The concentration of lead in fresh water is less than 3 ppb (Wedepohl, 1969) and the upper limit of guideline values of Jordanian standard for Pb concentration of effluent used for irrigation is 5ppm. The average concentration of Pb in the influent is 0.090ppm and in effluent of the plant is 0.083ppm (Table 3 and Fig. 3A), so the plant effluent used for irrigation purposes can be classified as uncontaminated with Pb.

Manganese (Mn)

Manganese occurs primarily as Mn^{2+} in the rocks forming silicates. The relatively low manganese content in the carbonate minerals is often due to a low concentration of this element in carbonate precipitating solutions such as sea water and other types of water (Talyor, 1983).

The upper limit of guideline values of the Jordan Institute of Standards and Metrology (JISM) for Mn concentration of effluent used for irrigation is 0.2ppm. The average concentration of Mn in the influent is 0.167ppm and in effluent of the plant is 0.156ppm (Table 3 and Fig. 3B), so the plant effluent used for irrigation purposes can be classified as uncontaminated with Mn.

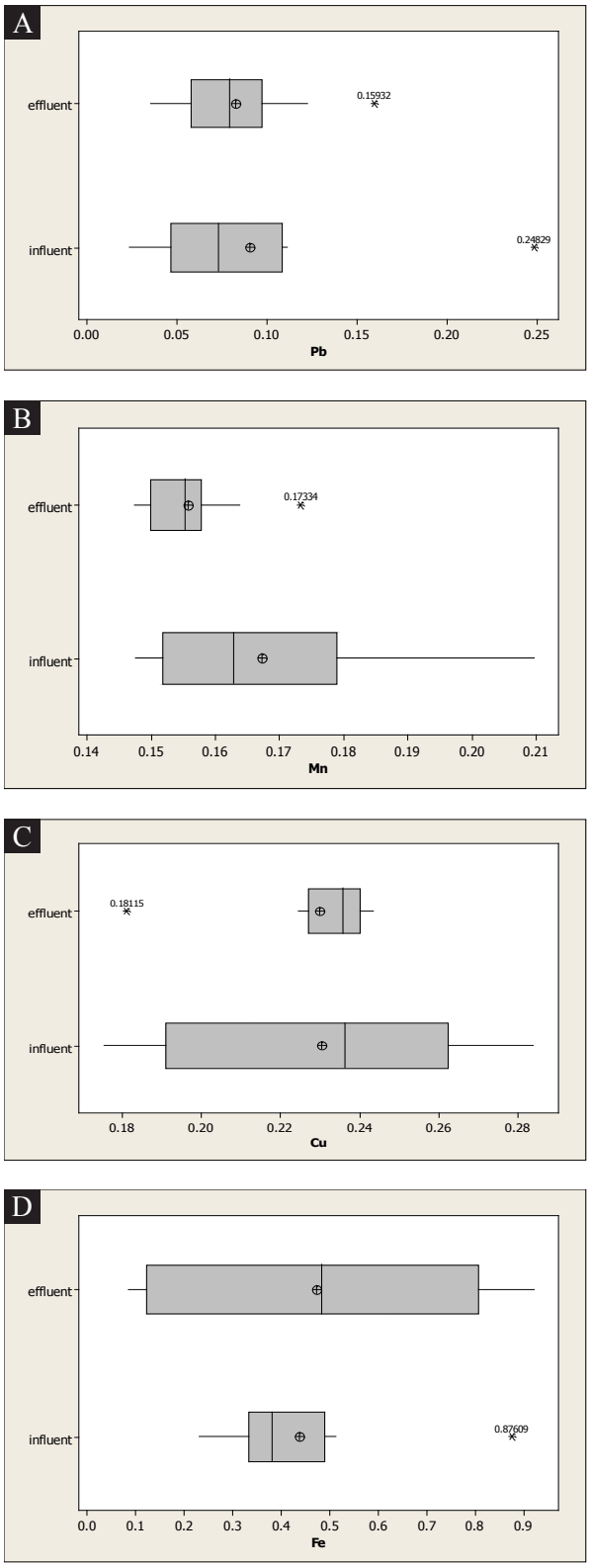

Figure 3: Box-plots show distribution of Pb(A), Mn (B), Cu (C) and Fe (D) concentrations in influent and effluent.

Copper (Cu)

Copper is widely distributed in nature in free state as well as in sulfides, arsenide, chlorides and carbonates.

The concentration of copper in fresh water is 3 ppb (Wedepohl, 1969) and the upper limit of guideline values of the Jordan Institute of Standards and Metrology (JISM) for Cu concentration of effluent used for irrigation is 0.2ppm. The average concentration of Cu in influent is 0.230ppm and in effluent of the plant is 0.230ppm (Table 3 and Fig. 3C), so the plant effluent used for irrigation purposes can be classified as slightly contaminated with Cu.

Iron (Fe)

Iron has several sources in sedimentary rocks. Iron minerals present in carbonate rocks are mostly ferric oxides formed by weathering.

The concentration of iron in river waters is 0.67ppm (Wedepohl,1969). The upper limit of guideline values of the Jordan Institute of Standards and Metrology (JISM) for Fe concentration of effluent used for irrigation is 5ppm. The average concentration of Fe in influent is 0.438ppm and in effluent of the plant is 0.472ppm (Table 3 and Fig. 3D), so the plant effluent used for irrigation purposes can be classified as uncontaminated with Fe.

Soils

Total Organic Matter (TOM %) in Soil

The organic matter of soil consists of mixture of plant and animal remains in various stages of decomposition.

Organic matter of a soil affects its color; it increases its cation exchange capacity and accounts for 20-90% of the adsorbing power of the soil.

The organic matter contents vary between 4.74 to 8.16 % in profile A, and from 4.3 to 7.9% in profile B (Table 4). The highest values were obtained at the surface with decreasing tendency with depth (Fig. 4A).

Table 4: The average and range of the concentration of heavy metals and total organic matter (TOM %) in the soil profiles and normal soils.

Tom% & Heavy Metals (PPm)	Average of Conc.		Range of Conc.		Average concentration in normal soils
	Profile A	Profile B	Profile A	Profile B	
TOM %	6.8	6.5	8.16-4.75	7.9-4.3	_____
Cd	ND	ND	ND	ND	0.1
Mn	767.35	644.76	737.27- 856.12	550.31 - 696.46	850
Pb	0.029	0.012	0.008-0.067	0.002-0.03	14
Zn	0.059	0.042	0.02-0.11	0.03-0.08	70
Cu	0.04	0.03	0.02-0.07	0.014-0.043	45
Fe	6.03	5.73	5.79-6.2	5.51-5.98	55

** Profile A, obtained soil samples non- irrigated by the plant effluent.
** Profile B, obtained soil samples irrigated by the plant effluent.
** ND: Not detect.

Heavy metals in soils

Cadmium (Cd)

The Cd concentration in all analyzed samples lies below the detectable limit of the atomic absorption spectrophotometer used.

The studied soils can be classified as uncontaminated with Cd.

Manganese (Mn)

Normal soils have an average content of Mn that ranges from 100 to 4000ppm with a mean value of 850ppm (NAS, 1973). Manganese is generally considered to be one of the most important toxic metals in acid soils. Several investigators pointed out that pH had the greatest effect on the availability of Mn, followed in order by organic matter and moisture (Christensen *et al*., 1951).

The concentration of Mn in the analyzed soil samples ranges from 550.31 to 856.12ppm (Table 4).The concentration of Mn in profile A (non -irrigated by plant effluent) ranges from 737.27 at the surface to 856.12ppm at 30cm depth, and in profile B (irrigated by plant effluent) 550.31ppm at the surface and 696.46 ppm at 30cm soil depth (Fig.4B).

The analysis shows that the Mn – concentration in general increases with depth in both profiles and decreases with irrigation (Profile B). It indicates that Mn is gradually washed out of soil by percolating rain and irrigation.

The obtained Mn-values are within the range given for normal soils; therefore, the studied soils can be classified as uncontaminated with Mn.

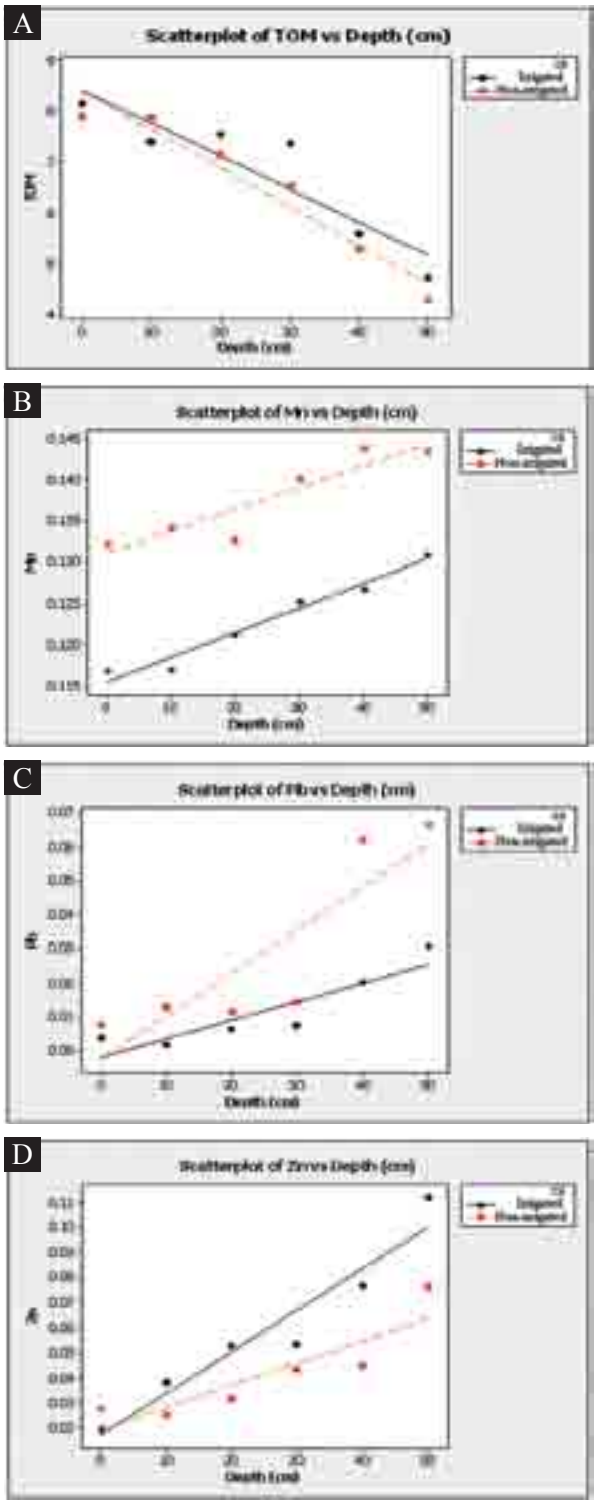

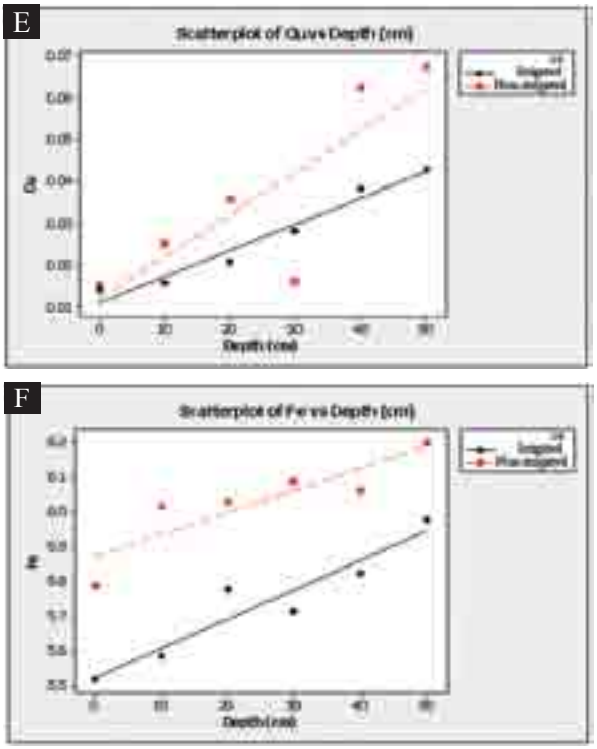

Figure 4: Variations of TOM(A), Mn(B), Pb(C), Zn(D), Cu(E) and Fe (F) in the studied profiles with depth.

Lead (Pb)

The average of Pb content in the earth's crust range from 13 to 16 ppm (Swaine, 1978).

Soils can have a wide range of Pb content, depending on a number of factors, such as the parent material and anthropogenic input (Adriano, 1986).

The concentration of Pb in the analyzed soil samples ranges from 0.002ppm to 0.067ppm (Table 4)

The increase tendency of lead with depth in both profiles (Fig. 4C) results from transport of lead from the surface probably at relatively lower pH to the bottom where higher pH-values are expected.

Comparison of the obtained Pb-values in the study area with Pb-values in normal soils indicated that the studied soils are uncontaminated with Pb.

Zinc (Zn)

The Zn-concentration in the study area ranges from 0.02 at the surface to 0.11ppm at 50cm depth in the non-irrigated soil, and from 0.03ppm at the surface to 0.08ppm at 50cm depth in the irrigated soil (Table 4 and Fig. 4D). This Soil can be classified as uncontaminated with Zn

Copper (Cu)

Copper is one of the important essential elements for plants and animals.

The average concentration of Cu in soils of the study area is 0.04ppm in profile A and 0.03ppm in profile B (Table 4 and Fig. 4E), so these soils can be classified as uncontaminated with Cu.

Iron (Fe)

The concentration of Fe in the analyzed soil samples ranges from 5.51 to 6.2ppm (Table 4). The concentration of Fe in profile A (non-irrigated by plant effluent) ranges from 5.79 at the surface to 6.2ppm at 50cm depth (average 6.03 ppm) and in profile B (irrigated by plant effluent) was 5.51ppm at the surface and 5.98ppm at 50cm soil depth (average 5.73 ppm).

The Paired T-Test analysis indicates significant difference in the Fe values between the two profiles as well as with the depth in the soil profile (Fig. 4F).

Generally, the Fe content of soils ranges from 10.00 to 100.00ppm (Mitchell, 1964). The distribution pattern of all measured elements shows an increasing tendency of the concentration with depth in irrigated and non-irrigated studied soils (Fig. 4F). This is probably caused by relatively increasing of pH with depth. However the obtained results are much lower than that given by Al-Ghazzawi (2009) for soils along Zarqa river and than that reported by Al-Kailani (2005) for soils irrigated by King Talal dam water. This can be explained by anthropogenic inputs to the Zarqa river, through the effluent of Khirbet Assamra and industrial waste discharged to the river.

The low values obtained in this study points to noncontamination of soils as well as the absence of anthropogenic heavy metals source in the area. The obtained results of heavy elements analyses in Al-Ramtha area are comparable with those reported by Rusan *et al.* (2006).

The effects of the upgrading of Al-Ramtha wastewater treatment plant

Different packages of Microsoft Office Word 2003, Excel 2003 and SPSS 8.0, chemical and biochemical data that covers ten years (2000-2009) have been used to find out the effect of upgrading that has been finished 2003 on the quality of the plant effluent.

BOD

The average percent removal of BOD in the old plant was 70.1% in summer and 67.94% in winter. This indicates that the effluent was not in agreement with the Jordanian standards, while the average removing of BOD in the new plant is 98.53% in summer and 98.5% in winter (Table 5 and Fig. 5A$_1$ & A$_2$). This complies with the Jordanian standards for reclaimed wastewater discharge to streams, ground water recharge, irrigation parks, reuse for irrigation of cooked vegetables, fruits, and trees, and for reclaimed wastewater reuse for fodder crops.

Table 5: The range, mean, and the standard deviation values (stdev) of the removing percentage of BOD for new plant and old plant in summer and winter seasons in the years 2000-2009.

Plant name	Seasons	Number of samples	Range of removing percentage	Mean	Stdev
New plant	summer	9	98.1%-99.3%	98.53%	0.35
New plant	winter	9	97.3%-98.9%	98.5%	0.49
Old plant	summer	9	62.5%-75.6%	70.1%	4.40
Old plant	winter	9	54.8%-75.3%	67.94%	6.43

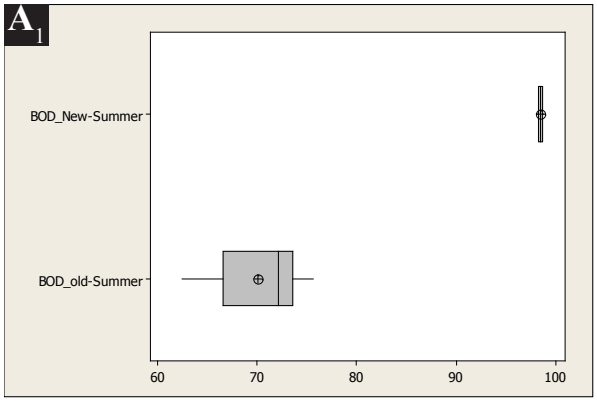

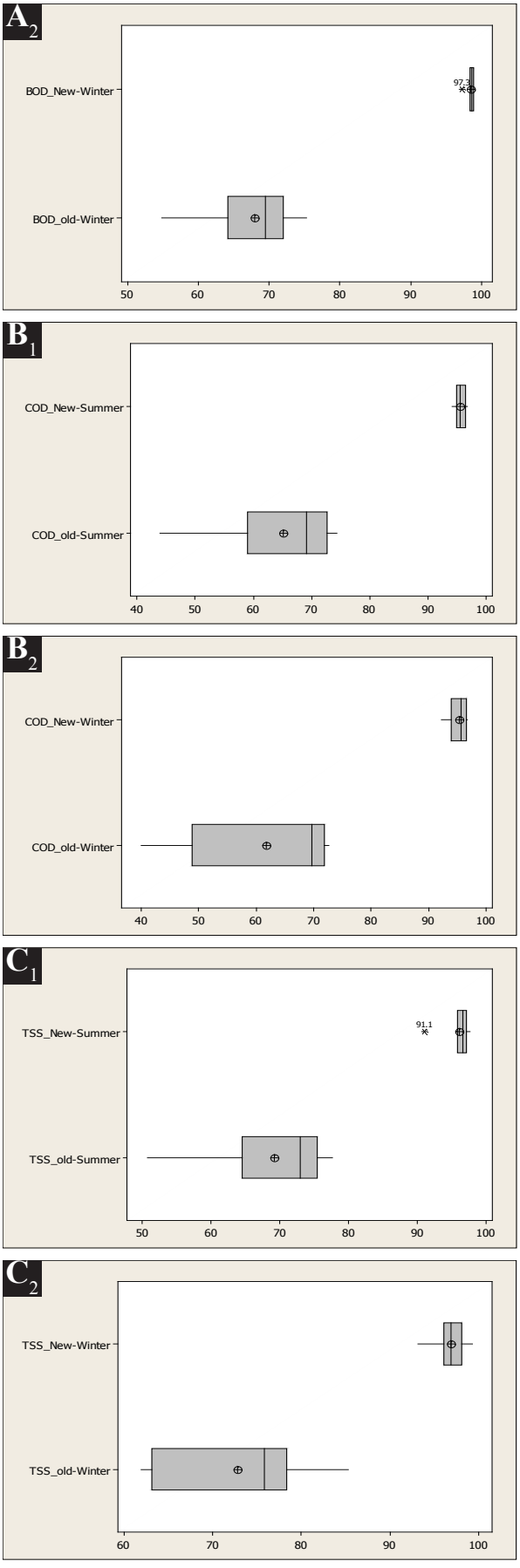

Figure 5: Box-plots show the removing percentages of BOD before and after upgrading in summer (A_1) and in winter (A_2), of COD before and after upgrading in summer (B_1) and winter (B_2) and of TSS before and after upgrading in summer (C_1) and winter (C_2).

COD

The average removal of COD in the old plant was 65.07% in summer and 61.67% in winter. The old plant effluent was not in agreement with the Jordanian standards, while the percentage removal of COD in the new plant is 95.53% in summer and 95.3% in winter (Table 6 and Fig. 5B_1 & B_2). The new plant effluent complies with Jordanian standards for reclaimed wastewater discharge to streams, ground water recharge, irrigation parks, reuse for irrigation of cooked vegetables, fruits, and trees, and for reclaimed wastewater reuse for fodder crops.

Table 6: The range, mean, and the standard deviation values of the removing percentage of COD for new plant and old plant in summer and winter seasons (2000-2009).

Plant name	Seasons	Number of samples	Range of removing percentage Of COD	Mean	Stdev
New plant	summer	9	94.1%-96.8%	95.53%	0.89
New plant	winter	9	92.3%-96.8%	95.3%	1.69
Old plant	summer	9	43.8%-74.3%	65.07%	9.81
Old plant	winter	9	39.9%-72.6%	61.67%	12.66

TSS

The average removal of TSS in the old plant is 69.17% in summer and 72.78% in winter. This indicates that the old plant TSS effluent was not in agreement with the Jordanian standards, while the average % removal of TSS in the new plant is 96.06% in summer and 96.86% in winter (Table 7 and Fig. 5C_1 & C_2). Therefore, the new plant TSS effluent complies with Jordanian standards for reclaimed wastewater discharge to streams, and water body, as also determined by Al-Zboon *et al*. (2008).

Table 7: The range, mean, and the standard deviation values of the removing percentage of TSS for new plant and old plant in summer and winter seasons (2000-2009).

Plant name	Seasons	Number of samples	Range of removing percentage	Mean	Stdev
New plant	summer	9	91.1%-97.7%	96.06%	1.97
New plant	winter	9	93.2%-99.3%	96.86%	1.75
Old plant	summer	9	50.6%-77.6%	69.17%	8.55
Old plant	winter	9	61.9%-85.3%	72.78%	8.32

4. Conclusions

1. The average temperature of influent wastewater in the treatment plant ranges from 15.4 to 20.4°C in winter, and from 21 to 26°C in summer. The minimum temperature in winter time is never less than 10°C; this is suitable for biodegradation of organic matter.
2. The wastewater generated in Al-Ramtha treatment plant is classified as strong in terms of total dissolved solid content, and the efficiency of the selected technologies in removing dissolved solids from wastewater is low. Also, the wastewater is classified as strong wastewater in terms of total suspended solid content, but the efficiency of the selected technologies in removing suspended solids is reasonably high (96.46%).
3. The treated wastewater is classified as strong wastewater in terms of BOD and COD contents, and the percent removals of BOD and COD are high.
4. The wastewater generated in Al-Ramtha is characterized as containing high nonbiodegradable organic matter, and there is a significant reduction of this matter in the treated wastewater in the treatment plant.

5. Regards to the selected elements in this study, the new plant effluent complies with Jordanian standards for irrigation parks, reuse for irrigation of cooked vegetables, fruits, and trees, and for reclaimed wastewater reuse for fodder crops, exception the upper limit of guideline values of the Jordan standards for TDS concentration of effluent used for irrigation purposes.
6. The effluent is not suitable for those vegetables that are eaten uncooked, such as tomato, carrot and green leaf vegetables.
7. The obtained concentration of all analyzed metals indicate that the studied soils are uncontaminated with respect to Cd, Zn, Mn, Pb, Cu and Fe (the soils are unpolluted in regarding to heavy metals).
8. The upgrading which took place on 2003 adds significant improvement in the process of plant treatment with respect to TSS, BOD and COD, but not with respect to TDS.

5. Recommendations

1. Construction additional treatment stage to reduced TDS in the plant effluent.
2. Further investigation is needed to study the effect of using treated water on food chain.
3. Organizing programs to increase the farmer's awareness for the right using of treated water, pesticides and fertilizers.

Acknowledgments

This work received financial support by the Yarmouk University (Project 2009/23); we wish to express our thanks for this support.

References

[1] Adriano, D.C., 1986. Trace elements in the terrestrial environmental. Springer Verlag. New York, pp. 533.
[2] Al-Ghazzawi, 2009. Soil pollution with heavy metals in farms along the upper course of Zarqa River. Unpublished M.Sc. thesis, Yarmouk University.
[3] Alkailani, A., 2005. Major and trace elements in soil profiles from selected Farms irrigated with King Talal dam water. Unpublished M.Sc. thesis, Yarmouk University.
[4] Al-Zboon, K., and Al-Ananzeh, N., 2008. Performance of wastewater treatment plants in Jordan and suitability for reuse. African Journal of Biotechnology, 7 (15): 2621-2629.
[5] Arceivala, S. J., 1981. Wastewater treatment and disposal: Engineering and ecology in pollution control. Marcel Dekker, New York. Pp. 53-600.
[6] Christensen, P.D., Toth, S. J., and Bear, F. E., 1951. Soil scisoc amproc 15: 279-282.
[7] Eckenfelder, W., 1989. Industrial water pollution control. McGraw-Hill Company, New York.
[8] FAO, 2008. Wastewater treatment. Corporate Document Repository. Food and Agriculture Organization of the United Nations. http://www.fao.org/docrep/T0551E/t0551e0b.htm. 25/4/2008.
[9] Gharaibeh, S., and Farhan, Y., 2000. Introduction to environmental science, Dar Ashoroq, pp. 415, (In Arabic).
[10] Loring, D. H. and Rantala, T. T., 1992. Manual for the geochemical analysis of marine sediments and suspended particulate matter. Earth science reviews, Vol.32, pp.235-263, Elsevier Science Publishers b. V., Amsterdam.
[11] Metcalf and Eddy, 1990. Wastewater engineering: Treatment, disposal, and reuse, McGraw-Hill Company, New York. pp. 56-118.
[12] Mitchell, R, L., 1964. Trace elements in soil. In: Chemistry of the soil. Ed. F. E. Bear. ACS monogragh No. 160. Reunhold Publishing, New York.
[13] National Academy of Science (NAS), 1973. Manganese. NAS, Washington, D.C. pp. 191.
[14] Parker, J.G., and Lyons, B.J., 1979. Factors influencing the treatment of food processing wastes by anaero-bic-aerobic lagoon systems. Progress in water technology, Volume 11, pp. 377-388.
[15] Rich, L., 1980. Low-maintenance and mechanically simple wastewater treatment systems. McGraw-Hill, New York, USA, pp. 53-129.
[16] Rusan, M., Hinnawi, S., Rusan, L., 2006. Long term effect of wastewater irrigation of forage crops on soil and plant quality parameters. Desalination, 215: 143–152.
[17] Sincero, A. and Sincero, G. 1996. Environmental engineering: A design Approach. Prentice Hall, New Jersey.
[18] Swaine, D. J., (1978): J. Royal Soc. new South Wales, 111: pp. 41-47.
[19] Talyor, J.H., 1983. The geochemistry of iron and manganese in the waters and sediments of bolstadfiord. Estuarine, Costal and shelf science, Volume 17, pp. 1-19.
[20] Wedepohl, K. H., 1969. Handbook of geochemistry. Springer Verlag, New York. pp. 297-319.

JJEES

Volume 6, Number 2, December, 2014
ISSN 1995-6681
Pages 93- 97

Jordan Journal of Earth and Environmental Sciences

Seasonal Variation of Temperature in Dhaka Metropolitan City, Bangladesh

Md. Zakaria Hossain[1], Md. Nazrul Islam Mondal[2*], Sarose Kumar Sarkar[3] and Md. Abdul Haque[4]

[1] Institute of Environmental Science, University of Rajshahi, Rajshah-6205, Bangladesh
[2] Department of Population Science, and Human Resource Development, University of Rajshahi, Rajshahi-6205, Bangladesh
[3] Department of Statistics, University of Rajshahi, Rajshahi-6205, Bangladesh
[4] Department of Applied Mathematics, University of Rajshahi, Rajshah-6205, Bangladesh

Received 8 December, 2013; Accepted 28 November, 2014

Abstract

The present study aims to analyze the impact of global climate change on the basis of seasonal variation of temperature in Dhaka city, Bangladesh. The daily data on temperature from the years 1953-2009 were used and collected from the Meteorological Department, Bangladesh. Pearson correlation analysis, least significant difference techniques and ratio to trend method were used to analyze the data. The results revealed that the temperature of pre-monsoon and winter seasons exhibited an insignificant positive correlation between the periods '1953-1971 and 1972-1990', '1972-1990 and 1991-2009', and '1953-1971 and 1991-2009'. However, the monsoonal and post-monsoonal temperature exhibited insignificant negative correlation between the periods '1953-1971 and 1991-2009', and positive correlation between the periods '1953-1971 and 1972-1990', '1972-1990 and 1991-2009'. The least significant difference technique identified the significant differences between the periods '1953-1971 and 1972-1990', '1972-1990 and 1991-2009', '1953-1971 and 1991-2009' during monsoon and winter seasons. It also identified the significant difference in all the periods of four seasons except the periods 1953-1971 and 1972-1990 during pre-monsoon season and the periods 1972-1990 and 1991-2009 during post-monsoon season. Again, the ratio to trend method identified that the lowest average temperature in January, it gradually increased until June, fluctuated in July-October, and then decreased until December.

Keywords: Global warming; Temperature fluctuation; Climate change; Seasonal variation; Ratio to trend method

1. Introduction

The global warming has induced the changes in natural calamity as well as precipitation in different regions of the world. Bangladesh is recently experiencing climate change impact related to hazards like cyclone, rainfall, flood, draught etc. Season is the climatic type at any place associated with a particular time of the year (Das, 1995). The change of season is mainly due to the change in angle of the earth's axis in relation to the position of the sun at a particular place (Manabe et al., 2011). Weather is the term that denotes the state of the atmosphere at a given time and place that is constantly changing sometimes from hour to hour and at other times from day to day (Brohan et al., 2006). Climate is the average state of atmosphere near the earth's surface over a long span of time (Chapman and Walsh, 1993). It refers to many elements including temperature, precipitation, humidity, air pressure, and wind direction and movement. Geographical location (latitude, coastal or continental position) and physical setting influence the climate of any country (Dee and Uppala, 2009; Jones et al., 1999). Bangladesh extends from $20^0 34'$N to $26^0 38'$N latitude and from $88^0 01'$E to $92^0 41'$E longitude. It is bordered by the Himalayas to the north and by the Bay of Bengal to the south. As the Tropic of Cancer passes through the middle of the country a tropical climate prevails there. The influence of the monsoonal wind is so strong that as a whole, the climate of Bangladesh is known as a tropical monsoon climate.

Bangladesh is one of the top most nations vulnerable to climate change (Harmeling, 2008). The Intergovernmental Panel on Climate Change (IPCC) recognizes Bangladesh as one of the most vulnerable countries in the world to the negative impacts of climate change. Consequences of climate change like recurring floods, river bank erosion, drought in dry season, salinity increase as a result of back water effect in the coastal region, downing ground water level during the dry season, have been contributing to augment the vulnerability of many regions. Nevertheless, many regions of Bangladesh this country remain outside the ambit of climate change related actions (Titumir and Basak, 2012). Warrick et al. (1994) studied the variation of temperature over Bangladesh and identified that the mean-annual temperatures have been expressed as departures from the reference period 1951-1980. It is evident that, on this time scale, the entire region of Bangladesh is getting warmer. Since the later part of the last century, there has been an overall mean increase in temperature by 0.5^oC which was comparable in magnitude to the observed global warming. However, a good numbers of studies have been carried out on trends of change in climatic parameters in the context of Bangladesh. Warrick et al. (1994), Karmakar and Shrestha (2000) and Debsarma (2003) provided the assessment of changes in temperature over Bangladesh, while Chowdhury and Debsarma (1992), and Mia (2003) reported the changes in temperature based on analysis of historical data of some selected weather stations

* Corresponding author. e-mail: nazrulupm@gmail.com

in Bangladesh. Karmakar and Nessa (1997), and Karmakar (2003) provided the assessment of the effects of climate change on natural disasters.

In and around Bangladesh rainy season is divided into three periods: (i) pre-monsoon (March-May), (ii) monsoon (June-September), and (iii) post-monsoon (October-November) periods (Das, 1995; Islam and Uyeda, 2007). The Fourth Assessment Report of IPCC observed that the 100-year linear trend (1906-2005) of global average surface temperature exhibited a 0.74 (0.56 to 0.92) ^{o}C increase, which is larger than the global corresponding increase of 0.6 (0.4 to 0.8)^{o}C in the years (1901-2000) (IPCC, 2007). The area impacted by drought in Bangladesh might have increased since the 1970s (IPCC, 2007). Modeling studies by Haque et al. (1992) indicated that the average increase in temperature would be 1.3^{o}C and 2.6^{o}C for the projected years of 2030 and 2075, respectively. Therefore, the main aim of this study is to provide an assessment of seasonal variation due to climate change in Dhaka city, Bangladesh based on the analytical results of historical data of temperature.

2. Methodology

In this study the daily data on temperature from the years 1953-2009 were used. The data were collected from the Meteorological Department, Bangladesh. The data were divided into three climatological periods as first period (1953-1971) less industrialization period, second period (1972-1990) moderate industrialization period and third period (1991-2009) modern industrialization period. These data were analyzed using different analytical programs. The seasonal variation of climatic data is identified by correlation analysis and least significant difference techniques among three periods. Beside these, monthly variations of indices were checked by ratio to trend method. The three tests are employed to ensure the variation of three periods for four climatological seasons e.g., pre-monsoon (March to May), monsoon (June to September), post-monsoon (October to November) and winter (December to February). Seasonal mean values have been computed for these four seasons.

3. Results

3.1. Temperature

Attempts were made to identify the correlation in seasonal variation of temperature for four seasons into three segments of 19 years period in Dhaka city, Bangladesh for the total period of 1953-2009. The variation of yearly mean seasonal variation of temperature for four climatological seasons over Dhaka city are shown in Figs. 1-4, respectively.

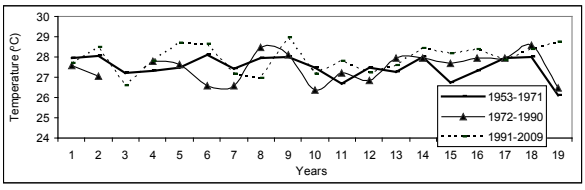

Figure 1: Variation of yearly seasonal mean temperature among three periods 1953-1971, 1972-1990, and 1991- 2009 during pre-monsoon season

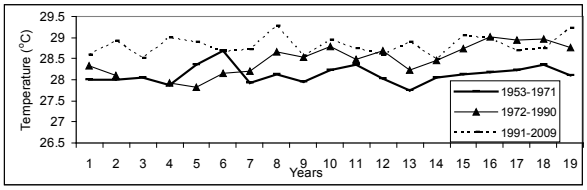

Figure 2: Variation of yearly seasonal mean temperature among three periods 1953-1971, 1972-1990, and 1991-2009 during monsoon season

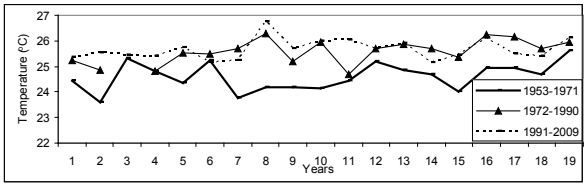

Figure 3: Variation of yearly seasonal mean temperature among three periods 1953-1971, 1972-1990, and 1991- 2009 during post-monsoon season

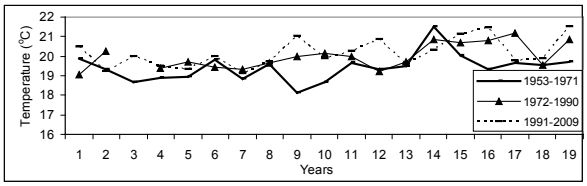

Figure 4: Variation of yearly seasonal mean temperature among three periods 1953-1971, 1972-1990, and 1991-2009 during winter season

The vertical axes of the figures of temperature represent temperature in ^{o}C and the horizontal axes represent year. Each of the data series of temperature exhibits period to period variation. From the figures, it is seen more seasonal variation in monsoon and post monsoon seasons and less seasonal variation occurred in pre-monsoon and winter seasons. The significant test of correlation in seasonal variation is shown below in Table 1.

Table 1: The correlation between the periods '1953-1971 and 1972-1990', '1972-1990 and 1991-2009', and '1953-1971 and 1991-2009' for temperature

Season	Period	Correlation coefficient (r)*	Degrees of freedom (df)
Pre-monsoon	1953-1971 and 1972-1990	0.34	11
	1972-1990 and 1991-2009	0.12	11
	1953-1971 and 1991-2009	0.06	11
Monsoon	1953-1971 and 1972-1990	0.16	11
	1972-1990 and 1991-2009	0.09	11
	1953-1971 and 1991-2009	-0.03	11
Post-monsoon	1953-1971 and 1972-1990	0.32	11
	1972-1990 and 1991-2009	0.39	11
	1953-1971 and 1991-2009	-0.01	11
Winter	1953-1971 and 1972-1990	0.34	11
	1972-1990 and 1991-2009	0.38	11
	1953-1971 and 1991-2009	0.18	11

***Note**: Significance of the correlation coefficients are carried out by t-test

From Table 1, it is seen that the correlation coefficients of temperature $r = 0.34$, $r = 0.12$, and $r = 0.06$ represent the insignificant positive correlation between the periods '1953-1971 and 1972-1990', '1972-1990 and 1991-2009', and '1953-1971 and 1991-2009', respectively, the during pre-monsoon season at 5% level of significance (Fig. 1). Again, the insignificant positive correlation coefficients $r = 0.16$ and $r = 0.09$ were found between the periods '1953-1971 and 1972-1990', and '1972-1990 and 1991-2009' respectively; the negative correlation coefficient $r = -0.03$ was found between the periods '1953-1971 and 1991-2009' during the monsoon season at the same level of significance (Fig. 2). Furthermore, the insignificant positive correlation coefficients $r = 0.32$ and $r = 0.39$ were found between the periods '1953-1971 and 1972-1990', '1972-1990 and 1991-2009' respectively; an insignificant negative correlation $r = -0.01$ was found between the periods '1953-1971 and 1972-1990' during the post monsoon season (Fig. 3). Likewise, the winter season also showed an insignificant positive correlation coefficients $r = 0.34$, $r = 0.38$, and $r = 0.18$ between the periods '1953-1971 and 1972-1990, '1972-1990 and 1991-2009', and '1953-1971 and 1991-2009' respectively (Fig. 4). Thus, the findings suggest that temperature goes up over time during most of the periods though the correlation coefficients of temperature are not statistically significant.

3.2. Test of least significant difference

The mean difference of temperature between the periods '1953-1971 and 1972-1990' were not statistically significant, but the difference between the periods '1953-1971 and 1991-2009', '1972-1990 and 1991-2009' were statistically significant at 5% level of significance during pre-monsoon season. Monsoon season shows highly significant mean difference of temperature at 0.1% level of significance between periods '1953-1971 and 1972-1990', '1953-7191 and 1991-2009', '1953-1971 and 1991-2009', and '1972-1990 and 1991-2009'. On the other hand, the mean differences of temperature between periods '1953-1971 and 1972-1990', and '1953-1971 and 1991-2009' were statistically significant at 1% level of significance during the post-monsoon and the winter seasons. These results are summarized in Table 2.

Table 2: Results of least significant difference test showing the mean differences of temperature between the periods during four seasons

Season	Period	Mean Difference	Standard Error	p-values
Pre-monsoon	1953-1971 and 1972-1990	0.01042	0.21271	0.961
	1972-1990 and 1991-2009	-0.43762	0.21271	0.045
	1953-1971 and 1991-2009	-0.42720	0.20982	0.047
Monsoon	1953-1971 and 1972-1990	-0.36513	0.09097	0.000
	1972-1990 and 1991-2009	-0.32171	0.09097	0.001
	1953-1971 and 1991-2009	-0.68684	0.08973	0.000
Post-monsoon	1953-1971 and 1972-1990	-0.97792	0.15803	0.000
	1972-1990 and 1991-2009	-0.08787	0.15803	0.581
	1953-1971 and 1991-2009	-1.06579	0.15588	0.000
Winter	1953-1971 and 1972-1990	-0.57305	0.23101	0.016
	1972-1990 and 1991-2009	-0.17086	0.23101	0.463
	1953-1971 and 1991-2009	-0.74391	0.22787	0.002

3.3. Seasonal variation of temperature using ratio to trend method

The results of trend values obtained by using ordinary least square method are presented in Table 3. Again, the results of monthly seasonal indices used ratio to trend method are presented in Table 4.

Table 3: Results of trend value by ordinary least squares method

Year	1	2	3	4	5	6	7	8	9	10	11	12
1991	25.616	25.619	25.621	25.624	25.626	25.629	25.631	25.634	25.636	25.639	25.641	25.644
1992	25.646	25.649	25.651	25.654	25.656	25.659	25.661	25.664	25.666	25.669	25.671	25.674
1993	25.676	25.679	25.681	25.684	25.686	25.689	25.691	25.694	25.696	25.699	25.701	25.704
1994	25.706	25.709	25.711	25.714	25.716	25.719	25.721	25.724	25.726	25.729	25.731	25.734
1995	25.736	25.739	25.741	25.744	25.746	25.749	25.751	25.754	25.756	25.759	25.761	25.764
1996	25.766	25.769	25.771	25.774	25.776	25.779	25.781	25.784	25.786	25.789	25.791	25.794
1997	25.796	25.799	25.801	25.804	25.806	25.809	25.811	25.814	25.816	25.819	25.821	25.824
1998	25.826	25.829	25.831	25.834	25.836	25.839	25.841	25.844	25.846	25.849	25.851	25.854
1999	25.856	25.859	25.861	25.864	25.866	25.869	25.871	25.874	25.876	25.879	25.881	25.884
2000	25.886	25.889	25.891	25.894	25.896	25.899	25.901	25.904	25.906	25.909	25.911	25.914
2001	25.916	25.919	25.921	25.924	25.926	25.929	25.931	25.934	25.936	25.939	25.941	25.944
2002	25.946	25.949	25.951	25.954	25.956	25.959	25.961	25.964	25.966	25.969	25.971	25.974
2003	25.976	25.979	25.981	25.984	25.986	25.989	25.991	25.994	25.996	25.999	26.001	26.004
2004	26.006	26.009	26.011	26.014	26.016	26.019	26.021	26.024	26.026	26.029	26.031	26.034
2005	26.036	26.039	26.041	26.044	26.046	26.049	26.051	26.054	26.056	26.059	26.061	26.064
2006	26.066	26.069	26.071	26.074	26.076	26.079	26.081	26.084	26.086	26.089	26.091	26.094
2007	26.096	26.099	26.101	26.104	26.106	26.109	26.111	26.114	26.116	26.119	26.121	26.124
2008	26.126	26.129	26.131	26.134	26.136	26.139	26.141	26.144	26.146	26.149	26.151	26.154
2009	26.156	26.159	26.161	26.164	26.166	26.169	26.171	26.174	26.176	26.179	26.181	26.184

Table 4: Results of monthly seasonal indices by ratio to trend method

Year	1	2	3	4	5	6	7	8	9	10	11	12
1991	73.39	90.17	104.99	112.01	106.92	110.81	113.53	112.74	108.83	106.48	91.26	76.43
1992	72.14	80.32	105.65	116.16	111.08	114.97	111.06	112.61	112.21	106.74	92.32	72.06
1993	69.32	87.23	96.179	107.46	106.67	111.72	111.32	110.53	110.13	105.84	92.21	77.03
1994	74.3	78.96	102.29	108.5	113.16	112.76	113.52	112.74	111.95	106.11	91.33	73.83
1995	68.77	82.37	101.39	116.14	116.91	113.79	111.06	112.99	111.04	107.15	92.78	73.75
1996	71.02	85.37	106.32	112.13	114.83	109.78	112.1	109.76	112.85	104.31	90.73	76.38
1997	68.23	80.62	103.48	100.37	111.99	112.36	111.19	113.12	108.07	102.64	92.95	73.58
1998	66.21	84.01	94.459	106.06	112.63	118.81	111.45	111.83	111.04	110.26	96.71	78.91
1999	72.71	90.1	107.11	118.31	110.57	112.1	110.16	110.15	108.98	106.65	91.96	80.75
2000	72.24	80.34	98.489	107.75	108.12	112.36	111.96	112.34	110.4	106.14	94.55	77.56
2001	71	87.2	102.62	112.25	106.84	107.99	111.06	113.75	110.66	106.4	94.44	76.32
2002	75.93	87.09	100.96	106.34	107.1	109.02	109.78	110.15	111.3	105.51	92.41	78.16
2003	62.36	85.07	93.914	111.22	113.52	109.28	112.73	113.1	109.63	106.93	92.3	78.83
2004	69.98	83.82	104.19	106.87	116.85	109.54	109.91	111.82	106.43	103.35	89.89	80.66
2005	72.98	89.87	103.3	111.35	109.8	114.02	109.78	111.31	110.91	103.61	91.71	80.19
2006	72.51	95.52	105.1	109.69	111.6	111.59	111.96	111.56	109.25	106.94	93.13	78.95
2007	68.98	82.38	97.313	107.65	114.92	109.92	108	111.44	109.89	103.76	91.5	75.79
2008	72.72	77.69	101.79	111.73	112.1	109.8	109.02	110.16	110.53	103.64	90.63	78
2009	75.32	89.07	103.21	115.04	111.21	115.4	110.81	110.42	110.02	105.43	93.96	78.52
Total	1350.11	1617.21	1932.75	2097.1	2116.84	2126.03	2110.42	2122.5	2094.14	2007.89	1756.77	1465.69
Average	71.06	85.12	101.72	110.37	111.41	111.90	111.07	111.71	110.22	105.68	92.46	77.14
(Adjusted) seasonal index	71.07	85.13	101.73	110.38	111.43	111.91	111.09	111.72	110.23	105.69	92.47	77.15

Note: Monthly Seasonal Indices are obtained by ratio to trend method and adjusted indices are obtained by the formula of adjusting factor, k = 1200/ total of the average indices

From the monthly seasonal indices obtained by the ratio to trend method, it is found that the lowest average temperature in the month of January and then gradually increased until June and then fluctuated in the month of July- October and then decreased until December. These findings suggest that the lower temperature (compared to 100) in the month of January, February, November and December do not influence the sufficient rainfall. That is, about four months remained dry in the Dhaka city. On the other hand, it is seen that the temperature is moderately higher from April-October and the average temperature remained 10% higher than the standard (100). Since the indices are unit free, so it is compared lower and higher relative to 100. These findings can also be achieved in the graphical form which is shown in Fig. 5.

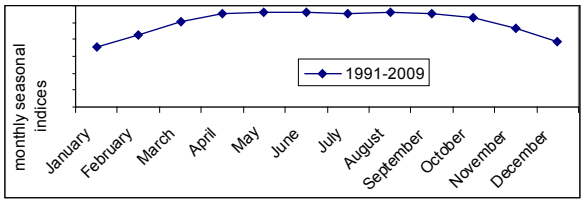

Figure 5: Changes in monthly seasonal indices of different month's temperature

4. Discussion

Though statistically insignificant positive correlations between the periods '1953-1971 and 1972-1990', '1972-1990 and 1991-2009', and '1953-1971 and 1991-2009' were found during the pre-monsoon season but trend of the temperature is upward. On the other hand, it was found an insignificant positive correlation between the periods '1953-1971 and 1972-1990', and '1972-1990 and 1991-2009', and negative correlation between the periods '1953-1971 and 1991-2009' during the monsoon season. Furthermore, it was seen that an insignificant positive correlation between the periods '1953-1971 and 1972-1990', and '1972-1990 and 1991-2009' but during the periods '1953-1971 and 1972-1990' exhibited an insignificant negative correlation during the post monsoon season. Likewise, the winter season also showed an insignificant positive correlation between the periods '1953-1971 and 1972-1990', '1972-1990 and 1991-2009', and '1953-1971 and 1991-2009'. It was found the significant difference in all pairs of four seasons except the periods '1953-1971 and 1972-1990' during the pre-monsoon and the periods '1972-1990 and 1991-2009' during the post-monsoon season using least significant difference method. On the other hand, by ratio to trend method, it was found that

the lowest average temperature in the month of January and then gradually increased until June and then fluctuated in the month of July-October and then decreased until December. In this regard, a study of Zaman et al. (2013) about trend analysis of temperature in Bangladesh due to global warming and found increasing average mean temperature in May, and July-October during 1979-2008.

The yearly seasonal mean temperature increased gradually in the periods '1953-1971', '1972-1990', and '1991-2009' and the rates of change of temperature were 0.01°C, 0.02°C, 0.04°C per year during the pre-monsoon and were 0.04°C, 0.07°C, 0.08°C per year during the winter season respectively. On the other hand, the yearly seasonal mean temperature was found to be increasing at a rate of 0.004°C, 0.05°C, 0.008°C per year during the monsoon and of 0.03°C, 0.05°C, 0.02°C during the post-monsoon in the periods '1953-1971', '19972-1990', and '1991-2009' respectively. But, the temperature in the winter season (December-February) increased at much higher rate than the summer season (June-August). The findings of this research are consistent with the results obtained by the IPCC (2007) and Zaman et al. (2013). Moreover, Basak et al (2013) studied the climate change in Bangladesh using a historical analysis of temperature and rainfall data where the yearly average was maximum temperature increased at all regions in Bangladesh during the period of 1976-2008. The above results are very close to this study.

5. Conclusion

The pre-monsoon and the winter seasons exhibited an insignificant positive correlations among the periods '1953-1971 and 1972-1990', '1972-1990 and 1991-2009', and '1953-1971 and 1991-2009'. The monsoon and the post-monsoon seasons showed the insignificant negative correlation between the periods '1953-1971 and 1991-2009' and positive correlation between the other two periods. From the test of least significant difference, it is found the significant difference in all pairs of four seasons except pair 1953-1971 and 1972-1990 during the pre-monsoon and pair 1972-1990 and 1991-2009 during the post-monsoon seasons. On the other hand, by ratio to trend method it is found that the lowest average temperature in the month of January and then gradually increased until June and then fluctuated in the month of July-October and then decreased until December.

Acknowledgments

This research work is supported by the grants from Rajshahi University and Climate Change Fund, Ministry of Environment and Forests, Government of the People's Republic of Bangladesh. The authors are very grateful to authority for this grant. Thanks are also to the editor and the referees for their comments and criticism, which lead to greatly improved version of this paper.

References

[1] Basak, J.K., Titumir, R.A.M., Dey, N.C. 2013. Climate change in Bangladesh: A Historical Analysis of Temperature and Rainfall Data. Journal of Environment, 2(2):41-46.

[2] Brohan, P., Kennedy, J. J., Harris, I., Tett, S. F. B., and Jones, P.D. 2006. Uncertainty estimate in regional and global observed temperature changes: A new data set from 1850. J. Geophys. Res., 111.

[3] Chapman, W. L., and Walsh, J. E. 1993. Recent variation of sea ice and air temperature in high latitudes. Bull. Amer. Meteor. Soc., 74: 33-47.

[4] Chowdhury, M.H.K., Debsarma, S.K. 1992. Climate change in Bangladesh- A statistical review. Report of IOC-UNEP Workshop on Impacts of Sea Level Rise due to Global Warming, NOAMI, November 16-19, 1992, Dhaka, Bangladesh.

[5] Das, P.K. 1995. The Monsoons, 3rd Ed. National Book Trust, New Delhi, India.

[6] Debsarma, S.K. 2003. Intra-annual and inter-annual variation of rainfall over different regions of Bangladesh. In: Proceedings of SAARC Seminar on Climate Variability in the South Asian Region and its Impacts, SMRC, December 20-24, 2002, Dhaka, Bangladesh.

[7] Dee, D. P., and Uppala, S. 2009. Variational bias correction of satellite radiance data in the ERA-Interim reanalysis. Quart. J. Roy. Meteor. Soc., 135: 1830-1841.

[8] Haque, M.Z., Quayyam, H.A., Hossian, M.M., and Islam, M.S. 1992. Occurrence of grain fertility in different rice crops. Proc. Intl. Bot. Conf., January 10-12, 1991, Bangladesh.

[9] Harmeling, S. 2008. Global Climate Risk Index 2009. Weather-related Loss and Their Impacts on Countries in 2007 and in a Long Term Comparison. Kaiserstr 201, Bonn, German watch e.V.: 5-8.

[10] IPCC. 2007. Summary for Policymakers. The Physical Science Basis. Contribution of Working Group I to the Fourth Assessment Report of the Intergovernmental Panel on Climate Change (IPCC). New York.

[11] Islam, M.N., Uyeda, H. 2007. Use of TRMM in determining the climatic characteristics of rainfall over Bangladesh. Remote Sens. Environ., 108: 264-276.

[12] Jones, P. D., New, M., Parker, D.E., Martin, S., and Rigor, I.G. 1999. Surface air temperature and its variation over the last 150 years. Rev. Geophys., 37: 173-199.

[13] Karmakar, S. 2003. Trends in the annual frequency of cyclonic disturbances and storms in the Bay of Bengal. Seminar on Climate Variability in the South Asian Region and its Impacts, December 20-24, 2002, Dhaka, Bangladesh.

[14] Karmakar, S., and Nessa, J. 1997. Climate change and its impacts on natural disasters and south-west monsoon in Bangladesh and the Bay of Bengal. Journal of Bangladesh of Academy of Sciences 21(2): 127-136.

[15] Karmakar, S., Shrestha, M.L. 2000. Recent Climate Change in Bangladesh. SMRC Series, no. 4. Dhaka, Bangladesh..

[16] Manabe, S., Ploshay, J., and Lau, N.C. 2011. Seasonal Variation of Surface Temperature Change during the Last Several Decades. J. Climate, 24:3817-3821.

[17] Mia, N.M. 2003. Variations of temperature in Bangladesh. Seminar on Climate Variability in the South Asian Region and its Impacts. December 20-24, 2002; Dhaka, Bangladesh.

[18] Titumir, R.A.M., and Basak, J.K. 2012. Effects of Climate Change on Crop Production and Climate Adaptive Techniques for Agriculture in Bangladesh. Social Science Review, the Dhaka University Studies, Part-D 29(1):215-232.

[19] Warrick, R.A., Bhuiya, A.H., and Mirza, M.Q. 1994. The Greenhouse Effect and Climate Change: Briefing Document No. 1. Unnayan Parishod, Dhaka, Bangladesh: 17-20

[20] Zaman, R., Malaker, P.K., Murad, K.F.I., and Sadat, M.A. 2013. Studies on trend analysis of changing temperature in Bangladesh due to global warming. Journal of Biodiversity and Environmental Science, 3: 32-28.

The Jordan Journal of Earth and Environmental Sciences (JJEES)

INSTRUCTIONS TO AUTHORS:

The Jordan Journal of Earth and Environmental Sciences (JJEES) is the national journal of Jordan in earth and environmental sciences. It is an internationally refreed journal dedicated to the advancement of knowledge. It publishes research papers that address both theoritical and applied valuable subjects and matters in both Arabic and English languages in the various fields of geoscience and environmental disciplines. JJEES is published quarterly by the Hashemite University.

Submitted articles are blindly and rigorously reviewed by distinguished specialists in their respected fields.

The articles submitted may be authenitic research papers, scientific reviews, technical/scientific notes.

SUBMISSION OF PAPERS

Online: For online submission upload one copy of the full paper including graphics and all figures at the online submission site, accessed via http://jjees.hu.edu.jo. The manuscript must be written in MS Word Format. All correspondence, including notification of the Editor's decision and requests for revision, takes place by e-mail and via the Author's homepage, removing the need for a hard-copy paper trail.

By Mail: Manuscripts (1 original and 3 copies) accompanied by a covering letter may be sent to the Editor-in-Chief. However, a copy of the original manuscript, including original figures, and the electronic files should be sent to the Editor-in-Chief. Authors should also submit electronic files on disk (one disk for text material and a separate disk for graphics), retaining a backup copy for reference and safety.

Note that contributions may be either submitted online or sent by mail. Please do NOT submit via both routes. This will cause confusion and may lead to delay in article publication. Online submission is preferred.

FORMATE GUIDE:

1. The research papers should be printed on one side of the paper, be duoble-line spaced, have a margin of 30 mm all around , and no more than 30 pages (7,500 words, font size 13). The title page must list the full title and the names and affiliations of all authers (first name, middle name and last name). Also, their addresses, including e-mail, and their ranks/positions must be included. Give the full address, including e-mail, telephone and fax, of the author who is to check the proof.

2. The research must contain the title and abstract, keywords, introduction, methodology, results, discussion, and recommendations if necessary. The system of international units must also be used. Scientific abbreviations may be used provided that they are mentioned when first used in the text. Include the name(s) of any sponsor(s)of the research contained in the paper, along with grant number(s).

3. Authors should submit with their paper two abstracts, one in the language of the paper and it should be typed at the beginning of the paper followed by the keywords before the introduction. As for the other abstract, it should be typed at the end of the paper on a separate sheet. Each abstract should not contain more than 200 words.

4. Captions and tables should be numbered consecutively according to their occurrence in the research with headings. When mentioned in the text, the same consecutive numbers should be used. Captions and tables must be typed on separate sheets of paper and placed at the end of the paper.

5. The author(s) should submit a written consent that he or she will not publish the paper in any other journal at the same time of its publication in JJEES. After the paper is approved for publication by the editorial board, the author does not have the right to translate, quote, cite, summarize or use the publication in the other mass media unless the editor-in-chief submits a written consent according to the policy of JJEES. Submitted material will not be returned to the author unless specifically requisted.

6. DOCUMENTATION:

- References:

a. To cite sources in the text, use the author-date method; list the last name(s) of the author(s), then the year. Examples: (Holmes, 1991); (Smith and Hutton 1997).

b. In the event that an author or reference is quoted or mentioned at the beginning of a paragraph or sentence or an author who has an innovative idea, the author's name is written followed by the year between two brackets. Example: Hallam(1990).

c. If the author's name is repeated more than once in the same volume, alphabets can be used. Example: (Wilson, 1994 a; Wilson, 1994 b).

d. Footnotes may be used to solve any ambiguity or explain something as in the case of a term that requires illustration. In this case, the term is given a number and the explanation is written in a footnote at the bottom of the page.

e. If the number of authors exceeds two, the last name of the first author followed by et al. is written in the text. Example: (Moore et al.). Full names are written in the references regardless of their number.

f. Prepare a reference section at the end of the paper listing all references in alphabetical order according to the first author's last name. This list should include only works that been cited.

- Books:

Hunt, J. 1996. Petroleum Geochemistry and Geology. 2nd Ed., H. W. Freeman and Company, New York.

- Chapter in a book:

Shinn E. A., 1983. Tidal Flat Environment, In: Carbonate Depositional Environments, edited by Scholle, P. A., Bebout, D. G., and Moore, C. H., The American Association of Petroleum Geologists, Tulsa, Oklahoma, U.S.A. pp. 171-210.

- Periodicals:

Sexton, P. F., Wilson, P. A.,and Pearson, P. N., 2006. Paleoecology of Late Middle Eocene Planktonic Foraminifera and Evolutionary Implication, Marine Micropaleontology, 60(1): 1-16.

- Conferences and Meetings:

Huber, B. T. 1991. Paleogene and Early Neogene Planktonic Foraninifer Biostratigraphy of Sites 738 and 744, Kerguelen Plateau (southern Indian Ocean). In: Barron, J., Larsen, B., et al. (Eds.), Proceedings of the Ocean Drilling Program. Scientific Results, vol. 119. Ocean Drilling Program, College station, TX, pp. 427-449.

- Dissertations:

Thawabteh, S. M. 2006. Sedimentology, Geochemistry, and Petrographic Study of Travertine Deposits along the Eastern Side of the Jordan Valley and Dead Sea, M. Sc. Thesis, The Hashemite University.

- Unpublished:

Makhlouf, I. M. and El-Haddad, A. 2006. Depositional Environments and Facies of the Late Triassic Abu Ruweis Formation, Jordan, J. Asian Earth Sciences, England, in Press.

- Illustrations:

a. Supply each illustration on a separate sheet, with the lead author's name, the figure number and the top of the figure indicated on the reverse side.

b. Supply original photographs; photocopies and previously printed material are not acceptable.

c. Line artwork must be high-quality laser output (not photocopies).

d. Tints are not acceptable; lettering must be of reasonable size that would still be clearly legible upon reduction, and consistent within each figure and set of figure.

e. Electronic versions of the artwork should be supplied at the intended size of printing; the maximum column width is 143 mm.

f. The cost of printing color illustrations in the Journal may be charged to the author(s).

7. Arranging articles in JJEES is based on the editorial policy.

8. The author should submit the original and two copies of the manuscript, together with a covering letter from the corresponding author to the Editor-in-Chief.

9. The editorial board's decisions regarding suitability for publication are final. The board reserves the right not to justify these decisions.

10. In case the paper was initially accepted, it will be reviewed by two specialized reviewers.

11. The accepted papers for publication shall be published according to the final date of acceptance.

12. If the author chooses to withdraw the article after it has been assessed, he/she shall reimburse JJEES the coast of reviewing the paper.

13. The author(s) will be provided with one copy of the issue in which the work appears in addition to 20 off prints for all authors. The author(s) must pay for any additional off prints of the published work.

14. Statement transferring copyright from the authors to the Hashemite University to enable the publisher to disseminate the author's work to the fullest extent is required before the manuscript can be accepted for publication. A copy of the Copyright Transfer Agreement to be used (which may be photocopied) can be found in the first issue of each volume of JJEES.

15. Articles, communications or editorials published by JJEES represent the sole opinion of the authors. The publisher bears no responsibility or liability whatsoever for the use or misuse of the information published by JJEES.

16. Submission address:

Prof. Dr. Eid A. Al-Tarazi
Editor-in-Chief,
Jordan Journal of Earth and Environmental Sciences,
The Hashemite University,
P.O. Box 150459, Zarqa, 13115, Jordan.
Phone: 00962-5-3903333 / Ext. 4229
Fax: 00962-5-3826823
E-Mail: jjees@hu.edu.jo
http:// jjees.hu.edu.jo/

المملكة الأردنية الهاشمية

الجامعة الهاشمية

المجلة الأردنية
لعلوم الأرض والبيئة

JJEES

مجلة علمية عالمية محكمة

http:// jjees.hu.edu.jo/

ISSN 1995-6681

المجلة الأردنية لعلوم الأرض والبيئة
مجلة علمية عالمية محكمة

المجلة الأردنية لعلوم الأرض والبيئة: مجلة علمية عالمية محكمة ومفهرسة ومصنفة، تصدر عن الجامعة الهاشمية وبدعم من صندوق البحث العلمي– وزارة التعليم العالي والبحث العلمي، الأردن.

هيئة التحرير

ترسل البحوث إلى العنوان التالي:

رئيس تحرير المجلة الأردنية لعلوم الأرض والبيئة

عمادة البحث العلمي والدراسات العليا

الجامعة الهاشمية

الزرقاء ١٣١٣٣ – الأردن

هاتف ٣٩٠٣٣٣٣–٥–٩٦٢+ فرعي ٤٢٢٩

Email: jjees@hu.edu.jo, Website: www.jjees.hu.edu.jo

المملكة الأردنية الهاشمية

الجامعة الهاشمية

المجلة الأردنية لعلوم الأرض والبيئة

JJEES

مجلة علمية عالمية محكمة

تصدر بدعم من صندوق دعم البحث العلمي

http://jjees.hu.edu.jo/

المجلد (٦) العدد (٢)

ISSN 1995-6681

كانون الأول ٢٠١٤ / ربيع الأول ١٤٣٦